Aus dem Charité Comprehensive Cancer Center
der Medizinischen Fakultät Charité – Universitätsmedizin Berlin

DISSERTATION

Extracellular vesicles as cancer liquid biopsy biomarker

zur Erlangung des akademischen Grades
Doctor medicinae (Dr. med.)

vorgelegt der Medizinischen Fakultät
Charité–Universitätsmedizin Berlin
von

Soo Ann Yap
aus Kuala Lumpur, Malaysia

Datum der Promotion:

4 Juni 2021

1. PREFACE

Certain parts of this thesis were used for the manuscript

Analysis of cancer related mutations in extracellular vesicles RNA by Droplet Digital PCR.

Yap S.A., Münster-Wandowski A., Nonnenmacher A., Keilholz U., Liebs S.

BioTechniques Journal, 25 June 2020

2. APPENDIX

2.1 List of abbreviations

1D plot	One-dimensional plot
2D plot	Two-dimensional plot
AJCC	American Joint Committee on Cancer
ALK	Anaplastic lymphoma receptor tyrosine kinase
ARTN	Artemin
AuTf	(Gold) Aurum-conjugated transferrin- receptor
BHQ1	Black hole quencher®
BSA	Bovine serum albumin
CDKN2A	Cyclin-dependent kinase inhibitor 2A
cDNA	Complementary DNA
cfDNA	Circulating cell-free DNA
CIMP	CpG island methylator phenotype
CML	Chronic myelogenous leukemia
CPM	Copies per microliter
CNS	Central nervous system
CRC	Colorectal cancer
CTC	Circulating tumor cells
ctDNA	Circulating tumor DNA
CTLA-4	Cytotoxic T lymphocyte-associated antigen 4
Cq	Cycle quantification
ddPCR	Droplet digital PCR™
DEPC	Diethyl pyrocarbonate
DMEM	Dulbecco's Modified Eagle Medium
DNA	Deoxyribonucleic acid
DSMZ	German Collection of Microorganisms and Cell Cultures
DTT	Dithiothreitol
dUTP	Deoxyuridine triphosphate
EDTA	Ethylenediaminetetraacetic acid
EGFR	Epidermal growth factor receptor
EMT	Epithelial to mesenchymal transition

EORTC	European Organization for Research and Treatment of Cancer
EpCAM	Epithelial cell adhesion molecule
ESCRT	Endosomal sorting complex required for transport
EV	Extracellular vesicles
Exo	Exosomes
FAP	Familial adenomatous polypopsis
FasL	Fas-ligand
FBS	Fetal bovine serum
FDA	U.S.A Food and Drug Administration
FFPE	Formalin-fixed paraffin-embedded
FPR	False positive rate
FWD	Forward
GD2	Disialoganglioside
gDNA	Genomic DNA
GM-CSF	Granulocyte-macrophage colony-stimulating factor
GTP	Guanosintriphosphat
HER2	Human epidermal growth factor receptor 2
HNB1	Hereditary neuroblastoma predisposition gene
HNPCC	Hereditary nonpolyposis colorectal cancer
IDRFs	Imaged-defined risk factors
ILV	Intraluminal vesicles
INFα	Interferon-alpha
INRGSS	International Neuroblastoma Risk Group Staging System
INSS	International Neuroblastoma Staging System
ISEV	International Society of Extracellular Vesicles
LDH	Lactate dehydrogenase
LNA	Locked nucleic acid
LOD	Limit of detection
MEK	Mitogen-activated protein kinase kinase (alias:MAPKK)
MIBG	Metaiodobenzylguanidine
MIR	Melanocortin-1-receptor
miRNA	Micro RNA
MITF	Microphthalmia-associated transcription factor
MM	Melanoma
MMR/MSI	Mismatch repair genes/microsatellite instability
mRNA	Messenger RNA
MUT	Mutation
MVB,MV	Multivesicular bodies

NB	Neuroblastoma
NEAA	Non-essential amino acid
Neg	Negative
nm	Nanometer
NSE	Neuron-specific enolase
nSMase2	Neutral sphingomyelinase 2
NRTN	Neurturin
qPCR	Quantitative PCR
PCR	Polymerase chain reaction
PD-L1	Programmed death ligand-1
PI3K	Phosphatidylinositol 3-kinase
Pos	Positive
PMMA	Polymethyl methacrylate
PSN	Persephin
PTA	Phosphotungstic acid
PVDF	Polyvinylidene difluoride membrane
RAB	RAS-related protein
REV	Reverse
RNA	Ribonucleic acid
RPMI	Roswell Park Memorial Institute
RRID	Resource Identification Initiative
RT	Room temperature
SEC	Size exclusion chromatography
TBS	Tris buffered saline
TBST	Tris buffered saline with Tween-20
TEM	Transmission electron microscope
TERT	Telomerase reverse transcriptase
THP	Tamm-Horsfall protein
TME	Total mesorectal excision
TNF	Tumor necrosis factor
TRAIL	TNF-related apoptosis-inducing ligand
UV	Ultraviolet
VEGF	Vascular endothelial growth factor
WB	Western blot
WT	Wildtype
WTA	Whole transcriptome amplification
Z/IB	Zen™/Iowa Black™ quencher

2.2 List of figures

Figure 1: Exocytosis of multivesicular endosome releasing exosomes 7
Figure 2: Biogenesis and release of EV from eukaryotic cells 9
Figure 3: Liquid biopsy components 14
Figure 4: Right versus left colon cancer 16
Figure 5: Colorectal cancer staging 17
Figure 6: Top 20 colorectal cancer genes 18
Figure 7: Top 20 genes in melanoma 23
Figure 8: Top 20 genes in neuroblastoma 30
Figure 9: Extracellular vesicles isolation from human-derived cell lines and plasma samples 46
Figure 10: Extracellular vesicles isolation from urine samples 48
Figure 11: Bio-Rad DG8 cartridges 52
Figure 12: Electron microscope validation of extracellular vesicle isolation protocol 57
Figure 13: Tamm-Horsfall protein in urine samples 58
Figure 14: Extracellular vesicles derived from urine 59
Figure 15: Transmission electron microscope 60
Figure 16: TEM image of cell-line derived extracellular vesicles 62
Figure 17: Enlarged TEM image of cell-line derived extracellular vesicles 62
Figure 18: Extracellular vesicles isolated from plasma of a healthy donor 63
Figure 19: Extracellular vesicles derived from a colorectal cancer patient 64
Figure 20: Characterization of extracellular vesicles by western immunoblotting 65
Figure 21: Multiple displacement amplification 66
Figure 22: Comparison of ddPCR prior to and after whole transcriptome amplification 66
Figure 23: Comparison of different primers 67
Figure 24: Schematic of the droplet digital PCR 68
Figure 25: Optimized duplex ddPCR 69
Figure 26: False positive rate for KRAS ^{G12C} assay 70
Figure 27: Limit of detection and WT/MUT ratio for KRAS ^{G12C} assay 71
Figure 28: Comparison of different quenchers for BRAF ^{V600K} assay 72
Figure 29: ddPCR optimization steps 73
Figure 30: ALK multiplex assay 74
Figure 31: BRAF multiplex assay 75
Figure 32: KRAS multiplex assay 76
Figure 33: DDPCR analysis of spiked samples 78
Figure 34: Whole mount immunoelectron analysis of spiked plasma sample 79
Figure 35: Liquid biopsy workflow 80

2.3 List of tables

Table 1: Melanoma staging (a) T category, (b) N category and (c) M category....21
Table 2: Neuroblastoma 5-year survival rate based on characteristics....25
Table 3: The INSS classification consists of 4 stages....27
Table 4: Neuroblastoma risk group classification....28
Table 5: Demographics, clinical characterization, and therapy information of participants for (a) colorectal cancer (b) melanoma and (c) neuroblastoma....43
Table 6: Concordance between gene status of extracellular vesicles and tumor tissue for (a) melanoma and (b) colorectal cancer cohort....82
Table 7: Cancer stages, tissue profiling and extracellular vesicles ddPCR results for (a) neuroblastoma (b) colorectal cancer and (c) melanoma cohort....83

TABLE OF CONTENTS

1. PREFACE ii
2. APPENDIX iii
   2.1 List of abbreviations iii
   2.2 List of figures vi
   2.3 List of tables vii
3. SUMMARY 1
4. ZUSAMMENFASSUNG 3
5. INTRODUCTION 5
   5.1 Extracellular vesicles 6
      5.1.1 Biogenesis and uptake of extracellular vesicles 8
      5.1.2 Physiological function of extracellular vesicles 11
      5.1.3 Extracellular vesicles and cancer 11
   5.2 Liquid biopsy 12
      5.2.1 Cancer biomarkers 13
   5.3 Colorectal cancer 15
      5.3.1 Colorectal cancer staging 16
      5.3.2 Genetic landscape 17
      5.3.3 Treatment 19
   5.4 Melanoma 20
      5.4.1 Melanoma staging 21
      5.4.2 Genetic landscape 23
      5.4.3 Treatment 24
   5.5 Neuroblastoma 25
      5.5.1 Neuroblastoma staging 26
      5.5.2 Genetic landscape 29
      5.5.3 Treatment 30
6. STUDY AIM 32
7. MATERIALS 33
   7.1 Commercially available kits 33
   7.2 Chemicals and solutions 34

7.3 Consumables 35
7.4 Antibodies 35
7.5 Devices 36
7.6 Software 36
7.7 Buffers and solutions 37
7.8 Primers and probes 38
7.9 Human-derived cell lines 40
8. METHODS 41
8.1 Patient materials 42
8.1.1 Patient samples 42
8.1.2 Patient demographics 42
8.2 Cell culture 45
8.2.1 Human-derived cell line cultivation and extracellular vesicle production 45
8.2.2 Extracellular vesicles isolation from cell lines 45
8.2.3 Extracellular vesicles isolation from plasma samples 46
8.2.4 Extracellular vesicles isolation from urine samples 47
8.3 RNA isolation and cDNA synthesis from cell lines 48
8.4 Extracellular vesicles-RNA isolation 48
8.5 Whole transcriptome amplification 49
8.6 Whole mount immunoelectron microscopy 49
8.7 Western blot 50
8.8 Designing primers and probes 50
8.9 Droplet digital polymerase chain reaction (ddPCR) 51
8.9.1 ddPCR multiplex 53
8.10 Data normalization and analysis 54
9. RESULTS 55
9.1 Culturing extracellular vesicles from cell lines 56
9.2 Extracellular vesicles isolation 56
9.2.1 Optimization of extracellular vesicles isolation 56
9.2.2 Purification of extracellular vesicles from urine 58
9.3 Extracellular vesicles characterization 59
9.3.1 Whole mount immunoelectron microscope analysis 59
9.3.2 Proteomic characterization 64
9.4 Whole transcriptome amplification 65
9.5 Mutational analysis 67

9.5.1 Primers and probes for extracellular vesicles mutational analysis 67
9.5.2 Mutational analysis via ddpcr 68
9.5.3 ddPCR multiplex 73
9.6 Sample collection and blood tube additives 76
9.7 Spiking 77
9.8 Patients 80
9.8.1 Sample preparation and workflow 80
9.8.2 Analysis of extracellular vesicles derived from patients 81
9.8.3 Discordant cases due to treatments 84
10. DISCUSSION 85
10.1 Isolation of extracellular vesicles 85
10.2 Extracellular vesicles from urine 87
10.3 Real-time PCR versus ddPCR 88
10.4 EV-based ddPCR patient analysis 89
10.5 Discordant results 90
10.6 Limitations in the pediatric neuroblastoma cohort 91
10.7 Clonal evolution 92
10.8 Challenges in extracellular vesicle research 93
11. FUTURE PERSPECTIVES 95
12. CONCLUSION 97
13. REFERENCES I
14. STATUTORY DECLARATION X
15. DECLARATION OF OWN CONTRIBUTION TO ANY PUBLICATIONS XI
16. CURRICULLUM VITAE XII
17. ACKNOWLEDGEMENTS XIII
18. PUBLICATION LIST XIV

3. SUMMARY

Extracellular vesicles (EV) are nanosized cup-shape vesicles, harboring a complex molecular repertoire of lipids, nucleic acids and protein. They exhibit the ability to carry molecular information from parental to target cells, along with playing vital roles in tumorigenesis, growth, progression, metastasis and drug resistance. Alongside circulating tumor cells and circulating cell-free DNA, EV are emerging as an important liquid biopsy component due to their ability to not only mirror information from cell of origin, but also the ability to protect their content in the circulation until arrival at the destination.

This thesis describes the isolation method of EV from cell lines, plasma and urine via differential centrifugation. Proteomic characterization was carried out with western blot, in which exosomal proteins, namely tetraspanins CD9 and CD81, were found to be enriched in the vesicles. Transmission electron microscope with anti-CD63 immunolabeling conjugated to 5 nm gold nanoparticles was used for the visualization of EV. Based on the defined criteria CD63-positive EV, varying from cup-shaped to round, 10-100 nm, with an intact membrane and central depression were identified.

KRAS, *BRAF* and *ALK* mutations from EV isolated from patients of colorectal cancer (CRC), melanoma (MM) and neuroblastoma (NB) were analyzed utilizing Droplet Digital PCR. EV-plasma samples collected post-therapy and tissue samples biopsied prior to treatment were compared, thus, allowing for the investigation of the vesicles' potential to monitor treatment response and disease progression. Mutated cDNA species were identified in ten of thirty-five cases. Concordance rates with corresponding tissues were 54%, 44% and 25% in CRC, MM and NB cohorts, respectively.

Furthermore, two discordant cases were highlighted due to their interesting medical background. In regards to both cases, a mutation switch after anti-*EGFR* or *BRAF/MEK* inhibitor therapy was detected prior to disease progression validated via cancer staging or repeated tissue genotyping, providing a prognosis for a disease relapse.

In conclusion, we proved that extracellular vesicles are able to provide information on tumor heterogeneity and prognosticate progression. The oncology field is being revolutionizing and advancing in the direction of targeted therapy to provide patients with a more precise approach. Liquid biopsy is therefore a good accompaniment to tissue biopsy in assisting the future development of targeted therapy, which requires the possibility of repetitive real-time monitoring to understand the dynamic changes within the disease. EV-derived nucleic acids may provide clinically relevant diagnostic information and mirror the evolution of the disease.

4. ZUSAMMENFASSUNG

Extrazelluläre Vesikel sind nanogroße, kelchförmige Vesikel mit komplexen molekularen Inhalten wie Lipiden, Nukleinsäuren und Proteinen. Sie können ihre molekularen Informationen von Mutterzellen an Zielzellen weitergeben und spielen daher eine wichtige Rolle bei Tumorentstehung, -wachstum und -progression, sowie beim Prozess der Metastasierung und dem Auftreten von Resistenzen gegen geläufige Therapiemethoden. Aufgrund ihres Vermögens nicht nur die Informationen von Mutterzellen widerzuspiegeln, sondern auch ihren molekularen Inhalt während des Transports durch die Blutzirkulation bis zur Ankunft am Zielort zu schützen, entwickeln sich EV neben zirkulierenden Tumorzellen und zell-freie DNA zu einer weiteren wichtigen Komponente der Liquid Biopsy.

Diese Dissertation beschreibt Methoden zur Isolierung von EV aus Zelllinien, Plasmen und Urin durch differentielle Zentrifugation. Die Charakterisierung der Proteine erfolgte durch Western Blots und ergab eine Anreicherung exosomaler Proteine (Tetraspanin CD9 und CD81) in den Vesikeln. Zur Visualisierung der Vesikel wurde ein Transmissionselektronenmikroskop mit anti-CD63 immunozytochemischer Markierung, konjugiert zu 5 nm Gold-Nanopartikeln, genutzt. Basierend auf definierten Kriterien wurden CD63 positive EV, mit variierender Form von rund bis kelchförmig, einer Größe von 10-100 nm, einer intakten Membran und zentraler Depression identifiziert.

Die aus Proben von Patienten mit kolorektalem Karzinom, Melanom und Neuroblastom isolierten EV wurden mit Hilfe von Droplet Digital PCRs auf Mutationen in *KRAS, BRAF* und *ALK* untersucht. Vergleiche von posttherapeutischen EV-Plasmaproben mit prätherapeutischen Biopsieproben ermöglichten die Abschätzung des Potentials von EV als Faktor zur Überwachung des Therapieanschlagens und Krankheitsverlaufs.

In 10 von 35 Fällen konnte eine Mutation in der cDNA festgestellt werden. Die Konkordanzrate mit dem dazugehörigen Tumorgewebe in den jeweiligen Kohorten waren 54% für kolorektale Karzinome, 44% für Melanome und 25% Neuroblastome.

Außerdem lassen sich zwei Fälle aufgrund ihrer Abweichungen und ihrem interessanten medizinischen Hintergrund hervorheben. In beide Fällen konnte eine Änderung der Mutation nach einer Therapie mit *EGFR*- oder *BRAF/MEK*-Inhibitoren vor der Progressionsbestätigung durch Krebs-Staging oder wiederholtes Feststellen des Gewebe-Genotyps detektiert werden und ermöglichte somit ein Krankheitsrezidiv zu prognostizieren. Zusammenfassend gesagt, sind extrazelluläre

Vesikel in der Lage Informationen über die Tumorheterogenität zu liefern, sowie eine Prognose über das Voranschreiten des Tumorwachstums zu ermöglichen.

Die onkologische Forschung bewegt sich in Richtung von personalisierten und patientenspezifischen Therapien. Dies erfordert die Möglichkeit einer wiederholbaren Echtzeitüberwachung der Krebserkrankung. Liquid Biopsy stellt daher einen guten und wichtigen Zusatz zur herkömmlichen Gewebebiopsie dar, um die dynamischen Veränderungen zu verstehen. Die in extrazellulären Vesikeln enthaltenen Nukleinsäuren können dabei klinische sowie diagnostische Information anbieten und folglich die Entwicklung der Krankheit widerspiegeln.

5. INTRODUCTION

Liquid biopsy is a minimally invasive diagnostic tool, providing information on miniscule nucleic acid in a single blood tube. It functions perfectly as an accompaniment to the gold standard tissue biopsy, and is efficient for the monitoring of disease progression and treatment response [1]. Extracellular vesicles (EV) are part of the liquid biopsy trio [1]. The vesicles are best known as a small delivery system, shuttling molecular information to designated cells [2]. This thesis highlights the value and importance of EV as a notable liquid biopsy component.

The study included the optimization of EV isolation via differential centrifugation from conditioned cell culture supernatant, plasma and urine samples. Proteomic content and morphological verification of EV were also studied. Primarily, mutational signatures in EV were analyzed with the novel platform droplet digital PCR, while comparing them to mutational analysis on tissue samples. EV could provide additional information on tissue samples, highlighting the heterogeneous nature of the disease. Tissue biopsy provides information originating from the location where tissue was probed, while liquid biopsy could capture a snapshot of the genomic landscape of the disease [3].

This thesis first introduces background information on EV (Section 4.1), a brief explanation of all three liquid biopsy components (Section 4.2) and the different tumor entities investigated in this study (Section 4.3 to 4.5). The main objectives of the study are further elaborated in Chapter 5. The materials used are listed in Chapter 6, Chapter 7 is concerned with the methodology applied for this study. Chapter 8 presents the findings of the research, focusing on the three key themes: proteomic, microscopic and PCR analysis, while especially highlighting discordant cases due to their interesting medical background. This thesis closes with a discussion of the findings in comparison to research literature (Chapter 9), future perspectives on EV studies (Chapter 10) and the conclusion (Chapter 11).

5.1 Extracellular vesicles

Extracellular vesicles (EV) are membrane vesicles released into the extracellular space, distinguished by size, composition and cellular origin. The vesicles are classified into subgroups based on their cellular biogenesis: microvesicles, exosomes and apoptotic bodies. Microvesicles are shed from the outward protrusion of the cell membranes. Exosomes, on the other hand are formed by inward budding and fusion of the plasma membrane upon release at the end of the endosomal recycling pathway [1]. Apoptotic bodies are membrane-bound vesicles formed during programmed cell death [2].

In the 1980s, two independent groups Pan and Johnstone [3] and Harding [4], with the assistance of a transmission electron microscope, witnessed an engulfment and the fusion of the vesicles with plasma membrane, a major discovery compared to previous findings, and mentioned exosomes as trash bags for molecular waste. Colloidal gold-conjugated transferrin-receptor (AuTf) particles were noticed to be taken up by reticulocyte transferrin receptors, specifically in small particles within the multivesicular bodies. The continuity of plasma membrane explained the fusion of multivesicular endosomes containing AuTf-labeled vesicles with plasma membrane [Figure 1(left)]. Post-fusion of the multivesicular endosomes and plasma membrane, and externalization of AuTf-labeled vesicles were observed [Figure 1(right)] [4].

Furthermore, Beckler *et al.* demonstrated the transfer of EV derived from mutant *KRAS* colorectal cancer cells to *KRAS* wild type (WT) cells, altering the *KRAS* gene sequence from wild type to mutant or acceleration the three-dimensional growth of *KRAS* wild type cells [5]. This demonstrates the ingestion of vesicles by cells and the vesicles' ability to alter the nature of the cells, thereby promoting intercellular communication. Extracellular vesicles are defined today as being 10 nm – 100 nm, and cup-shaped with a central indentation and bilayer phospholipid membrane. Proteins, nucleic acids and lipids make up the cargo sorted into EV, which depending on their fate are followed by either lysosomal degradation or fusion with plasma membrane of recipient cells [6]. Upon envelopment by recipient cells, the vesicular content of EV heavily influences the function of the recipient cells. Since their renewed discovery, there is a growing interest in multiple disciplines: cardiovascular [7], urology [8], endocrinology [9] and oncology [10,11].

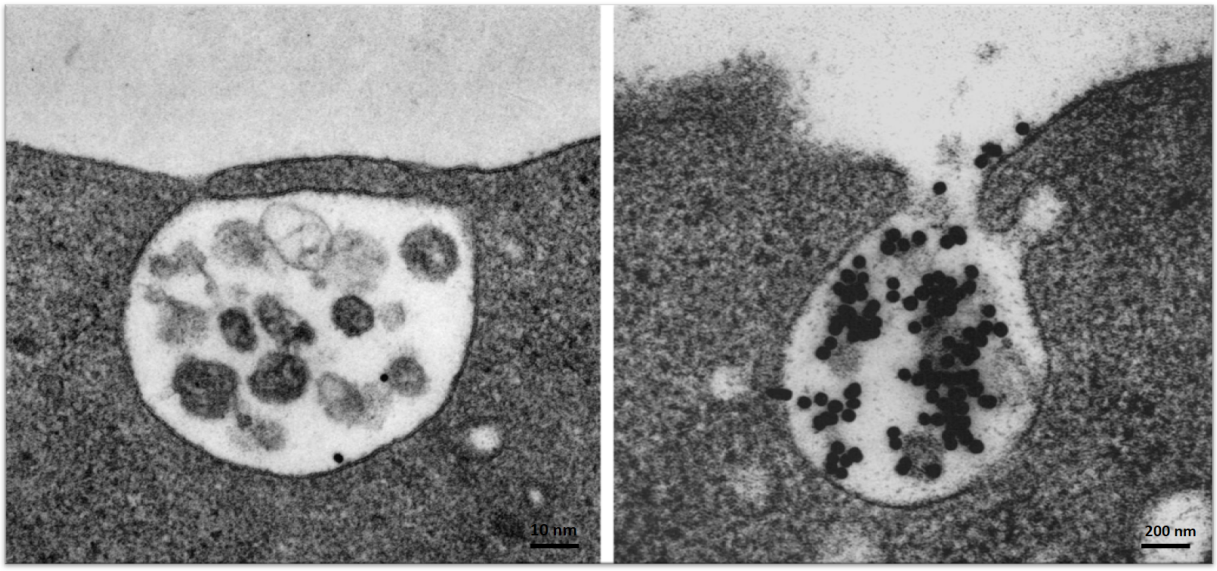

Figure 1: Exocytosis of multivesicular endosome releasing exosomes

Harding et al. visualized the internalization of the vesicles and the subsequent fusion of multivesicular endosomes and AuTf-labeled vesicles. Bar, 10 nm (left). This was followed by the externalization of vesicles. Bar, 200 nm (right). Adapted from Harding (1983) [4].

There has been a constant debate on utilizing the nomenclature extracellular vesicles or exosomes [12]. The Oxford Classical Greek Dictionary defines 'exo' as outside and 'soma' as from the body, forming the term exosomes [13]. In the scientific community, exosomes as described by multiple publications are vesicles formed in endosomal secretion and released upon fusion with plasma membrane [6,14,15]. To date, there is no isolation protocol that specifically separates the different vesicular subsets based on biogenesis or morphology. There is always a risk that subpopulations of the vesicles remain amongst the mix. Furthermore, there are also no proposed lists of EV-specific markers to segregate the different EV subsets. Therefore, the International Society of Extracellular Vesicles (ISEV) recommended the more generic term 'extracellular vesicles' for all particles released from cells with a bilayer lipid membrane [16].

5.1.1 Biogenesis and uptake of extracellular vesicles

Multivesicular bodies (MVBs) are endocytic structures formed by the budding of endosomal membrane into the lumen of compartments. After vesicular accumulation, MVBs are sorted either for cargo degradation in lysosomes or the invagination of endosomal membrane. The invagination of the endosomal membranes forms intraluminal vesicles (ILV) within MVBs. ILV then fuse with plasma membrane and are released into the extracellular space as EV [17] [Figure 2].

Endosomal sorting complex required for transport (ESCRT) has been revealed to be vital for the formation and cargo sorting of the intraluminal vesicles. The ESCRT machinery consists of 4 complexes associated with proteins Alix and VPS4, both enriched in EV [18]. ESCRT-0 is responsible mainly for EV secretion, ESCRT-I, and -II are involved in membrane formation by recognition and recruitment of proteins in endosomal membrane, and ESCRT-III mediates vesicle scission [19].

Trajkovic *et al.* mentioned the ability of ceramide to induce inward budding of endosomal membrane, due to the areas abundant with sphingolipids [20]. In another study, it was reported that EV are composed of lipid rafts, after investigating associated proteins such as flotillin-1 and stomatin. There, the direct involvement of lipids in vesicle structure, budding, ubiquitin-based sorting platform and apoptosis regulation was proven [21].

Additionally, tetraspanins are another vital player in EV biogenesis and have been thoroughly studied are tetraspanins. In the absence of ESCRT machinery, tetraspanins as proteins are fundamental for the biogenesis of lysosomal-related organelles [22]. Furthermore, the intricate formation of the tetraspanins web contributes to the role of cargo sorting and protein trafficking into EV [23].

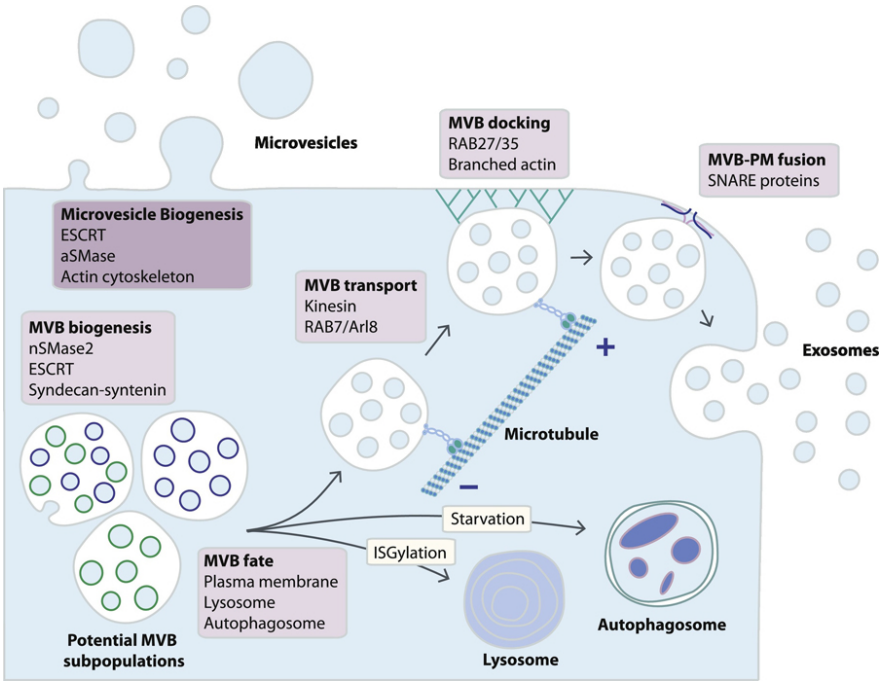

Figure 2: Biogenesis and release of EV from eukaryotic cells

Early endosome formation later develops into late endosomes (multivesicular bodies). Multivesicular bodies are sorted for either lysosomal degradation or invagination of endosomal membrane. Thereafter, EV are formed when intraluminal vesicles fuse with plasma membrane, bud outwardly, and are released into the extracellular space. SNAREs play a role in the fusion of multivesicular bodies with plasma membrane. RAB proteins take part in the transportation of the vesicles. ESCRT machinery and tetraspanins are tasked for the formation and cargo sorting of intraluminal vesicles. Lipids are vital for the structure of the vesicles, the ubiquitin-based sorting platform and apoptosis regulation. Adapted from Bebelman (2014) [24].

Several publications habe highlighted the involvement of Rab GTPase proteins, which are majorly involved in intracellular vesicle transport and docking [25]. Rab11 is involved in the discharge of the vesicles [26]. EV secretion is regulated by Rab27 and Rab35 [27,28].

After secretion, the nanovesicles are internalized through several mechanisms: phagocytosis, macropinocytosis, vesicle-cell fusion, and lipid-raft dependent- and receptor-mediated-endocytosis. Phagocytosis is an actin-, phosphatidylinositol 3-kinase (PI3K), - and dynamin-2 mediated engulfment of the vesicles by specialized cells (macrophages and monocytes). Through this process, extracellular materials are internalized by a form of envelopment [29]. Macropinocytosis internalizes smaller particles upon activation of phosphatidylserine and is Na^+-dependent, almost similarly to phagocytosis [30].

Cell-to-cell signaling has been demonstrated from tumor-derived EV, such as soluble signaling, which involves cleaving ligands from the surface of the vesicles, or via alternative splicing and juxtacrine signaling, which requires a close contact between ligands and receptors on the surface [25]. Transmembrane proteins such as Fas ligand (FasL), tumor necrosis factor (TNF) and TNF-related apoptosis-inducing ligand (TRAIL) signal apoptosis via receptors, and their membrane-bound form has been reported to have superior pro-apoptotic activity when compared to their soluble form [31].This mechanism was seen in EV isolated from plasma of ovarian cancer patients, which expressed Fas ligand. Fas ligand associated with cancer-derived vesicles induced T-lymphocyte apoptosis. Moreover, the presence of the plasma-derived EV suppressed T-cell receptor/CD3-ζ expression in T-lymphocytes of patients and correlated with the induction of apoptosis and caspase-3 within the T-cells. [32].

The direct merging of the plasma membrane of a cell and vesicle or vesicle-cell fusion also contributes to the internalization of EV [25]. Other forms of vesicle uptake include endocytosis involving either caveolin-dependent or lipid raft-dependent (caveolin-independent) endocytosis. Caveolar endocytosis is clathrin-independent endocytic process with plasma membrane invaginations, known as caveolae and the membrane proteins cavins. Some caveolae bud off from the plasma membrane, while some fuse back with the plasma membrane [33]. The mechanisms of lipid raft-dependent and caveolae-dependent endocytosis are similar [21].

Multiple studies have demonstrated transcriptomic content in EV, including mRNAs and miRNAs [25,26,27]. Thakur *et al.* proved the existence of double-stranded DNA in the vesicles while confirming mutations in cancer cells [37]. Proteomic content has been identified in many studies [38–40], and lipid content in the vesicles contributes to both the structural integrity and functions of the vesicles [21]. EV content including proteins, mRNA and miRNA are documented in ExoCarta [41].

5.1.2 Physiological function of extracellular vesicles

EV were studied and identified from diverse body fluids such as blood [42], urine [43], cerebrospinal fluid [44] and saliva [45], exhibiting their secretion in vivo. As mentioned above, EV transport proteomic and nucleic acid contents to distant cells and therefore modulate the function of the target cells. Upon release, EV protect cargo from phagocytosis, thereby protecting their content from the host response of the recipient cell. This transportation mode can also function in favor of pathogenic components to attack the host response [46]. Furthermore, EV isolated from infected macrophages activate pro-inflammatory mediators, including tumor necrosis factor–alpha (TNF-α) and RANTES (up-regulation of iNOS expression). These mediators in turn release cytokines, which are important for achieving immunity [47].

Formation of coagulation complexes and promotion of tissue factor activity could be facilitated by phosphatidylserine, found on membranes of platelet- and monocyte-derived EV [48]. Phosphatidylserine is a phospholipid and an important element in regulating blood coagulation and apoptosis. Platelet-derived vesicles encourage monocyte adhesion to endothelium and further stimulate prostacyclin synthesis and thromboxane A2 production, promoting platelet activation to aggregation [49–51].

5.1.3 Extracellular vesicles and cancer

EV from tumor cells can induce malignant transformation in normal cells, as well as accelerating existing tumorigenesis. Cargo internalized by EV has been known to influence oncogenic transformation, for example miR-125b, 130b, and 155 in prostate cancer [52], and pre-miRNA, RISC loading complex for breast cancer cells [53].

Several studies reported that the uptake of EV by cells encourages tumorigenesis. EV from chronic myelogenous leukemia (CML) promote growth of the tumor cells by stimulating the stromal cells in bone marrow to produce interleukin-8 [54]. Colon cancer cell lines when incubated with ΔNp73-enchanced EV proliferate greatly [55]. Angiogenesis is vital for the tumor to be continuously supplemented. Pro-angiogenic influences have been detected in EV with miR-105 in breast cancer cells [56], miR-92a in leukemic cells [57] and miR-135b in multiple myeloma cells undergoing hypoxia [58].

EV-integrins upregulate proinflammatory protein S100 expression and prepare pre-metastatic niches for the ideal microenvironment for tumor cells to colonize and disseminate to distant organ sites [59]. Chen *et al.* conducted experiments on mice and concluded that EV express programmed death ligand-1 (PD-L1) on their surface, promote tumor growth and reduce T-cell production. When the EV enriched with PD-L1 arrives at the pre-metastatic sites, the immune system is then inhibited and pre-metastatic niches are developed [60].

EV have been studied for their ability to reduce the efficacy of cancer treatment regimen through the transfer of multidrug resistance-associated protein. Metabolites and drugs could be encapsulated, transported by EV and able to modulate their binding to tumor cells, thereby negating the effect of the antibody drugs [15]. Bone marrow stromal cell-derived EV were seen to be able to induce multiple myeloma cells to be resistant to drugs like bortezomib, lenalidomide and thalidomide [61]. Furthermore, Wang *et al.* realized that bone marrow stromal cell-derived EV inhibit apoptosis, induced by bortezomib which instate the activation of caspase-3 and -9 [61]. In a breast cancer study, EV from HER2 overexpressing cancer cells were able to bind to trastuzumab (Her2 antibody) and inhibit its effect [62].

5.2 Liquid biopsy

Precision medicine is an approach which provides the opportunity to design therapy frameworks for patients based on genetic screening. The foundation of precision medicine is the introduction of targeted therapy, such as immune checkpoint inhibitors, which are used to target and terminate cancer cells while avoiding off-targets effects [63]. However, like the survival of the fittest, tumor cell populations evolve to survive under such conditions [64]. The initial promise of improved patient survival and tumor regression were subsequently met with secondary resistance. Cancer cells aggressively develop and adapt over the course of the targeted therapy, for example by developing a mechanism of resistance to escape immune recognition or by completely dysregulating the immune system, thus, inevitably causing disease relapse and ineffectiveness of the targeted therapy [65].

The current gold standard for genetic testing is tissue biopsy, which is arduous and meager in terms of the information it provides. It is strenuous for the patients to have repetitive tissue

biopsy due to its invasiveness, especially for pediatric patients, or due to the inconvenient location of the tumor. Furthermore, mutational analysis of tissue biopsy only provides information on the specific location where tissue was acquired. Cancer, as is known, can be heterogeneous and tissue biopsy is unable to adequately reflect this information [66].

The introduction of liquid biopsy could complement tissue biopsy in making up for insufficient mapping of the tumor heterogeneity. Due to its non-invasiveness, it is an advantageous in patient stratification, disease screening, treatment monitoring and prognostication of residual disease.

5.2.1 Cancer biomarkers

Three major players in liquid biopsy are circulating tumor cells (CTCs), cell free DNA (cfDNA) and extracellular vesicles (EV) [68] [Figure 3]. Circulating tumor cells (CTCs) are cells emanating from primary tumor or metastatic sites into the vasculature. The heterogeneity of CTCs could be due to the diverse location of the tumor they were released from. CTCs are described as viable cells with an intact nucleus, positively selected with cytokeratin and epithelial cell adhesion molecule (EpCAM) and negatively selected with CD45 (a leucocyte common antigen) [66]. They are detectable in cancer patients, rarely in healthy blood, and it has been reported that about one to ten CTCs were detected in one milliliter of blood [69]. Some CTCs undergo a special process known as epithelial to mesenchymal transition (EMT). This changes their characteristics and behavior. EMT has been known to increase tumor invasiveness, and overcome anoikis resistance *(anoikis: programmed cell death that occurs in anchorage-dependent cells when cells detach from the surrounding extracellular matrix*) and cell survival [70–72]. Unfortunately, the frequency of detectable CTCs is also highly dependent on the different technologies used for isolation. Furthermore, it is vital to isolate CTCs from whole blood within 96 hours after blood is drawn [73]. Its rarity has been proven to be a technical challenge.

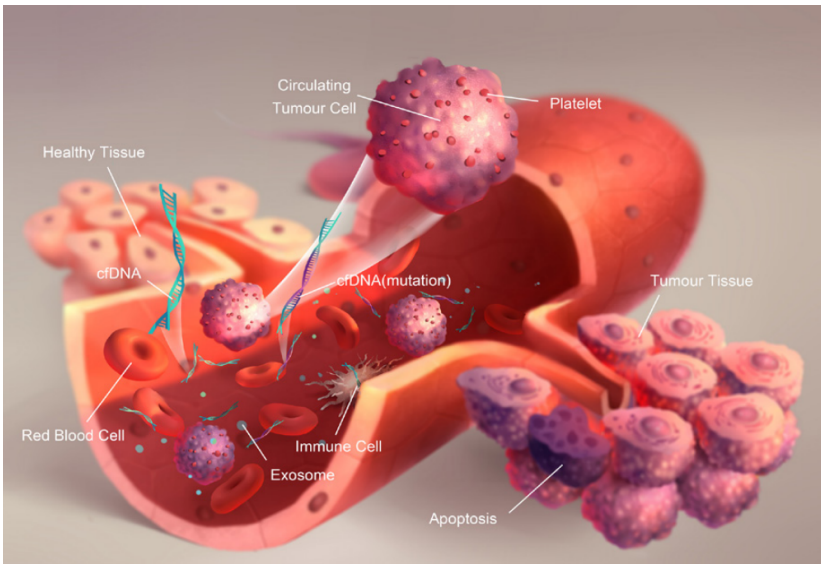

Figure 3: Liquid biopsy components

Representation of cfDNA, CTCs and exosome (extracellular vesicles) in the blood stream. Exosomes are released from a variety of cell types. cfDNA are released when cells undergo apoptosis. CTCs could escape from tumor tissue due to tumor growth or mechanical interruption due to surgery. Additionally, platelets could facilitate CTC adhesion to distant organs. Adapted from Zhang (2017) [67].

CTCs: circulating tumor cells, cfDNA: circulating cell free-DNA.

Circulating cell-free DNA (cfDNA) is released passively through apoptosis. In normal individuals or early cancer stages about 3 to 9 ng of cell-free DNA per milliliter of plasma were detected, whereas the amount increased by more than 10-fold in advanced cancer patients [74]. The challenge here is the rare detection of circulating tumor DNA (ctDNA) which carries mutant genes in the midst of normal cfDNA. Nevertheless, CancerSEEK , a recently established ctDNA blood-based diagnostic, achieved a sensitivity ranging from 69 to 98% across five cancer types, affirming ctDNA as worthwhile for cancer detection [75].

Both CTCs and cfDNA have been used to study the mutational status of the disease via different platforms such as droplet digital PCR and next generation sequencing. In comparison, the use of EV as a blood-based biomarker is still in its infancy. They are gaining an improved reputation as feasible cancer biomarkers due to their ability to protect their biological cargo in the circulation [76]. EV are more abundant and can be analyzed from both fresh and frozen biobanked samples, unlike CTCs which required fresh samples (67,75). Both cfDNA and EV require at least one milliliter of plasma for analysis. However, EV are more efficient in searching for mutations, whereas cfDNA samples are populated with a high wild-type environment [68,78].

Even though liquid biopsy could complement tissue biopsy well to provide information for a better understanding of the disease and therapy stratification, isolation is tedious, and it is challenging to gather enough nucleic acid from the different liquid biopsy components.

5.3 Colorectal cancer

Colorectal cancer (CRC) originates in the colon or rectum. Its growth is frequently initiated with the development of polyps in the inner lining of the colon or rectum, which then turn malignant [79]. As most polyps are benign and only 1% are potentially precancerous, polyps correlate with the development of CRC. The following factors are taken into consideration as an increased risk of CRC development: if a polyp is larger than 1 cm, the occurrence of more than two polyps, and the appearance of dysplasia after removal of polyps (*Dysplasia: a precancerous condition, in which cells appear morphologically abnormal*) [79].

CRC is accountable as the third most common cancer for male population after prostate and lung cancer, and the second most common cancer for the female population after breast cancer, with 63,000 new cases every year [80]. When evaluating CRC patients, the location of the primary tumor has been given importance, on the grounds that it differs in clinical symptoms and prognosis, and could influence therapy outcome. Due to the different embryologic origins and with the splenic flexure as a border, the right colon (proximal) arises from the midgut and left colon (distal) arises from the hindgut [81] [Figure 4]. Right colon cancer is more common with older females and presents itself initially with iron deficiency anemia, while left colon cancer presents itself clinically with hematochezia and bowel habit changes, and has a better prognosis [82]. Furthermore, right colon cancer frequently develops through *MMR/MSI* or *CIMP* pathways with a high frequency of *PI3K*, *BRAF* or *RAS* mutations when compared to left colon cancer [83]. On the other hand, *TP53* mutation occurs more frequently in left colon cancer [84].

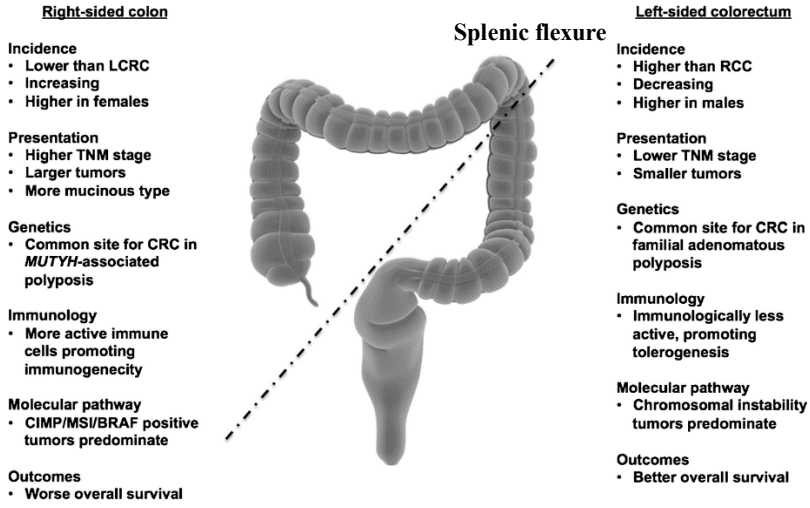

Figure 4: Right versus left colon cancer

Clinicopathological characteristics of right and left colon cancer with the splenic flexure as a border. Adapted from Ghidini (2018)[85].

5.3.1 Colorectal cancer staging

Colorectal cancer is staged based on the TNM concept: primary tumor (T), regional lymph nodes (N) and distant metastasis (M). American Joint Committee on Cancer (AJCC) staging is more commonly used to define cancer stages from stage 0 (very early), stage 1 through stage 4 (late), based on the TNM concept [Figure 5]. AJCC staging uses the surgical or pathological stage by examining tissue extracted during surgery and is more accurate when compared to clinical staging (physical examinations, biopsies and imaging diagnostics prior to surgery) [86].

Dukes classification entails histopathological examination [87].

Stage A : Tumor limited to mucosa

Stage B1 : Tumor limited to submucosa, without lymph node invasion

Stage B2 : Tumor confined to muscle layer, without lymph node invasion

Stage C1 : Tumor did not exceed bowel wall, with lymph node metastasis

Stage C2 : Tumor exceeded intestinal wall, with lymph node metastasis

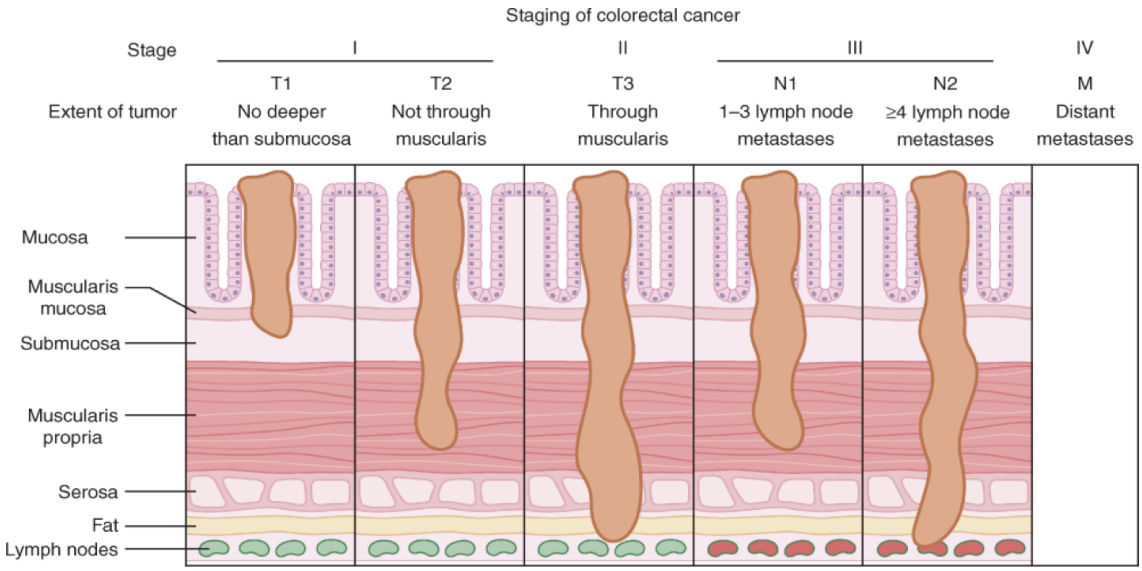

Figure 5: Colorectal cancer staging

Colorectal cancer staging based on the TNM concept: primary tumor (T), regional lymph nodes (N) and distant metastasis (M). American Joint Committee on Cancer (AJCC) classification is defined in stages. In stage I, cancer spreads from the mucosa of the colon wall to the submucosa of the muscle layer. Stage II cancer spreads through the muscle layer of the colon wall to the serosa. Stage III cancer spreads through all layers and infiltrates lymph nodes or tissues close to lymph nodes. In stage IV, the cancer metastasizes to distant locations, including the lung, liver, abdominal wall or ovary. Adapted from DiPiro (2017) [88].

5.3.2 Genetic landscape

Lynch syndrome or hereditary nonpolyposis colorectal cancer (HNPCC) is a common predisposition for colorectal cancer and autosomal dominant genetic syndrome with defective DNA mismatch repair *(MMR) - mutL homologue 1 (MLH1), mutS homologue 2 (MSH2), MSH6* or *postmeiotic segregation increased 2 (PMS2)* [79,89].

Commonly manifested, microsatellite instability (MSI) involves short tandem repeats with alternate size repetitive DNA sequences, and it occurs because of the defective DNA mismatch repair system. This phenotype affiliates with disease staging and improved prognosis [90].

The second most common hereditary colorectal cancer is the autosomal dominant familial adenomatous polyposis (FAP), caused by *APC* gene mutation. *APC* is a tumor suppressor protein in Wnt signaling, degrades ß-Catenin and associates with deletion in chromosome 5 [79].

MUYTH-associated polyposis is a less common autosomal recessive syndrome. Its clinical presentation resembles FAP closely, except that this syndrome have typically has less than 100 polyps. The *MUYTH* gene encodes the protein, which is part of the DNA base excision repair system which answers to oxidative stress [79].

Besides hereditary genetic disorders, which are also a predisposition for CRC, certain gene mutations are given more attention than others as they affect therapeutic decisions. *KRAS* (32%) mutations are most frequently found in CRC, followed by *TP53* (43%), *BRAF* (12%) and *PIK3CA* (12%) [91]. Figure 6 depicts the top 20 genes found in CRC.

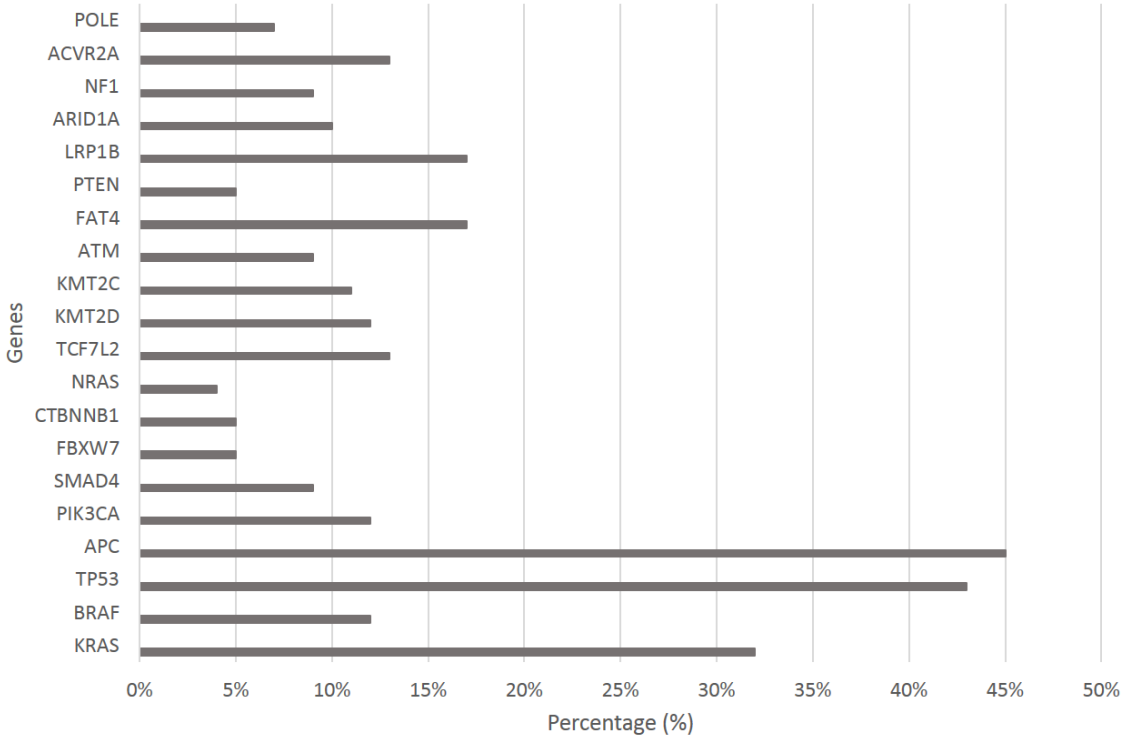

Figure 6: Top 20 colorectal cancer genes

Adapted from COSMIC [91].

5.3.3 Treatment

Total mesorectal excision (TME) is the standard operative procedure which removes rectal tumor and pararectal lymph node. TME reduces local recurrences by at least 10%. For a better overall survival rate and improvement of local recurrences, radiotherapy is combined with 5-Fluorouracil [79].

Additionally, current standard chemotherapy schemes include FOLFOX 4 (folinic acid, 5-fluorouracil, oxaliplatin), modified FOLFOX 6 (oxaliplatin, folinic acid, 5-fluorouracil) and Xelox (oxaliplatin, capecitabine) [92].

Alongside chemotherapy, a new generation of treatments including signaling inhibitors and monoclonal antibodies were introduced to target specific mechanisms. Current approved monoclonal antibodies include cetuximab, bevacizumab and panitumumab [79]. Cetuximab and panitumumab work against *epidermal growth factor receptor* (*EGFR*), which regulates tumor proliferation. Bevacizumab, on the other hand ,targets *vascular endothelial growth factor* (*VEGF*), and therefore functions as an anti-angiogenesis agent [93,94].

5.4 Melanoma

Melanoma is a malignant tumor from melanocytes (*cells that produce pigment*) which undergo tumorigenesis and turn aggressive. The melanocytes arise from neural crest, and then migrate to the skin, meninges, mucous membrane, upper esophagus and eyes [79]. Malignant melanoma, although only liable for 5% of cutaneous malignancies, is accountable for being the most lethal, and the highest number of deaths caused by cutaneous malignancies [95]. Unlike the early stages of the disease which are easily treatable, when melanoma begins to metastasize and approach advanced stages, surgery is no longer sufficient, and the disease proves to be challenging to treat [79].

In central European countries, the incidence rate of melanoma is reported as 15 to 18 cases per 100,000 people per year. The highest worldwide disease incidence rate is reported to be in Australia, with up to 60 cases in a population of 100,000 [96]. The incidence rate increment can be discussed across different ethnicities, geographical locations, ages and genders [79]. In comparison to other cancers, melanoma is known to be more common among fair-skinned Caucasian populations. This is attributed partly to a lower level of photo protection from the reduced melanin presence in melanocytes. In a darker-pigmented individual, the melanin photo barrier absorbs large amounts of Ultraviolet (UV) A and B radiation, thus reducing its penetration through skin [97]. Geographical location also plays a major role in influencing the incidence rate. As previously mentioned, the highest melanoma incidence rate is in Australia as the country lies close to the equator, thus having a higher degree of sun exposure [97].

The risk of contracting melanoma peaks when the patient is between 70 to 80 years old. The risk is much lower for patients younger than 40 years of age. However, adolescent and young adult women are more affected, and the increment of incidence in this patient group be could due to the popular tanning culture, which is associated with increased risk of cutaneous malignancy. After the age of 40, men are more susceptible to melanoma [79].

5.4.1 Melanoma staging

Melanoma skin cancer staging is defined with the five different stages of the American Joint Committee on Cancer (AJCC) TNM classification, which is also able to define a 15-year relative survival rate. The disease stage is defined after pathological analysis of biopsied tissue (T), ultrasound of regional lymphatic nodules (N) and radiological analysis of distant metastasis (M) [79] [Table 1].

Table 1: Melanoma staging (a) T category, (b) N category and (c) M category

(a)

T Category	Thickness	Ulceration/ mitoses
Tx	Primary tumor thickness cannot be assessed	Not applicable
T0	No evidence of primary tumor	Not applicable
Tis	Melanoma in situ	Not applicable
T1	≤ 1.00 mm	a: without ulceration
		b: with ulceration
T2	> 1.0-2.0 mm	a: without ulceration
		b: with ulceration
T3	> 2.0-4.0 mm	a: without ulceration
		b: with ulceration
T4	> 4.0 mm	a: without ulceration
		b: with ulceration

(b)

N Category	Amount	Nodal burden
N0	0	Not applicable
N1	1	a: micrometastases
		b: macrometastases
N2	2-3	a: micrometastases
N3	> 4	b: macrometastases
		c: in-transit metastases or satellite lesions without metastatic nodes

(c)

M Category	Anatomic site	LDH level
M0	No evidence of distant metastasis	Not applicable
M1	Evidence of distant metastasis	
M1a	Distant metastasis to skin, soft tissue including muscle, and/or non-regional lymph node	Unspecified
M1a (0)		Not elevated
M1a (1)		Elevated
M1b	Distant metastasis to lung with or without M1a sites of disease	Unspecified
M1b (0)		Not elevated
M1b (1)		Elevated
M1c	Distant metastasis to non-CNS visceral sites with or without M1a or M1b sites of disease	Unspecified
M1c (0)		Not elevated
M1c (1)		Elevated
M1d	Distant metastasis to CNS with or without M1a, M1b or M1c sites of disease	Unspecified
M1d (0)		Not elevated
M1d (1)		Elevated

CNS: central nervous system, LDH: lactate dehydrogenase.

AJCC Cancer staging based on TNM categories. Adapted from Cutaneous melanoma: ESMO Clinical Practice Guidelines for diagnosis, treatment and follow up [100].

5.4.2 Genetic landscape

Family history of the disease is a significant risk factor for melanoma. About 20% – 40% of hereditary melanoma is due to germline mutations of *Cyclin-dependent kinase inhibitor 2A (CDKN2A)* locus. This locus is responsible for the encoding of two tumor suppressor proteins: p16 and p14ARF. P14ARF inhibits p53, while p16 inhibits the CD4/6-mediated phosphorylation. Although presumed to be rare, CDK4 is also a hereditary predisposition for melanoma contraction and is located on the chromosome 12q13 [79].

Melanoma-lineage-specific oncogene *microphthalmia-associated transcription factor (MITF)* increase the tendency for the development of sporadic and hereditary melanoma. Another gene which contributes to the hereditary factor of the disease is *melanocortin-1-receptor* (MIR), for which upregulation is induced by sunlight [79].

The *RAS* pathway in melanoma has been thoroughly studied as it could provide a glimmer of hope to patients with metastatic melanoma. *RAS* and *BRAF* are part of the MAP-kinase signaling pathway and are drivers of melanoma proliferation [98]. The top mutated genes in melanoma consist of *BRAF* (41%), *NRAS* (15%), *HRAS* (11%) and *TP53* (26%) and *KIT* (7%) [Figure 7] [99]. Mutational testing is highly recommendable for patients in late stages (stage 3 to stage 4).

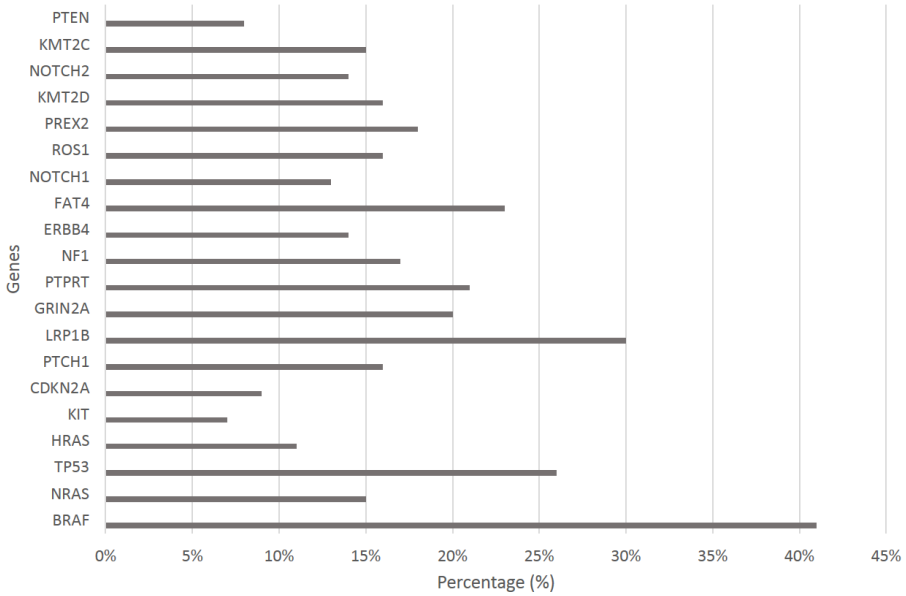

Figure 7: Top 20 genes in melanoma

Adapted from COSMIC [91].

5.4.3 Treatment

Localized diseases are treated with the wide local excision of primary tumors, and lymph node dissection. For lentigo maligna, radiotherapy is the choice of treatment. On the other hand, non-resectable tumors are addressed with systemic treatment which includes the administration of interferon-alpha (INFα) and tumor necrosis factor alpha (TNFα) [79].

Although interferon alpha (INFα) demonstrated significant improvement in disease-free survival in 14 randomized controlled trials with 8,122 patients demonstrated significant improvement in disease-free survival, its significant toxicity has confined its application to only in patients with ulcerated stage 2c or when other drugs are not accessible [100,101].

Ipilimumab is a monoclonal antibody against cytotoxic T-lymphocyte-associated antigen 4 (CTLA- 4). Based on a European Organization for Research and Treatment of Cancer (EORTC) 18071 trial, ipilimumab in comparison to placebo proved to improve the recurrence-free survival rate (median of 26.1 months versus 17.1 months) and 3-year recurrence-free survival rate of 46.5% versus 34.8% respectively [102]. However, ipilimumab presents itself with adverse reactions, including endocrinopathies and colitis, thereby, shifting the focus to other treatments, including PD-L1 inhibitors (anti-PD-L1) or dabrafenib/ trametinib [100].

Nivolumab is an anti-PD-L1 agent which promises significant recurrence-free survival benefit for late melanoma stages and reduces toxic adverse events compared to toxic ipilimumab [100]. When comparing the recurrence-free survival of patients treated with high dose ipilimumab to nivolumab, 60% of the patients were relapse-free versus 70% at 12 months, 53% versus 66% at 18 months, and 50% versus 63% at 24 months, respectively [103]. Another anti-PD-L1 agent is pembrolizumab, and both anti-PD-L1 treatments are approved in the adjuvant setting as of August and December 2018, respectively [100].

Dabrafenib/trametinib (*BRAF/MEK* inhibitor) combination therapy is the only currently approved targeted therapy used for adjuvant treatment for melanoma patients [100]. The COMBI-AD study comparing dabrafenib/trametinib combination therapy versus two placebos in fully resected high-risk stage 3 melanoma demonstrated an improved recurrence-free survival rate of 58% versus 39% at 3 years and improved overall survival of 86% versus 77%,respectively [104].

5.5 Neuroblastoma

Neuroblastoma (NB) is the most common malignant solid pediatric tumor arising from the neural crest with unpredictable clinical behaviors reflected by spontaneous regression, ganglioneuroblastoma or ganglioneuroma maturation and life-threatening progression [105]. Most infants experience complete regression with minimal therapy; however, older patients approach vigorous metastatic disease despite intensive multimodality therapy. Typically, the disease metastasizes to regional lymph nodes, bone and bone marrow. Uniquely with infants, the disease primarily spreads to the liver and skin [105].

NB is the most common extracranial childhood solid tumor, accountable for 7.2% of all cancers among children below the age of 15. The 5-year survival rate is variable and highly dependent on age and disease stage. It has been reported that survival is highest among infants and patients with local or regional disease. Older children and patients with distant metastasis have poorer survival rates. Table 2 defines the 5-year survival rate based on gender, age and stage.

Table 2: Neuroblastoma 5-year survival rate based on characteristics

5-year relative survival rate (%)	
Characteristics	**%**
Male	64
Female	65
< 1 year old at diagnosis	86
1-4 years old at diagnosis	54
5-9 years old at diagnosis	44
10-14 years old at diagnosis	61
Local and regional stages (all ages)	85
Local and regional stages (< 1 year old)	95
Local and regional stages (≥ 1 year old)	80
Distant metastatic stage (all ages)	48
Distant metastatic stage (< 1 year old)	77
Distant metastatic stage (≥ 1 year old)	34

Based on Surveillance, Epidemiology and End Results Program (SEER) registry data 1985 to 2000.

5.5.1 Neuroblastoma staging

Two systems are currently used for NB staging. The first is the International Neuroblastoma Risk Group Staging System (INRGSS). This classification utilizes results from imaging test prior to treatment. The International Neuroblastoma Staging System (INSS) is based on the extent of surgical removal of the tumor [Table 3].

The INRGSS uses image-defined risk factors and consists of 4 stages [114]:

L1: Locoregional tumor without image-defined risk factors (IDRFs)

L2: Locoregional tumor with one or more IDRFs

M: Distant metastasis

Ms: Metastasis in skin, liver, and /or bone marrow.

Table 3: The INSS classification consists of 4 stages

Tumor stage	Description
1	Localized tumor with complete gross excision, with or without microscopic residual disease. Representative ipsilateral lymph nodes negative for tumor microscopically. Nodes attached to and removed with primary tumor may be positive.
2A	Localized tumor with incomplete gross excision; ipsilateral non-adherent lymph nodes negative for tumor microscopically.
2B	Localized tumor with or without complete gross excision, with ipsilateral non-adherent lymph nodes positive for tumor. Enlarged contralateral lymph nodes must be negative microscopically.
3	Unresectable unilateral tumor infiltrating across midline, with or without regional lymph node involvement; or localized unilateral tumor with contralateral regional lymph node involvement; or midline tumor with bilateral extension by infiltration or lymph node involvement. The midline is defined as vertebral column. Tumors originating on one side and crossing the midline must infiltrate to or beyond the opposite side of the vertebral column.
4	Primary tumor with dissemination to distant lymph nodes, bone, bone marrow, liver, skin, and/or other organs.
4S	(special neuroblastoma) Localized primary tumor, as defined for stage 1, 2A or 2B with dissemination limited to skin, liver, and/or bone marrow. Age group is limited to infants younger than 12 months. Bone marrow involvement should be less than 10% of total nucleated cells identified as malignant by bone marrow biopsy or aspiration. MIBG scan should be negative for disease in bone marrow.

MIBG: metaiodobenzylguanidine

Adapted from American Cancer Society [115].

Besides both classifications mentioned above, the risk group classification for NB patients combined with the INRGSS stage of the disease is vital for the decision on treatment regimen [Table 4] [116].

Table 4: Neuroblastoma risk group classification

Risk groups	Characteristics
Low Risk	- Stage 1
Intermediate Risk	- Stage 2A or 2B, < 1 year old - Stage 2A or 2B, ≥ 1 year old, without *MYCN* amplification - Stage 2A or 2B, ≥ 1 year old, favorable histology, *MYCN* amplification - Stage 4S, < 1 year old, favorable histology without *MYCN* amplification
High Risk	- Stage 3, < 1 year old, without *MYCN* amplification - Stage 3, ≥ 1 year old, favorable histology, without *MYCN* amplification - Stage 4, < 1 year old, without *MYCN* amplification - Stage 4S, < 1 year old, unfavorable histology, without *MYCN* amplification, normal DNA ploidy
	- Stage 2A or 2B, ≥ 1 year old, unfavorable histology, *MYCN* amplification - Stage 3, < 1 year old, *MYCN* amplification - Stage 3, ≥ 1 year old, *MYCN* amplification - Stage 3, ≥ 18 months old, unfavorable histology - Stage 4, any age group, *MYCN* amplification - Stage 4, ≥ 18 months old - Stage 4, between 12 and 18 months old, unfavorable histology, *MYCN* amplification, and/or normal DNA ploidy - Stage 4S, < 1 year old, *MYCN* amplification

Favorable histology is defined by ganglioneuroma mature (stroma-dominant, ganglioneuroma maturing (stroma-dominant), ganglioneuroblastoma intermixed (stroma rich), neuroblastoma (stroma-poor), differentiating or poorly differentiated with low/intermediate mitosis-karyorrhexis index in patients < 1.5 years at diagnosis, and neuroblastoma (stroma-poor), differentiating with low mitosis-karyorrhexis index in patients 1.5 to 5 years at diagnosis.

Unfavorable histology is defined by ganglioneuroblastoma, nodular (stroma-rich/ stroma-dominant and stroma-poor) and neuroblastoma (stroma-poor)[116].

Adapted from American Cancer Society [115].

5.5.2 Genetic landscape

Neuroblastoma has a heterogenous mutation spectrum with few recurrent mutated genes and a low mutation frequency [105], which explains the broad clinical presentation and treatment response.

Hirschsprung disease-related genes (*RET, EDNRB, EDN3, GDNF, ECE1 and ZHFX1B, RET, GDNF, BDNF and PHOX2B*) have been linked to the occurrence of NB [106]. *GDNF, neurturin (NRTN), artemin (ARTN)* and *persephin (PSN)* are part of the receptor system of RET tyrosin kinase and glycosylphosphatidylinositol-anchored co-receptor (GFR alpha 1-4) [107]. Maris *et al.* reported the appearance of *hereditary neuroblastoma predisposition gene (HNB1)* on the distal short arm of chromosome 16 as an inherited disease when at least two putative familial neuroblastoma predisposition loci are reported [108].

The most frequent genes with somatic mutation frequencies in NB include *ALK* (9.2%), *PTPN11* (2.9%), *ATRX* (2.5% and 7.1% with focal deletion), *MYCN* (1.7%) and *NRAS* (9.83%) [109] [Figure 8], with *ALK, MYCN* and TERT as major NB oncogenic transformation drivers [99,110]. *Telemerase reverse transcriptase (TERT*) (31%) occur only in high risk NB and exist exclusively with *MYCN* amplification and *ATRX* mutation [111,112]. *MYCN* amplification is used as a vital biomarker used, as well as an important prognostic factor for NB. Therefore, it has also been studied for inhibition and indirect targeting. Targeting *MYCN* can be challenging due to the lack of appropriate drug-binding sites on its DNA binding domain [113].

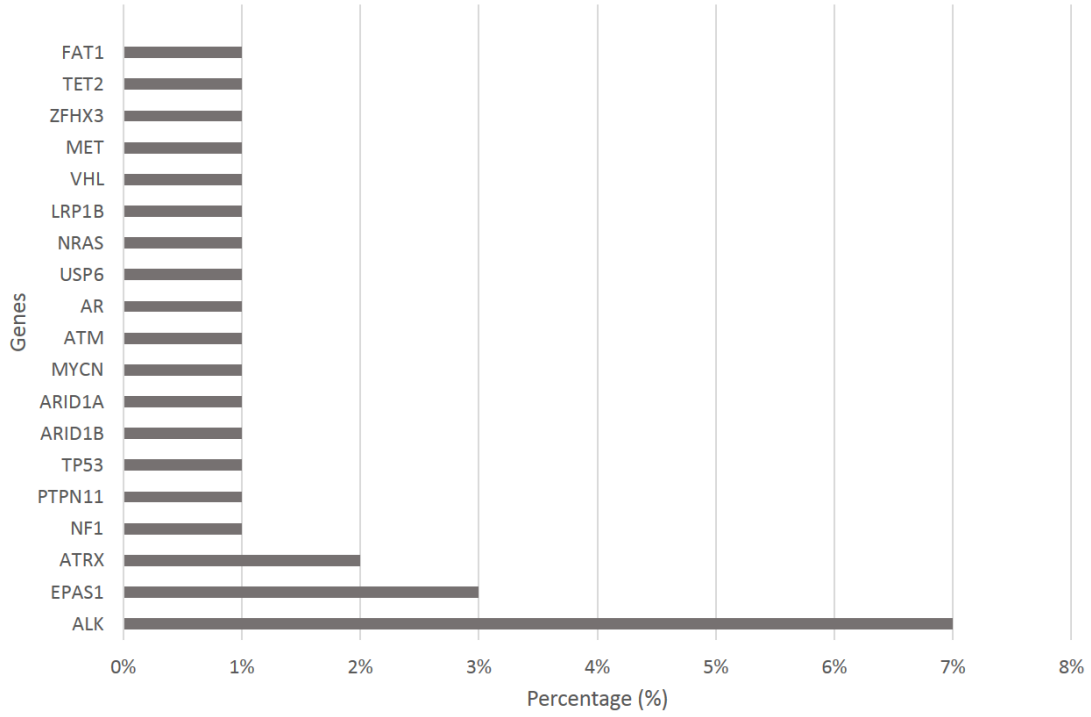

Figure 8: Top 20 genes in neuroblastoma

Adapted from COSMIC [91]

5.5.3 Treatment

Low risk NB is curable with no or minimal therapy and is associated with spontaneous regression, especially for infants. When treatment is necessary, surgical resection is a feasible option [117]. Symptomatic low-risk patients and patients classified in the intermediate risk group receive chemotherapy regimen consisting of carboplatin, cyclophosphamide, doxorubicin and etoposide [118].

High risk NB patients receive treatment in three phases: induction, consolidation and post consolidation. The induction phase includes dose-intensive cisplatin cycles and etoposide alternating with vincristine, cyclophosphamide and doxorubicin, followed by resection of the primary tumor when applicable [119].

The consolidation phase includes myeloablative chemotherapy and stem cell transplant [120]. The post consolidation phase aims to eradicate minimal residual disease after stem cell trans-

plantation. In this phase, dinutuximab is combined with granulocyte-macrophage colony stimulating factor (GM-CSF), interleukin-2 and isoretinoin and has demonstrated improved event-free survival [121].

The current most extensively studied targeted therapy in NB is the *ALK* inhibitor crizotinib. Crizotinib is FDA approved for adult *ALK*-translocated non-small cell lung cancer and is a competitive inhibitor of ALK and MET kinase activity. The usage of crizotinib was evaluated in patients with *ALK* aberrant NB and a resistance challenge appeared, which was resolved by combination with chemotherapy, topotecan and cyclophosphamide. The results of the trial demonstrated complete response 24 weeks after the end of therapy [122].

6. STUDY AIM

The work described in this thesis was concerned with the characterization of the proteomic content and morphology of the extracellular vesicles, as well as to analyze mutational signatures in the vesicles. Isolation of extracellular vesicles via differential centrifugation was first tested according to a fundamental protocol from Thèry *et al*. [4] and further optimized. Initial extracellular vesicles isolation from cell lines was then expanded to the isolation of extracellular vesicles derived from plasma and urine samples.

Western blot analysis was used to characterize proteomic content in the extracellular vesicles isolated from cell lines and plasma samples. Furthermore, transmission electron microscopy using immunogold CD63 labelling was utilized to understand the morphological structure of the vesicles.

As a significant player in liquid biopsy, mutational signatures (*KRAS, BRAF and ALK)* were detected with the novel platform Droplet Digital PCR™ (ddPCR). The ddPCR analysis of extracellular vesicles derived from plasma samples was compared to corresponding tissue samples for concordance rate. Discordant cases were evaluated to understand extracellular vesicles as potential therapy monitoring platform for patients. Also included in the study are three samples which were simultaneously analyzed for mutational signatures in cfDNA. Furthermore, multiplex ddPCR assays as a screening platform with various point mutations for *KRAS, BRAF* and *ALK* were optimized and established.

7. MATERIALS

This chapter lists various kits, chemicals and solutions, consumables, antibodies, devices, software and cell lines used when conducting experiments related to this thesis. Section 6.5 compiles components of different buffers prepared in-house for western blot analysis. Primers and probe sequences, as well as PCR conditions are listed in Section 6.8.

7.1 Commercially available kits

Kits	**Producers**
Bolt Bis-Tris 4-12% gradient gel	Thermo Fisher Scientific, Massachusetts, USA
Centricon Plus-70	Merck KGaA, Darmstadt, Germany
ExoAB antibody sampler kit	System Bioscience, California, USA
ExoRNEASY midi kit	Qiagen, Hilden, Germany
ddPCR™ Supermix for Probes (No dUTP)	Bio-Rad Laboratories, California, USA
miRNeasy Micro Kit	Qiagen, Hilden, Germany
miRCURY RNA isolation-cell & plant	Exiqon, Denmark
miRCURY RNA isolation- biofluids	Exiqon, Denmark
Pierce™ BCA Protein Assay kit	Thermo Fisher Scientific, Massachusetts, USA
Promokine PCR Mycoplasma Test Kit I/C	PromoCell GmbH, Heidelberg, Germany
Repli-G WTA single cell	Qiagen, Hilden, Germany
RNA clean and concentrator	Zymo Research, California, USA
RNeasy mini kit	Qiagen, Hilden, Germany
QuantiTect Reverse Transcription Kit	Qiagen, Hilden, Germany

7.2 Chemicals and solutions

Chemicals and Solutions	Producers
Advanced DMEM	Thermo Fisher Scientific, Massachusetts, USA
Advanced RPMI 1640	Thermo Fisher Scientific, Massachusetts, USA
Bolt™ 4-12% Bis-Tris Plus gels	Thermo Fisher Scientific, Massachusetts, USA
BSA (Bovine Serum albumin)	Thermo Fisher Scientific, Massachusetts, USA
Chloroform	Carl Roth, Karlsruhe, Germany
DDPCR™ Buffer control for Probes	Bio-Rad Laboratories, California, USA
DMEM (Dulbecco's Modified Eagle Medium)	Thermo Fisher Scientific, Massachusetts, USA
Dulbecco's PBS	Life Technologies, California, USA
Ethanol	Carl Roth, Karlsruhe, Germany
Fetal bovine serum (FBS)	Thermo Fisher Scientific, Massachusetts, USA
Glycine	Sigma-Aldrich, Munich, Germany
Halt™ Protease inhibitor cocktail	Thermo Fisher Scientific, Massachusetts, USA
Isopropanol	Carl Roth, Karlsruhe, Germany
L-Alanyl-Glutamine 200 mM	Biochrom, Berlin, Germany
Lithium dodecyl sulfate (LDS)	Thermo Fisher Scientific, Massachusetts, USA
MEM Non-essential amino acid	Thermo Fisher Scientific, Massachusetts, USA
Methanol	Carl Roth, Karlsruhe, Germany
MOPS	Carl Roth, Karlsruhe, Germany
NaCl	Merck Group, Darmstadt, Germany
Na Deoxycholate	Sigma-Aldrich, Munich, Germany
Nuclease-free water	Thermo Fisher Scientific, Massachusetts, USA
Non-essential amino acid (100x)	Life Technologies, California, USA
Non-fat dried milk powder	Applichem, Darmstadt, Germany
Page Ruler prestained™ protein ladder	Thermo Fisher Scientific, Massachusetts, USA
Penicillin/Streptomycin	Thermo Fisher Scientific, Massachusetts, USA
Pierce™ ECL Plus western blotting substrate	Thermo Fisher Scientific, Massachusetts, USA
Reduction Agent	Thermo Fisher Scientific, Massachusetts, USA
RPMI 1640	Thermo Fisher Scientific, Massachusetts, USA
SDS page	Promega, Wisconsin, USA
Streptomycin/ penicillin (200 U/mL)	Thermo Fisher Scientific, Massachusetts, USA
Transfer membrane, PVDF	Sigma-Aldrich, Munich, Germany
Tris/HCL pH 7.2-7.4	Carl Roth, Karlsruhe, Germany

Chemicals and Solutions	Producers
Triton X-100	Sigma-Aldrich, Munich, Germany
Trypsin 0.25% EDTA	Sigma-Aldrich, Munich, Germany
Tween-20	Carl Roth, Karlsruhe, Germany

7.3 Consumables

Consumables	Producers
10 ml Open-Top Thickwall Polycarbonate tube	Beckman Coulter, California, USA

7.4 Antibodies

Antibodies	Producers
CD63 unconjugated	Bio-Rad Laboratories, California, USA
GM130/ Golga 2 (1:1000)	System bioscience, California, USA

7.5 Devices

Devices	Producers
CO^2 cell culture incubator	Binder, Tuttlingen, Germany
Electric weighing scale	Kern und Sohn GmbH, Balingen. Germany
Li-Cor odyssey imaging system	Li-Cor, Nebraska, USA
Mini Gel Tank	Thermo Scientific, Massachusetts, USA
Mini Trans-Blot® Cell	Bio-Rad Laboratories, California, USA
pH meter	Fisher Scientific, Massachusetts, USA
PHO Mo microplate reader	Autobio, Zhengzhou, China
PowerPac Universal Power Supply	Bio-Rad Laboratories, California, USA
PowerPRO 300 Power Supply	Cleaver scientific, Warwickshire, UK
Proscan 2K, Slow-Scan CCD-Camera	Zeiss, Oberkochen, Germany
Sorvall Discovery 90 SE ultracentrifuge	Thermo Scientific, Massachusetts, USA
T-100 Thermal cycler	Bio-Rad Laboratories, California, USA
T1270 ultracentrifuge rotor	Thermo Scientific, Massachusetts, USA
QX200 droplet generator	Bio-Rad Laboratories, California, USA
QX200 droplet reader	Bio-Rad Laboratories, California, USA
Zeiss transmission electron microscope	Zeiss, Oberkochen, Germany

7.6 Software

Software	Producers
iTEM Olympus	Olympus, Tokyo, Japan
QuantaSoft™ version 1.7.4	Bio-Rad, California, USA
Microsoft Excel	Microsoft, Washington, USA

7.7 Buffers and solutions

Transfer buffer		**Tris buffered saline (TBS)**	
10x stock solution		10x stock solution	
288 g	Glycine	60.6 g	Tris
60.56 g	Tris	87.6 g	NaCL
20%	SDS	1 M	HCl (for pH adjustment)
20%	Methanol	1L	$_dH_2O$
20x MOPS running buffer		**TBST**	
209.2 g	MOPS	1x solution	
121 g	Tris	100 mL	10x TBS
100 ml	20% SDS	900 mL	$_dH_2O$
41 ml	0.5 M EDTA	1000 µl	Tween 20
RIPA buffer		**EDTA 0.5 M (pH 8.0)**	
50 mM	Tris/HCL pH 7.2- 7.4	186.1 g	Disodium EDTA 2 H_2O
150 mM	NaCl	800 ml	$_dH_2O$
0.1%	SDS		
1%	Na Deoxycholat		
1%	Triton X 100		

7.8 Primers and probes

Primers/ Probes	Sequences (5'-3')	Annealing Temp.	Conc.	Amplicon length
	DDPCR Duplex Assays			
KRAS (old)				
FWD	TTTCGGACTGGGAGCGA	61°C	900 nm	170 bp
REV	CTGAATTAGCTGTATCGTCAA		900 nm	
KRAS				
FWD	CCAGGTGCGGGAGAGAG		900 nm	
REV	TGCCTTGACGATACAGCTAA		900 nm	
WT	HEX-TGTGGTAGTTGGAGCTGGTGGC-BHQ-1		250 nm	
G12A	FAM-TGTGGTAGTTGGAGCTGCTGGC-BHQ-1	59 °C	250 nm	98 bp
G12C	FAM-TGTGGTAGTTGGAGCTTGTGGC-BHQ-1	59 °C	250 nm	
G12D	FAM-TGTGGTAGTTGGAGCTGGTGGC-BHQ-1	59 °C	450 nm	
G12V	FAM-TGTGGTAGTTGGAGCTGTTGGC-BHQ-1	60 °C	450 nm	
G13D	FAM-TGTGGTAGTTGGAGCTGGTGAC-BHQ-1	60 °C	450 nm	
BRAF				
FWD	TTCATGAAGACCTCACAGTAAA		900 nm	
REV	TTTGTGGATGGCACCAG		900 nm	
WT	HEX-TTTGGTCTAGCTACAGTGAAATCTCG-BHQ-1		250 nm	
V600E	FAM-TTTGGTCTAGCTACAGAGAAATCTCG-BHQ-1	61°C	350 nm	98 bp
V600K	FAM-TTTGGTCTAGCTACAAAGAAATCTCG-Z/IB	58°C	400 nm	
ALK F1174L				
FWD	GGACGAACTGGATTTCCTCAT		900 nm	
REV	GTGAGCCTGCAATCCCTG		900 nm	96 bp
WT	HEX-CAGCAAATTCAACCACCAGAACAT-BHQ-1		400 nm	
F1174L	FAM-CAGCAAATTAAACCACCAGAACAT-BHQ-1	59°C	400 nm	
ALK R1275Q				
FWD	CTGGAAGAGTGGCCAAGAT		900 nm	
REV	ATAGAAAGGGAGGCTGTGC		900 nm	82 bp
WT	HEX-CCGAGACATCTACAGGGCGAGCTA-Z/IB		350 nm	
R1275Q	FAM-CCAAGACATCTACAGGGCGAGCTA-Z/IB	61°C	350 nm	

FWD: forward, REV: reverse, WT: wild-type, Temp.: Temperature, Conc.: concentration

Primers/ Probes	Sequences (5'-3')	Annealing Temp.	Conc.	Amplicon length
	DDPCR Multiplex Assays			
KRAS Multiplex				
FWD	CCAGGTGCGGGAGAGAG		900 nm	
REV	TGCCTTGACGATACAGCTAA		900 nm	
WT	HEX-TGTGGTAGTTGGAGCTGGTGGC-BHQ-1		250 nm	
G12A	FAM-TGTGGTAGTTGGAGCTGCTGGC-BHQ-1	59°C	350 nm	98 bp
G12D	FAM-TGTGGTAGTTGGAGCTGGTGGC-BHQ-1		450 nm	
G12V	FAM-TGTGGTAGTTGGAGCTGTTGGC-BHQ-1		250 nm	
BRAF Multiplex				
FWD	TTCATGAAGACCTCACAGTAAA		900 nm	
REV	TTTGTGGATGGCACCAG		900 nm	
WT	HEX-TTTGGTCTAGCTACAGTGAAATCTCG-BHQ-1	60°C	250 nm	98 bp
V600E	FAM-TTTGGTCTAGCTACAGAGAAATCTCG-BHQ-1		250 nm	
V600K	FAM-TTTGGTCTAGCTACAAAGAAATCTCG-Z/IB		500 nm	
ALK Multiplex				
ALK F1174L				
FWD	GGACGAACTGGATTTCCTCAT		900 nm	
REV	GTGAGCCTGCAATCCCTG		900 nm	
WT	HEX-CAGCAAATTCAACCACCAGAACAT-BHQ-1		250 nm	
F1174L	FAM-CAGCAAATTAAACCACCAGAACAT-BHQ-1		250 nm	
ALK R1275Q		60°C		96 bp
FWD	CTGGAAGAGTGGCCAAGAT		900 nm	
REV	ATAGAAAGGGAGGCTGTGC		900 nm	
WT	HEX-CCGAGACATCTACAGGGCGAGCTA-Z/IB		350 nm	
R1275Q	FAM-CCAAGACATCTACAGGGCGAGCTA-Z/IB		350 nm	

FWD: forward, REV: reverse, WT: wild-type, Temp.: temperature, Conc.: concentration

7.9 Human-derived cell lines

RRID[1]	Cell line	Disease[1]	Gene mutation	Medium	Source
CVCL_9529	CLB-Ga	Neuroblastoma	*ALK* ^{F1174L}	DMEM	AG Deubzer
CVCL_0291	HCT 116	Colon carcinoma	*KRAS* ^{G13D}	RPMI-1640	DSMZ
CVCL_0030	HELA	Endocervical adenocarcinoma	Wild-type	DMEM	DSMZ
CVCL_1303	IGR-1	Groin lymph node Melanoma	*BRAF* ^{V600K}	DMEM	DSMZ
CVCL_0346	IMR-32	Neuroblastoma	Wild-type	DMEM	AG Deubzer
CVCL_2092	Kelly	Neuroblastoma	*ALK* ^{R1275Q}	RPMI-1640	AG Deubzer
CVCL_1384	LS174T	Colon adenocarcinoma	*KRAS* ^{G12D}	RPMI-1640	Sigma-Aldrich
CVCL_0428	MIA PaCa-2	Pancreatic ductal adenocarcinoma	*KRAS* ^{G12C}	DMEM	ATCC
CVCL_0041	RPMI-8226	Plasma cell myeloma	*KRAS* ^{G12A}	RPMI-1640	DSMZ
CVCL_0526	SK-MEL-28	Cutaneous melanoma	*BRAF* ^{V600E}	RPMI-1640	ATCC

All cell lines were authenticated by single nucleotide polymorphism profiling by Multiplexion GmbH (Friedrichshafen, Germany) and tested negative for mycoplasma.

DMEM: Dulbecco's Modified Eagle Medium, RPMI: Roswell Park Memorial Institute, DSMZ: German Collection of Microorganisms and Cell Cultures (Braunschweig, Germany), Sigma-Aldrich (Merck KGaA, Darmstadt, Germany), ATCC: American Type Culture Collection (Manassas, USA), RRID: Resource Identification Initiative[1].

[1] Artimo P, Jonnalagedda M, Arnold K, Baratin D, Csardi G, de Castro E, Duvaud S, Flegel V, Fortier A, Gasteiger E, Grosdidier A, Hernandez C, Ioannidis V, Kuznetsov D, Liechti R, Moretti S, Mostaguir K, Redaschi N, Rossier G, Xenarios I, and Stockinger H. ExPASy: SIB bioinformatic resource portal, Nucleic Acids Res, 40(W1):W597-W603, 2012.

8. METHODS

Most methods from section 7 have been published in:

Analysis of cancer related mutations in extracellular vesicles RNA by Droplet Digital PCR.

Yap S.A., Münster-Wandowski A., Nonnenmacher A., Keilholz U., Liebs S.

BioTechniques Journal, 25 June 2020.

8.1 Patient materials

8.1.1 Patient samples

Four NB patients, thirteen advanced CRC and eighteen MM patients were enrolled in our study from the Department of Oncology and Hematology, the Skin Tumor Center and the Department of Pediatrics, Division of Oncology and Hematology of the Charité Medical University. Among the thirty-five samples, three patients originated from the OncoTrack project and were recruited from the Charité and the Medical University Graz [124]. All patients consented for blood donation. The study was approved by the ethics committee from of both Charité University Medicine (EA1/069/11, EA4/090/08, EA4/063/13, NB2004 and NB2016) and Medical University Graz (23-015 ex 10/11).

Peripheral blood from patients was collected in BD Vacutainer® EDTA tubes (BD, Franklin Lakes, USA). For urine analysis, 10 milliliters of urine from NB patients were collected in BD Vacutainer® Plus urinalysis tubes (BD, Franklin Lakes, USA).

8.1.2 Patient demographics

Thirteen advanced CRC patients, all of whom were characterized as American Joint Committee on Cancer (AJCC) stage 4, were recruited into our study. Among the patients, eleven were male and two were female, with a median age of 59. Five patients were diagnosed with right-sided colon cancer while five patients were diagnosed with left-sided colon cancer. Three patients were diagnosed with rectal cancer. Based on the patients' database, seven patients were profiled with *KRAS* mutation and six with *KRAS* wild type. Furthermore, three patients underwent therapy with cetuximab, and three with FOLFOX. Combination therapy of FOLFOX and bevacizumab was prescribed to six patients, whereas one patient received a combination of FOLFOX, bevacizumab and panitumumab.

Eighteen MM patients were recruited into our study. Among the patients, twelve were male and six were female with the median age of 54. The patient cohort varied in stages. Tumor tissues from 13 patients were profiled to be *BRAF* positive and for 5 patients with *BRAF* wild type. Moreover, two patients received nivolumab and seven patients received a combination of nivolumab

and ipilimumab. Two patients were treated with *MEK* inhibitor and seven patients were treated with combination of *BRAF/MEK* inhibitor.

NB patients ranged from ages 3 to 5 and belonged to the high-risk groups. Three patients were diagnosed with the primary tumor in the adrenal gland and one patient with the primary tumor located in retroperitoneal and intraabdominal cavity. All patients had an increment in tumor marker neuron-specific enolase (NSE), and in three patients there was also an increment in homovanillic acid and vanillylmandelic acid in urine. All patients received NB 5 (valenzen, vindesin, etoposid and cisplatin) and NB 6 (vincristin, dacarbazin, ifosfamid and doxorubicin) block therapies and anti-GD2 antibody (dinutuximub), while two patients underwent debulking surgery. One of four patients eventually received palliative anti-GD2 therapy and unfortunately passed away during the course of our study. Patient demographics are listed in Table 5.

Table 5: Demographics, clinical characterization, and therapy information of participants for (a) colorectal cancer (b) melanoma and (c) neuroblastoma

(a)

Colorectal cancer (CRC)	
Total patients (n =13)	Number
Gender	
Male	11
Female	2
Age	59 (median)
Localization	
Right-sided colon cancer	5
Left-sided colon cancer	5
Rectum	3
AJCC	
1	0
2	0
3	0
4	13
KRAS MUT	7
KRAS WT	6
Therapy	
cetuximab	3
FOLFOX + cetuximab	3
FOLFOX + bevacizumab	6
FOLFOX + bevacizumab + panitumumab	1

(b)

Melanoma (MM)	
Total patients (n= 18)	Number
Gender	
Male	12
Female	6
Age	54 (median)
Stage	
1	2
2	0
3	3
4	13
BRAF MUT	13
BRAF WT	5
Therapy	
nivolumab	2
nivolumab/ipilimumab	7
MEK inhibitor	2
BRAF + *MEK* inhibitor	7

(c)

Neuroblastoma (NB) Total patients (n = 4)	Number
Gender	
Male	2
Female	2
Age	4 (median)
Localization	
Adrenal gland	3
Retroperitoneal,	1
Abdominal cavity	
Risk groups	
Low	0
Intermediate	0
High	4
Stage (INSS)	
1	0
2	0
3	0
4	4
Tumor markers	
NSE	4
Homovanillic acid	3
Vanillylmandelic acid	3
MYCN amplification	3
ALK ^{F1174L}	2
Therapy	
NB 5	4
NB 6	4
Anti-GD 2 antibody	4

INSS: international neuroblastoma staging system
NSE: neuron-specific enolase
NB 5: valenzen, vindesin, etoposid, cisplatin
NB 6: vincristin, dacarbazin, ifosfamid, doxorubicin

8.2 Cell culture

8.2.1 Human-derived cell line cultivation and extracellular vesicle production

The validation of cell lines was carried out with single nucleotide polymorphism profiling by Multiplexion GmbH (Friedrichshafen, Germany). Prior to culturing cells for EV harvesting, the cell lines were tested negative for mycoplasma using the Promokine PCR Mycoplasma Test KIT I/C based on the manufacturer's instructions (PromoCell GmbH, Heidelberg, Germany). Cells were cultured in the respective medium listed in Section 5.8 and maintained at 37°C and 5% CO_2. All cell lines were supplemented with 1% penicillin/streptomycin (Gibco®, Thermo Fisher Scientific, Massachusetts, USA) and 2% L-glutamine (Gibco®, Thermo Fisher Scientific, Massachusetts, USA). The NB cell line Kelly was additionally supplemented with 1% MEM non-essential amino acid (NEAA) (Thermo Fisher Scientific, Massachusetts, USA).

Isolated EV were cultured from the corresponding cell lines: SK-MEL-28, IGR-1, RPMI 8226, MIA PaCa-2, LS174T, SW480, HCT 116, Kelly and CLB-Ga, which express mutations of *BRAF* $^{V600E/K}$, *KRAS* $^{G12A/C/D/V}$, *KRAS* ^{G13D} and *ALK* $^{F1174L/R1275Q}$, respectively (ref: Section 5.8). Cells were seeded in TC-treated cell culture dishes (Eppendorf, Hamburg, Germany) until 80% confluent, thn the primary fetal bovine serum (FBS) was then removed by rinsing adherent cells twice with PBS and recultured with Advanced DMEM or Advanced RPMI (Thermo Fischer Scientific, Massachusetts, USA) without FBS.

8.2.2 Extracellular vesicles isolation from cell lines

EV-rich supernatant was harvested after 48 hours of incubation at 37°C and 5% CO_2. The remaining cells were pelleted at 2,000 x g for 20 minutes at 4°C and the supernatant was filtered with a 0.22 µM cellulose acetate filter (Merck, Darmstadt, Germany) to remove larger particles. The supernatant was concentrated with the Centricon Plus-70 Filter (Merck, Darmstadt, Germany) following the supplier's instructions. The concentrated samples were filtered again, followed by two cycles of ultracentrifugation at 100,000 x g the first round for 70 minutes and the second round

for 60 minutes at 4°C as shown in Figure 9(a) in thickwall polycarbonate tubes. This was conducted with the Sorvall Discovery 90 SE ultracentrifuge and a T-1270 fixed angle titanium rotor (Thermo Scientific, Massachusetts, USA).

8.2.3 Extracellular vesicles isolation from plasma samples

Whole blood samples were centrifuged at 1,811 x g for 7 minutes and 3,060 x g for 10 minutes at room temperature. Plasma was stored in DNA low-binding 1.5 ml tubes (Eppendorf, Hamburg, Germany) at -80°C until further processing. One milliliter of plasma was thawed at room temperature and resuspended with 1x PBS to isolate EV via serial centrifugation as shown in Figure 9(b). The resuspended plasma was centrifuged twice at 4°C and the pellet was discarded in both steps: 3,000 x g for 5 minutes and 10,000 x g for 20 minutes. The supernatant was then subjected to two rounds of ultracentrifugation at 100,000 x g for 2 hours at 4°C in thickwall polycarbonate tubes, followed by filtration of the supernatant with a 0.22 µm cellulose acetate filter before proceeding with a second round of ultracentrifugation at 100,000 x g for 70 minutes.

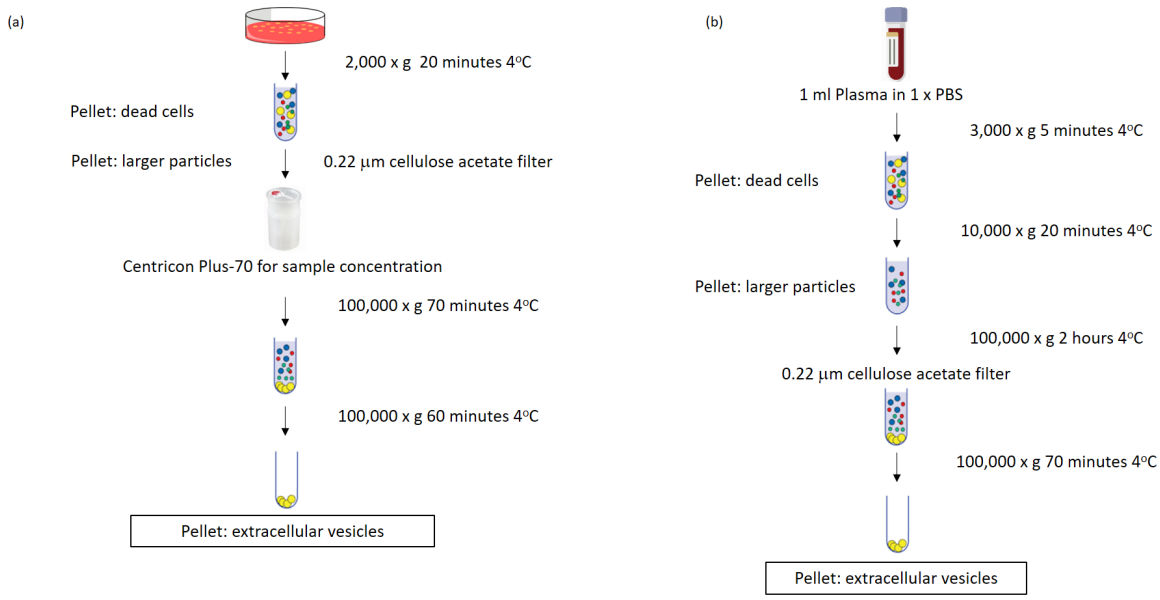

Figure 9: Extracellular vesicles isolation from human-derived cell lines and plasma samples

(a) The cell line supernatant was centrifuged at 2,000 x g for 20 minutes before filtering with the 0.22 µm cellulose acetate filter. The filtered supernatant was concentrated with Centricon Plus-70 before undergoing two rounds of ultracentrifugation to pellet extracellular vesicles.

(b) One millimeter of plasma was diluted with 1x PBS and centrifuged twice at 3,000 x g for 5 minutes, followed by 10,000 x g for 20 minutes to pellet dead cells and larger particles. The Resuspended pellet was filtered once with 0.22 µm cellulose acetate filter in between the two ultracentrifugation cycles.

8.2.4 Extracellular vesicles isolation from urine samples

Ten milliliters of urine was collected in BD Vacutainer® Plus urinalysis tubes (BD, Franklin Lakes, USA) from NB patients. Prior to storing at -80°C, 1x Halt™ Protease Inhibitor Cocktail (Thermo Scientific, Massachusetts, USA) was added to the urine samples when intended for proteomic characterization. Urine samples used for other analyses were stored at -80°C without additives until further processing. The urine samples were thawed at room temperature followed by 5 minutes of vortexing and subjected to serial centrifugation at 4°C: 2,000 x g for 10 minutes, 17,000 x g for 45 minutes and 200,000 x g for 65 minutes in thickwall polycarbonate tubes. Dithiothreitol (DTT) (200 mg/ml) (Carl Roth, Karlsruhe, Germany) was used to resuspend the EV pellet to rid samples of Tamm-Horsfall protein (uromodulin). The suspended sample was then subjected to a final round of ultracentrifugation at 200,000 x g for 65 minutes at 4°C [Figure 10].

When used for transmission electron microscopic (TEM) analysis, the EV pellet was resuspended in 20 µl of PBS. EV used for western blot (WB) analysis were immediately lysed with RIPA buffer before storage at -80°C, and for mutational analysis, EV-RNA was immediately isolated prior to storage in -80°C.

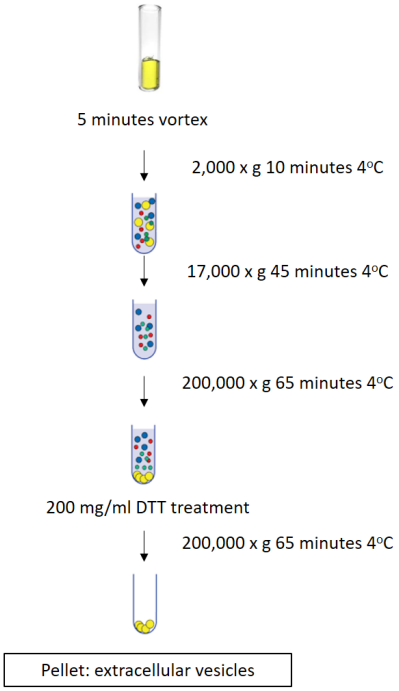

Figure 10: Extracellular vesicles isolation from urine samples

Extracellular vesicles derived from 10 millimeters of urine samples were isolated via differential centrifugation. Prior to the final ultracentrifugation step, 200 mg/ml of DTT were added to rid the sample of Tamm-Horsfall protein.

8.3 RNA isolation and cDNA synthesis from cell lines

Ribonucleic acid (RNA) was isolated from cell lines with the commercial kit RNeasy Mini Kit (Qiagen, Hilden, Germany) based on the manufacturer's instructions. This was followed by cDNA synthesis and gDNA removal with a QuantiTect Reverse Transcription Kit (Qiagen, Hilden, Germany) following the manufacturer's instructions.

8.4 Extracellular vesicles-RNA isolation

EV-RNA was isolated immediately after EV isolation using the miRCURY RNA Isolation Kit-Cell & Plants (Exiqon, Denmark) for cell line-derived EV and the miRCURY RNA Isolation Kit-Biofluids (Exiqon, Denmark) for EV derived from plasma. MiRneasy Micro Kit (Qiagen, Hilden, Germany) was used as a substitution for the remaininghalf of the samples, due to the discontinuation of both kits from Exiqon. EV-RNA was isolated according to slightly modified manufacturer's instructions. DNase (1U/µl) (Thermo Scientific, Massachusetts, USA) was added to the RNA samples to

rid the sample of possible DNA contamination. The samples were cleaned and concentrated with the RNA clean & concentrator kit (Zymo Research, California, USA) and eluted in 10 µl nuclease-free DEPC treated water (Carl Roth, Karlsruhe, Germany) based on the manufacturer's instructions. EV-RNA was stored in -80°C until further usage.

8.5 Whole transcriptome amplification

Whole transcriptome amplification (WTA) was performed with REPLI-g WTA kit (Qiagen, Hilden, Germany) according to supplier's instructions. EV-RNA were converted into cDNA and amplified, resulting in 19 µl amplified cDNA. Samples were purified, concentrated with the RNA Clean & Concentrator™-5 kit (Zymo Research, California, USA) and eluted in 30 µl nuclease-free DEPC treated water (Carl Roth, Karlsruhe, Germany) based on the manufacturer's proposition.

8.6 Whole mount immunoelectron microscopy

EV pellets were fixed and deposited on Formvar carbon-coated (Plano, Wetzlar, Germany) glow-discharged (MED020, Leica) nickel grids. The grids were washed in PBS and incubated in a blocking buffer containing 1% bovine serum albumin (BSA, Sigma-Aldrich, Darmstadt, Germany) in PBS. Subsequently, the grids were exposed to primary antibody CD63 produced in mouse (Bio-Rad, California, USA) for one hour and secondary antibody goat anti-mouse IgG conjugated to 5 nm gold particles (Plano, Wetzlar, Germany) for 30 minutes. The grids were stained with 2% phosphotungstic acid (PTA, Sigma-Aldrich, Darmstadt, Germany), pH = 7.0, for 10 minutes, before transferring to a mixture of 2% methyl-cellulose with 4% uranyl acetate (Merck, Darmstadt, Germany) for 10 minutes on ice. Stainless steel loops were used to remove grids. The excess fluid was gently blotted on Whatman Grade 1 qualitative cellulose filter paper (Merck, Darmstadt, Germany) and the grids were left to dry. The analysis was carried out with a Zeiss transmission electron microscope 912 equipped with a digital camera (Proscan 2K, Slow-Scan CCD-Camera, Zeiss, Oberkochen, Germany). Image analysis was carried out with iTEM Olympus software. For negative controls, the primary antibodies were omitted. Microscopic analyzation and data interpretation was kindly performed by Dr. Münster-Wandowski and technical assistant Heike Heilmann (Institute of Integrative Neuroanatomy, Charité Universitätsmedizin Berlin).

8.7 Western blot

When collecting cell culture supernatant for EV isolation,the cells were harvested to be used as controls for all western blot analysis. EV pellets and cells were homogenized in RIPA lysis buffer (ref: Section 5.4), supplemented with Protease Inhibitor Cocktail (Thermo Scientific, Massachusetts, USA) and boiled for 95°C for 10 minutes. The Pierce™ BCA Protein Assay Kit (Thermo Scientific, Massachusetts, USA) was used for quantification of total protein following the manufacturer's instructions and analyzed with a PHO Mo microplate reader (Autobio, Zhengzhou, China). Twenty micrograms of protein and 5 µl of PageRuler™ Prestained Protein Ladder (Thermo Fisher Scientific, Massachusetts, USA) were loaded in 4-15% gradient Mini Protean® TGX™ Precast Gels (Bio-Rad, California, USA). The western blot was performed with MOPS running buffer (ref: Section 5.4) in the Mini Gel Tank (Thermo Scientific, Massachusetts, USA). The electrophoresis ran first at 75 V for 15 minutes to separate the bands and continued at 120 V for 60 minutes.

The proteins were electrophoretically transferred to polyvinylidene difluoride membranes (PVDF) with the Trans-Blot® tank blot system (Bio-Rad, California, USA) at 300 mA for one hour. The membrane was blocked in 5% BSA in TBST (0.1% Tween-20) for one hour, before overnight incubation with exosomal antibodies against CD9 (1:1000 dilution) (Exiqon, Denmark), CD81 (1:500 dilution) (Exiqon, Denmark) and non-exosomal antibody GM130 (1:1000 dilution) (System Bioscience, California, USA), followed by a one hour incubation with the secondary antibody. All antibodies were diluted with 5% BSA in TBST (ref: Section 5.4). Protein bands were detected by enhanced chemiluminescences using Pierce™ ECL Plus Western Blotting Substrate (Thermo Scientific, Massachusetts, USA) and visualized via Li-Cor Odyssey Imaging System (Li-Cor, Nebraska, USA). Western blot analysis was repeated once.

8.8 Designing primers and probes

Primers and probes for ddPCR assays were designed using Primer blast [125]. The important criteria taken into consideration when designing primers were: including GC content of 50 to 60%, the primer melting temperature being between 50 and 65°C, avoidance of Gs and Cs repetitions longer than 3 bases, placement of Gs and Cs at the 3'-end of primers, and avoidance of secondary

structure or primer-dimers. All primers used in the ddPCR assays for EV analysis were smaller than 100 based-pairs [126].

When the probes were designed, the following parameters were considered: the sequence should lie in between the amplicons of both primers, the probes melting temperature ranged from 3 to 10°C above that of the primers, GC content of 30 to 80°C, and avoidance of G nucleotide at the 5'-end of the probes. All probes were labeled with Black Hole Quencher (BHQ1) at 3'-end of the sequences, except for *BRAF* ^{V600K} and *ALK* ^{R1275Q} wild-type and mutated probes, which were labeled with a Zen™/Iowa Black™ (Z/IB) quencher [126,127]. Furthermore, mutant probes were labeled with FAM reporter dyes, while wild-type probes were labeled with HEX reporter dyes at the 5'-end of the probes to enable analyzation in the two-color detection system.

All primers and probes were resuspended in nuclease-free DEPC treated water (Carl Roth, Karlsruhe, Germany), allocated in Eppendorf 1.5 ml tubes (Eppendorf, Hamburg, Germany) to avoid repetitive freeze-thaw cycles and stored at -20°C until used. Primers and probes sequences are listed in Section 7.8.

8.9 Droplet digital polymerase chain reaction (ddPCR)

Two microliters of cDNA and twenty microliters of total reaction volume, consisting of primers, wild-type (WT) and mutation (MUT) probes and ddPCR Supermix for Probes (no dUTP) were prepared in Eppendorf 1.5 ml tubes (Eppendorf, Hamburg, Germany). Twenty microliters of PCR reaction was then transferred into the middle row of a DG 8™ Cartridges for QX200™ Droplet generator (Bio-Rad, California, USA), and 70 µl of droplet generation oil (Bio-Rad, California, USA) into the bottom wells of the DG8™ Cartridges (Bio-Rad, California, USA). Unused wells in the cartridges were filled with 1x ddPCR buffer control (Bio-Rad, California, USA). A gasket (Bio-Rad, California, USA) was then attached across the top of the DG8™ Cartridges (Bio-Rad, California, USA) before placing them into the QX200 droplet generator [Figure 11]. Droplet-partitioned samples were transferred to a 96-well plate using a Rainin Pipet-Lite multi pipette L8-200 XLS+ (Mettler Toledo, Ohio, USA) and VWR pipette tips (Avantor, Pennsylvania, USA) to ensure a smooth transfer of the droplets.

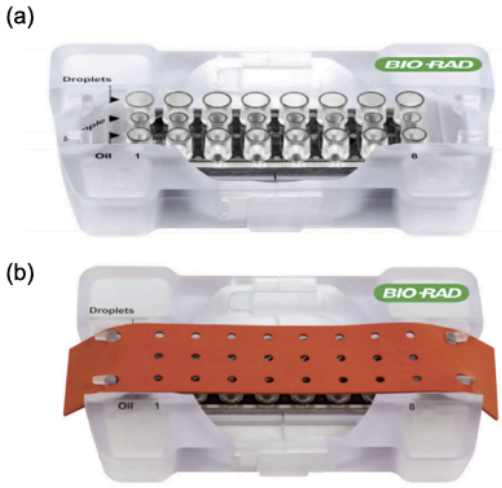

Figure 11: Bio-Rad DG8 cartridges

(a) The bottom row of the cartridge is filled with droplet generation oil and samples are pipetted into the middle row. Top wells contained generated droplets.
(b) Prior to placing the cartridge into the QX200 droplet generator, a gasket is placed over the plastic cartridge. Adapted from Bio-Rad Droplet Digital™ PCR applications guide [126].

PCR was performed with a T-100 Thermal cycler (Bio-Rad, California, USA) with the following protocol: 95°c for 10 minutes, followed by 40 cycles of 94°C for 30 seconds, 61°C (annealing temperature) for 1 minute and 98°C for 10 minutes. The annealing temperature varied in regards to different mutation assays. The primer and probe sequences and PCR conditions are listed in Section 7.8. DDPCR samples were analyzed as duplicates in the FAM (MUT) and HEX (WT) channels using the QX200™ Droplet Reader (Bio-Rad, California, USA). For the optimization of the ddPCR assays, cDNA from cell lines were used. Each ddPCR run included non-template control: PCR water (Carl Roth, Karlsruhe, Germany), cDNA from cell lines and the finalized mutation assays were repeated as triplicates. Prior to analysis on patient samples, EV derived from the cell lines were utilized to validate mutational detection.

DDPCR assays were optimized first as a singleplex, using only one probe at the concentration of 250 nm and a thermal gradient cycling program with an annealing temperature between 56°C to 63°C for 1 minute. The thermal gradient ddPCR was repeated as duplex with both wild-type and mutant probes, followed by testing of various probe concentrations (250 nm, 350 nm, 450 nm) to secure the ideal annealing temperature and probe concentration of both wild-type and mutant probes.

The false positive rate (FPR) was validated for each assay. Prior to running FPR experiments, serial dilution of wild-type derived cDNA was carried out to estimate the concentration of sample input

accountable for 500 copies/µl and 100 copies/µl of wild-type derived cDNA. Once confirmed, assays consisting of eight wells of non-template control, four wells of 500 copies/µl of wild-type cDNA and four wells of 100 copies/µl of wild-type cDNA were cycled.

Due to the intention to detect rare mutations, verifying limit of detection (LOD) was important to ensure the assay's sensitivity. Similarly to the preparation for FPR experiments, serial dilution of mutant-derived cDNA was carried out to estimate sample input concentration accountable for 100, 10, 1, 0.1 and 0.01 copies/µl. The assays were then analyzed with 10-fold serially diluted mutant-derived cDNA in a background of constant wild-type derived cDNA (100 copies/µl).This assay was also simultaneously used to estimate the WT/MUT ratio to identify the performance of the primers and probes.

The assays were also tested for specificity to ensure that the probes did not bind to another mutation with the same nucleotide position. Cell lines from cDNA representing different point mutations were used for validation. For the validation of *BRAF* mutation assays, SK-MEL-28, IGR-1, and WM115 representing *BRAF* $^{V600E/K/D}$ were used. On the other hand, for *KRAS* mutation assay validation, RPMI8226, SW480, LS174T, Mia Paca2 and HCT 116 representing *KRAS* $^{G12A/V/D/C}$ and *KRAS* ^{G13D} were used. The specificity test for *ALK* mutation assays included Kelly and CLB-GA representing *ALK* ^{F1174L} and *ALK* ^{R1275Q}.

8.9.1 ddPCR multiplex

Multiplex on the ddPCR platform includes the detection of more than two probes and analyzation of the different positive populations on the 2-D amplitude plot. *BRAF* multiplex assay has an annealing temperature of 60°C and the concentrations of the different probes V600E, V600K and wild-type are 250 nm, 500 nm and 250 nm, respectively.

KRAS multiplex assays consist of wild type and mutations G12D, G12A and G12V with an annealing temperature of 61°C and the concentrations of wild-type, G12D, G12A and G12V probes are 250 nm, 450 nm, 350 nm and 250 nm, respectively.

ALK multiplex assay includes two sets of primers and four probes with an annealing temperature of 60°C. The concentrations of both *ALK* ^{R1275Q} wild-type and mutant probes are 350 nm, and for both *ALK* ^{F1174L} wild-type and mutant probes are 250 nm. Multiplex assay conditions are listed in Section 7.8.

8.10 Data normalization and analysis

Protein concentrations were normalized with Microsoft Excel.

The rare mutation detection (RMD) function was used when analyzing the PCR products with QuantaSoft™ Software version 1.7.4 (Bio-Rad, California, USA). Droplet fluorescence data were viewed as 1-D and 2-D plot with QuantaSoft™ Software version 1.7.4 (Bio-Rad, California, USA) and were expressed as copies/µl. The results were then calculated as:

$CPM = \frac{copies\ of\ target\ x\ template\ volume}{volume\ analyzed\ of\ the\ duplicates}$ [126].

Microscopic analysis was carried with iTEM Olympus software.

9. RESULTS

Most of the results from section 8 have been published in:

Analysis of cancer related mutations in extracellular vesicles RNA by Droplet Digital PCR.

Yap S.A., Münster-Wandowski A., Nonnenmacher A., Keilholz U., Liebs S.

BioTechniques Journal, 25 June 2020

9.1 Culturing extracellular vesicles from cell lines

Fetal bovine serum (FBS) is often used as a cell culture supplement to facilitate cell maintenance and proliferation [128]. However, EV can also be secreted from FBS. Therefore, it is vital to eliminate vesicles in FBS prior to culturing cell lines for the purpose of EV production. Initially, we produced EV-depleted FBS to be used as a supplement in our culture medium. FBS was centrifuged at 120,000 x g for 8 hours and filtered with a 0.22 µm cellulose acetate filter, based on a protocol proposed by Shelke *et al.* [129]. While the cells were growing well with the addition of EV-depleted FBS, FBS was disrupting EV purification and concentration by clogging the Centricon Plus-70 Filter (Millipore) (ref: Section 6.3.2). Therefore, it was decided to remove the addition of EV-depleted FBS in medium-producing EV altogether by rinsing primary FBS twice with PBS when the cells were 80% confluent, and the culture medium was replaced with fresh medium without the FBS supplement. Neuroblastoma cell lines were unfortunately unable to survive after 24 hours without the addition of FBS. Depending on the cell lines, we then utilized Advanced DMEM or RPMI (Thermo Fischer Scientific, Massachusetts, USA) without FBS to replacethe primary culture medium when cells reached a confluency of 80%. Advanced DMEM and RPMI are cell culture media which allow the culture of mammalian cells with reduced FBS and are commonly used when culturing stem cell-derived cell lines [130].

9.2 Extracellular vesicles isolation

9.2.1 Optimization of extracellular vesicles isolation

The fundamental protocol for EV isolation was adapted from Thèry *et al.* [123]. Supernatant from the cell culture was centrifuged at 300 x g, 200 x g and 10,000 x g for 10 minutes, 10 minutes and 30 minutes to pellet cells, dead cells and cell debris respectively followed by two cycles of ultracentrifugation at 100,000 x g for 70 minutes [123]. Based on this protocol, vesicles of different morphology and sizes, as well as cell debris were visible with the transmission electron microscope [Figure 8]. The background of cellular debris and visibility of other vesicle populations complicated the identification of the vesicles of interest. Therefore, the isolation protocol was optimized by replacing the initial serial centrifugal strength with a filtration step through a 0.22 µm cellulose acetate filter and the sample concentration with the Centricon Plus-70 filter (Millipore)

(ref: Section 6.3.2). The Centricon Plus-70 filter (Millipore, Massachusetts, USA) is a centrifugation-based concentrating device with a 10 K nominal molecular weight limit used to concentrate 70 milliliters of cell culture supernatant to 350 µl of concentrated medium [131]. EV isolated with the optimized protocol mproved the visualization of homogenously sized and shaped vesicles with less impurities in the background [Figure 12].

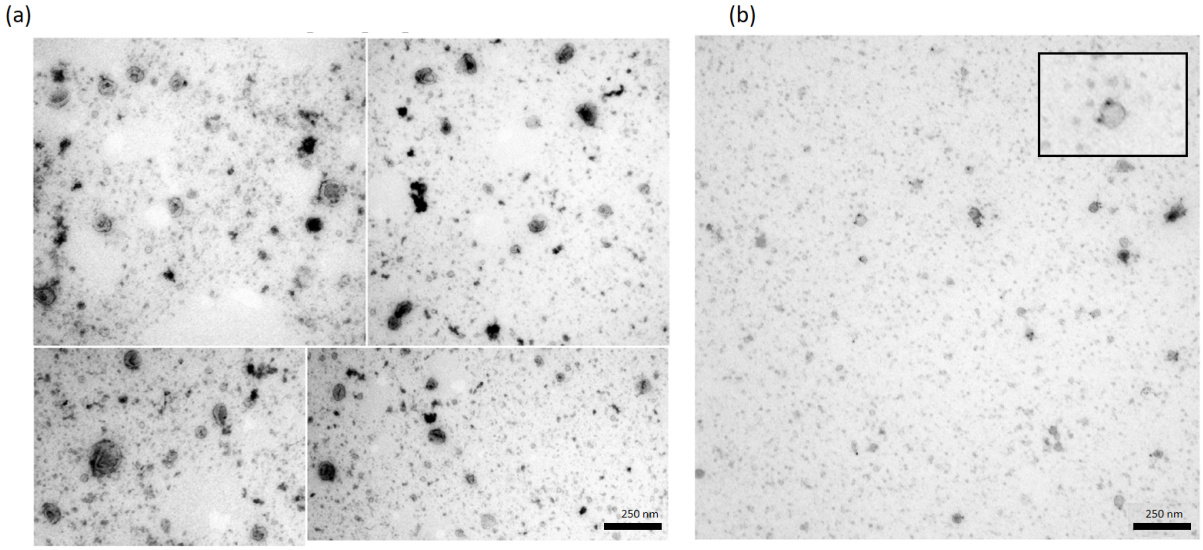

Figure 12: Electron microscope validation of extracellular vesicle isolation protocol

(a) Extracellular vesicles from SW-620 (colorectal cancer cell line) were isolated based on Thèry's protocol. Extracellular vesicle fractions were heavily accompanied with larger vesicles and cellular debris. Bar, 250 nm.
(b) The isolation protocol was optimized and EV-SW620 were isolated. Extracellular vesicle fractions appeared to be less contaminated with larger vesicles and cellular debris. Inset: zoomed-in CD63-positive extracellular vesicles. Bar, 250 nm.

9.2.2 Purification of extracellular vesicles from urine

As NB occurs in pediatric patients, the volume of blood drawn is limited. EV isolation from urine is a promising alternative to blood-based liquid biopsies due to its true invasiveness, and is abundantly available unlike blood. Its function as a potential biomarker is promising, as shown in patients with renal diseases [8], urothelial bladder carcinoma [132] and prostate cancer [133].

The physiological existence of Tamm-Horsfall glycoprotein (THP) or uromodulin in the urine reduces EV yield due to fibrin matrices trapping the vesicles [Figure 10]. Therefore, to increase EV yield, it is important to reduce amount of THP in the urine sample [134]. The entrapment can be eliminated by chemical reduction of disulfide bonds with 200 mg/ml of 1.2 - dithiothreitol (DTT), thereby depolymerizing the THP. The isolation protocol was adapted from Cheng *et al.* [135]. When comparing with and without the addition of DTT, significant improvement was noticed when DTT was added [Figure 13]. Protocol verification was assisted by transmission electron microscopy. Based on the morphological appearance of the vesicles and existence of fibrins and cellular fragments in the sample, we concluded that the protocol with the DTT supplement is superior to the other one [Figure 14].

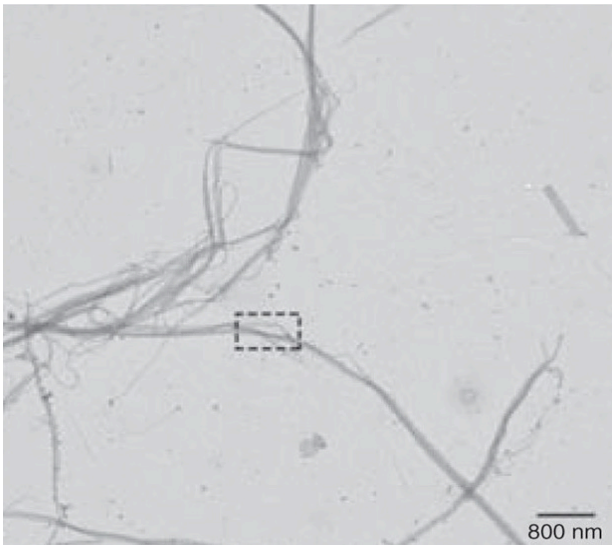

Figure 13: Tamm-Horsfall protein in urine samples
Fibrin matrices of the Tamm-Horsfall protein traps vesicles and reduce the yield of the vesicles.
Bar: 800 nm. Adapted from Llama et al. (2010) [134].

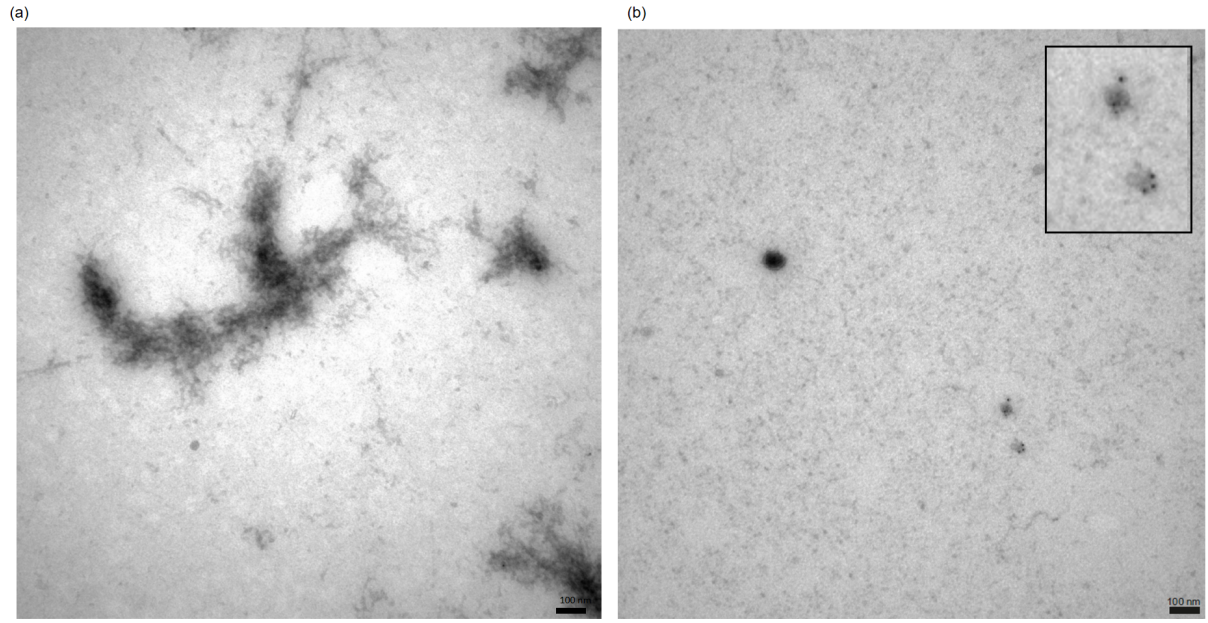

Figure 14: Extracellular vesicles derived from urine

Whole mount immunoelectron microscope analysis of extracellular vesicles isolated from the urine of neuroblastoma patients. (a) Representation of Ttamm-Horsfall protein in isolated EV fraction from urine sample. Bar, 100 nm (b) With the addition of DTT,the appearance of Tamm-Horsfall protein was reduced and more vesicles were seen. Inset: zoomed-in CD63-positive extracellular vesicles. Bar, 100 nm.

9.3 Extracellular vesicles characterization

9.3.1 Whole mount immunoelectron microscope analysis

Various EV including exosomes and microvesicles were examined using whole mount immunoelectron microscopy and were studied based on their size, morphology and immunoreactivity for protein enriched in the vesicles [131,136,137]. Immunoelectron microscope samples were prepared initially by fixing and dehydration and followed by embedment (ref: Section 6.7). The transmission electron microscope (TEM) utilizes electric beams to irradiate through the samples and the electrons can either be diffracted or transmitted by the samples. The transmitted electrons for bright-field images are then be collected by a fluorescent screen or charge-couple device. Scattered electrons are gathered to generate dark-field images, uncovering higher-contrasted structures [138,139] [Figure 15].

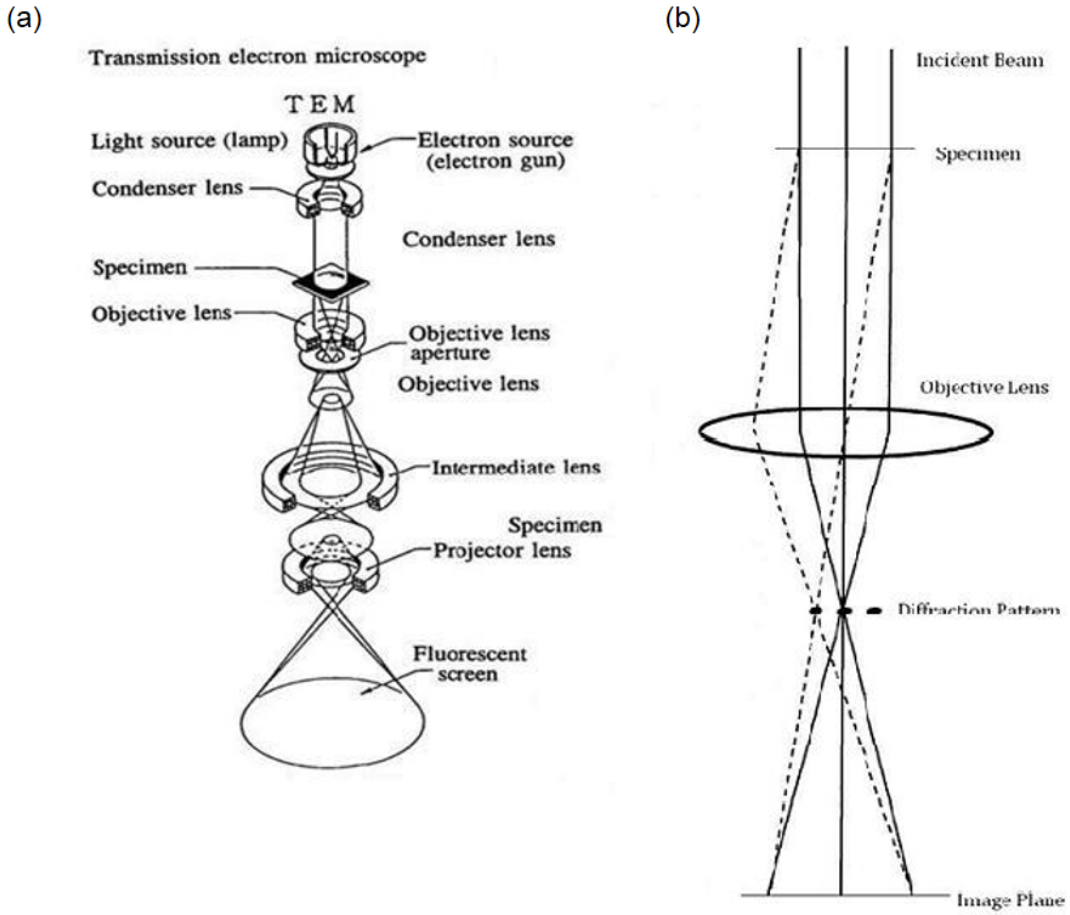

Figure 15: Transmission electron microscope

(a) Layout of a transmission electron microscope.

(b) Ray diagram describing the diffraction mechanism in a transmission electron microscope.

The diagram describes electron beams in a transmission electron microscope. As electrons pass through the sample, they are scattered by the electrostatic potential set up by the constituent elements in the specimen as it passes through the sample. The electron then passes through the electromagnetic objective lens, which focuses scattered electrons from one point of the specimen to one point in the image plane. The dotted line illustrates the collection of scattered electrons in the same direction into a single point.

Adapted from Williams and Carter (1996)[140].

Anti-CD63 conjugated to 5 nm gold nanoparticle immune labeling was performed to confirm a specific subset of vesicles with an endocytic origin based on a method described by Théry *et al.* [123]. Based on these criteria, CD63-positive vesicles, ranging from 10 nm – 100 nm, that were spherical with an intact membrane and a central depression were detected in EV. Examples of

EV are illustrated below: EV-IMR-32 (neuroblastoma cell line) [Figures 16 and 17], and EV isolated from plasma of a healthy donor [Figure 18] and a colorectal cancer patient [Figure 19].

In this study, 2% phosphotungstic acid and 4% uranyl acetate were included as controls to confirm the typical morphology of EV that was previously reported by György [141] and Théry, Ostrowski, and Segura [142]. Phosphotungstic acid was used to negatively stain the sample. This assisted the understanding of the structural and morphological details in the specimens. The particles were surrounded with electron-dense material, thereby revealing the surface by contrasting the stain (dark) and specimen (light). Hence the nomenclature, negative staining [143,144]. For positive staining, the specimen was incubated with uranyl acetate. Uranyl acetate enhanced the contrast by interacting with proteins or glycogens [145].

The expression level of tetraspanins varies greatly between different EV populations and was not homogenous within the EV fractions. Some EV were labeled more than others, while larger unlabeled EV populations with a similar morphology were also detected (> 100 nm). [Figure 16]. The cup-shaped form of the vesicles has been reported to be due to the dehydration step required by the TEM [131]. When the vesicles were visualized by the scanning electron microscope, they were more round [146,147], while some reported them as more saucer-shaped [148].

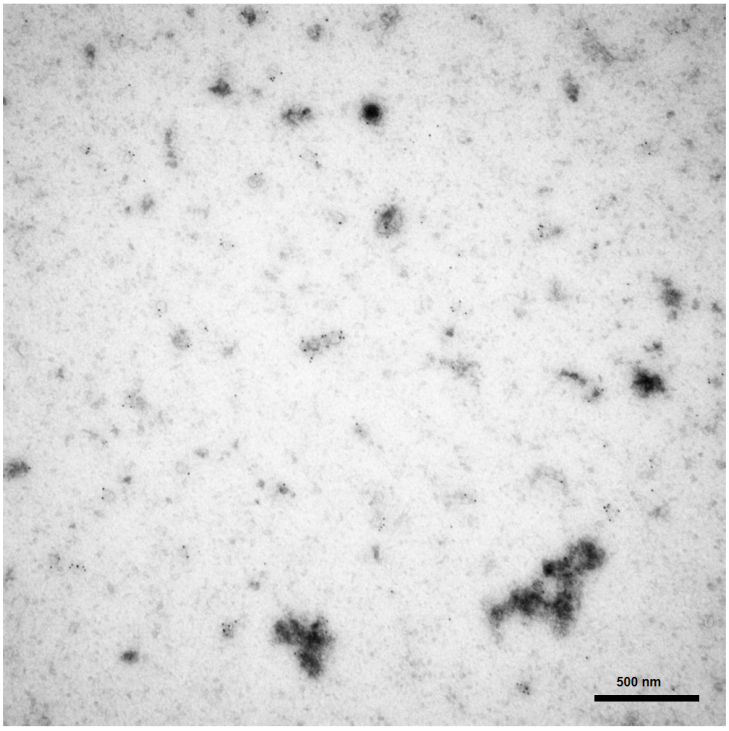

Figure 16: TEM image of cell-line derived extracellular vesicles

The figure illustrates a sample fraction of isolated extracellular vesicles from theneuroblastoma cell line (IMR-32). Bar, 500 nm.

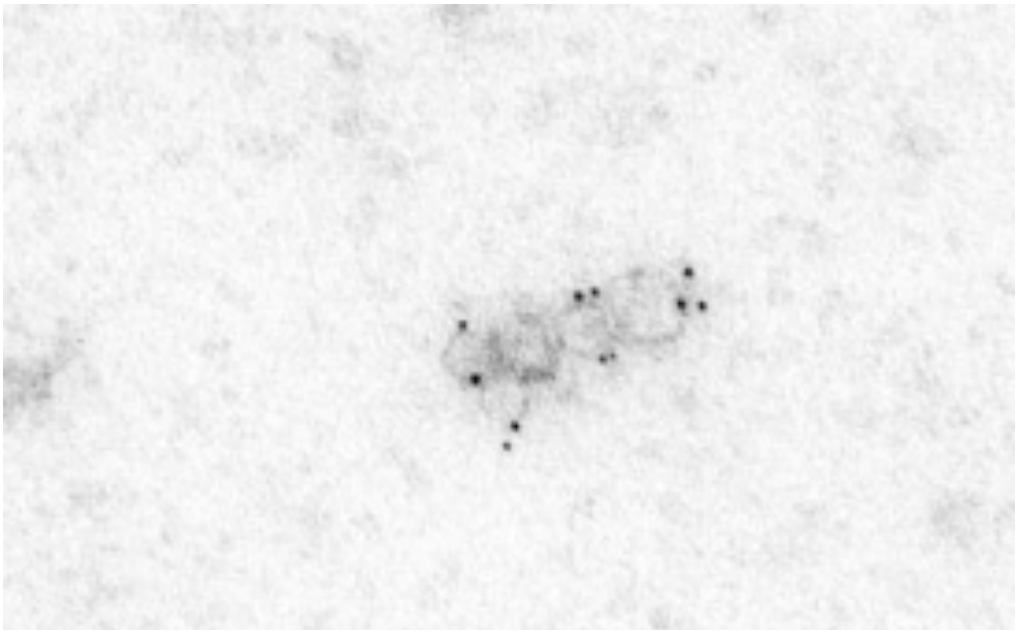

Figure 17: Enlarged TEM image of cell-line derived extracellular vesicles

Figure 17 illustrate magnified image of extracellular vesicles (from Figure 16). Vesicles were labeled with anti-CD63 gold nanoparticles and appeared to be cup-shaped with a central depression and a bilayer lipid membrane.

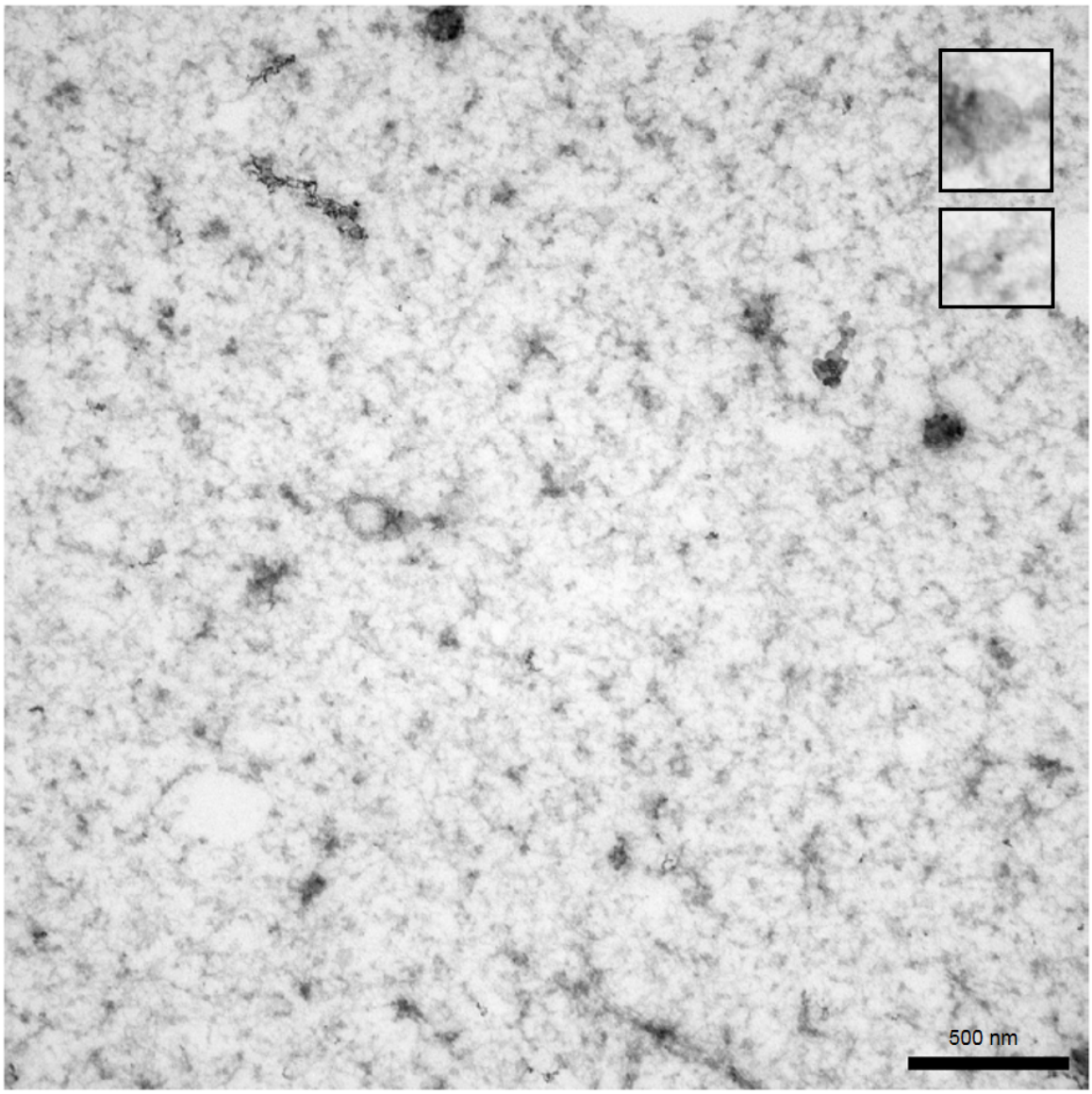

Figure 18: Extracellular vesicles isolated from plasma of a healthy donor

Anti-CD63 vesicles were visible in EV plasma isolated from a healthy donor, although in comparison to patient samples the appearance of vesicles is much sparser. Inset: magnified image of CD63 vesicles.
Bar, 500nm.

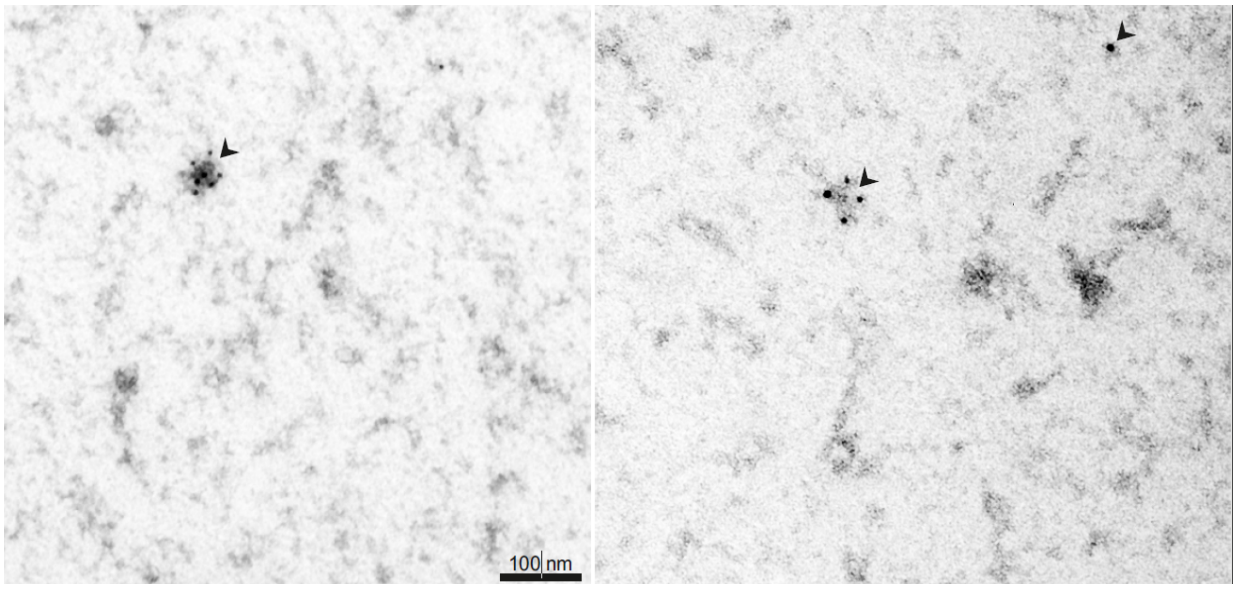

Figure 19: Extracellular vesicles derived from a colorectal cancer patient

CD63 gold-labeled vesicles fitting the profile of a typical extracellular vesicle in an EV fraction isolated from a colorectal cancer patient. Arrowheads indicate CD63-positive extracellular vesicles (5 nm immunogold particles). *Bar, 100 nm.*

9.3.2 Proteomic characterization

The EV proteins that are identified as found in the cytosol, endocytic compartments or plasma membranes and proteins of nuclear, mitochondrial, endoplasmic-reticulum or Golgi-apparatus are typically not seen in extracellular vesicles. This confirms the endosomal origin of the vesicles [18]. Based on proteomic profiling on ExoCarta [41], EV have been described to be enriched in tetraspanins, and therefore tetraspanins have been frequently identified as exosomal markers [18]. The tetraspanins CD9 and CD81 (Exiqon, Denmark) were chosen as antibodies to be included in the western blot analysis, along with CD63 (Bio-Rad Laboratories, California, USA) in the microscopic analysis.

Based on the western blot results, both CD9 and CD81 were found to be positive in EV derived from cell lines and patients' plasma. Depending on cell lines, the tetraspanins CD9 and CD81 were either present or absent. Due to the lack of a specific marker found ubiquitously in EV, GM130 (System bioscience, California, USA), a cis-matrix Golgi marker, was included as a negative control to label cell line-derived proteins which are not present in the vesicles [Figure 20].

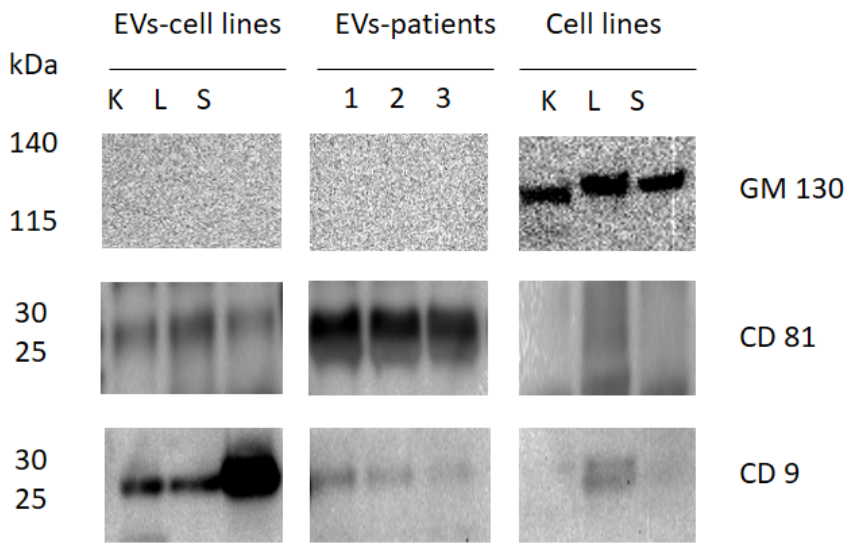

Figure 20: Characterization of extracellular vesicles by western immunoblotting

Extracellular vesicles derived from cell lines and plasma from three patients were analyzed by immunoblotting with antibodies against the exosomal proteins CD9 and CD81 and the non-exosomal protein GM130. Whole cell lysates were included as positive control for GM130.
K: Kelly, L: LS174T, S: SK-Mel-28

9.4 Whole transcriptome amplification

Working with cell lines promised optimal conditions which unfortunately do not represent real-life situations when working with patient samples. Whole transcriptome amplification was included into our workflow to allow us to remain true to our aim of using 6 to 10 milliliters (one tube) of peripheral blood. We used REPLI-g amplification kit (Qiagen, Hilden, Germany), which applies the multiple displacement amplification technology for cDNA amplification.

The multiple displacement amplification reaction initiates when multiple primer hexamers anneal to the template. When DNA synthesis proceeds to the next starting site, the polymerase DNA strand continues its elongation. The strand displacement generates newly synthesized single-stranded DNA template for more primers to anneal. To separate the DNA branching network, S1 nuclease are used to cleave the fragments at displacement sites [149] [Figure 21].

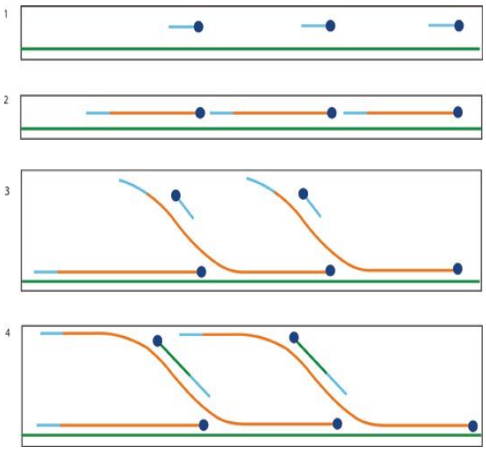

Figure 21: Multiple displacement amplification

1. Random hexamers (blue line) bind to denatured DNA (green line).

2. DNA polymerase (blue circle) elongates until it reaches the newly synthetized double – stranded DNA (orange line).

3. Enzyme displaces strands and continues polymerization; meanwhile primers bind to newly synthesized DNA.

4. Polymerization embarks on new strand.

Adapted from Spits et al. (2006) [150].

Whole transcriptome amplification was tested with EV derived from the heterogeneous NB cell line CLB-Ga (EV-CLB-Ga), with 50% less starting material than was previously used. With a reduction of starting material, non-amplified EV-CLB-Ga, which expresses *ALK* ^{R1275Q}, was not detectable, whereas the amplified EV-sample demonstrated a saturation of positive droplets in both FAM (MUT) and HEX (WT) channels [Figure 22].

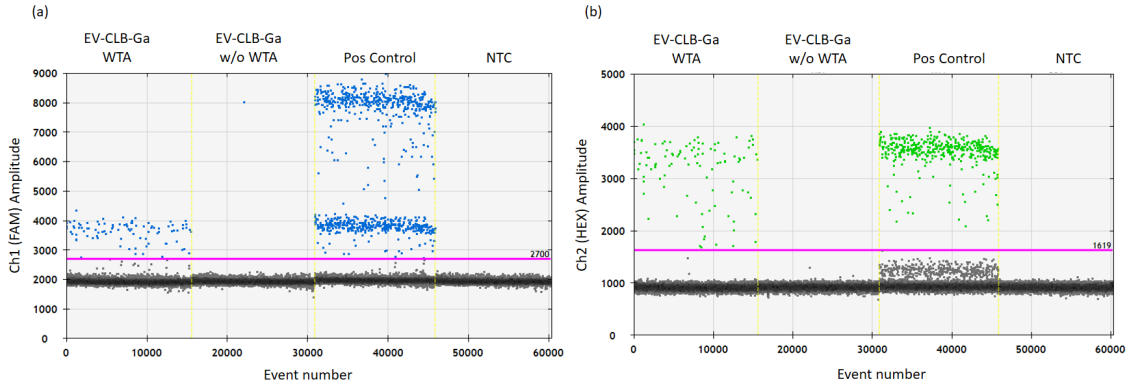

Figure 22: Comparison of ddPCR prior to and after whole transcriptome amplification.

Heterogeneous EV-CLB-Ga (neuroblastoma cell line) were isolated and underwent whole transcriptomic amplification. Amplified cDNA from EV-CLB-Ga was compared to non-amplified EV-CLB-Ga, demonstrating significant improvement after amplification. The PCR controls included were cDNA from cell line CLB-Ga as positive control and non-template control as negative control.

WTA: whole transcriptome amplification, w/o: without, Pos: positive, NTC: non template control (PCR-grade water)

9.5 Mutational analysis

9.5.1 Primers and probes for extracellular vesicles mutational analysis

Primers designed for the *KRAS* assay initially have a PCR product size of 170 base pairs. The optimized ddPCR fitted the ideal expectations when analyzed with cDNA derived from cell lines. However, when analyzing EV derived from cell lines, no results were attainable from the ddPCR. New primers with a product size smaller than 100 base pairs were designed, with the assumption that vesicles occurred more commonly at a shorter fragment length. This became the new standard for primers designed for EV analysis. Figure 23 depicts the results of cDNA from EV and cell lines when analyzed with primer pairs with a product size of 170 base pairs [Figure 23(a,b)] and 98 base pairs [Figure 23(c,d)]. By using the primers with the smaller product size, EV cell lines were detectable with the ddPCR.

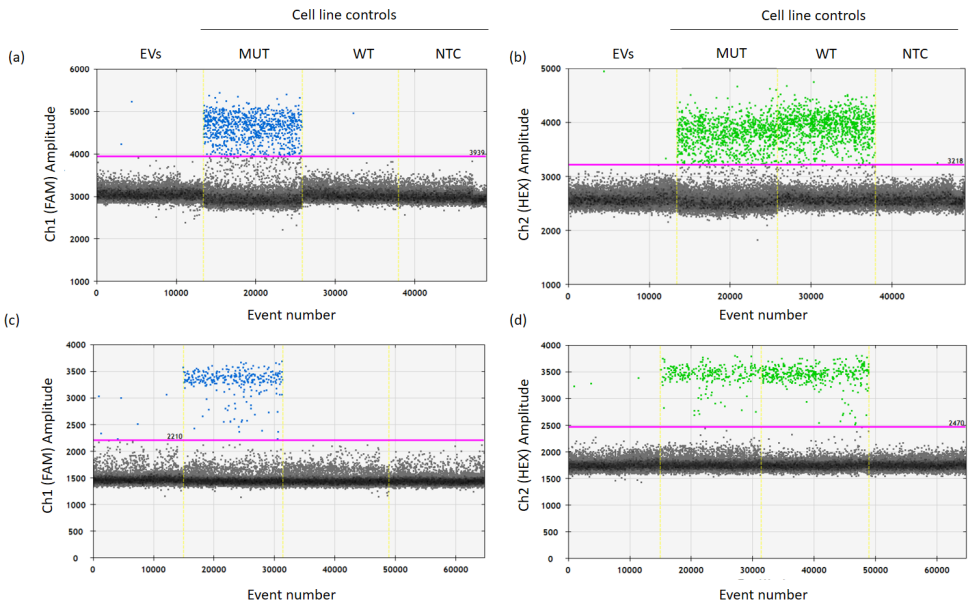

Figure 23: Comparison of different primers

KRAS ^{G12D} assays with a PCR product size of (a) and (b) 170 base pairs and (c) and (d) 98 base pairs were tested with heterogeneous EV-LS174T (colorectal cancer cell line). PCR controls included cDNA from mutant heterogeneous cell line LS174T (MUT), cDNA from wild-type cell line HeLa (WT) and non-template control (NTC) as negative control. Heterogeneous EV-LS174T were only detectable in KRAS ^{G12D} with a smaller product size (c) and (d). Mutant probes were labeled with FAM fluorophores (blue), while wild-type probes were labeled with HEX fluorophores (green).

9.5.2 Mutational analysis via ddpcr

Droplet digital™ PCR (ddPCR) is a novel emulsion-chemistry-based system which partitions 20 µl of TaqMan PCR reaction volume into approximately 20,000 oil-encapsulated nanodroplets, allowing independent amplification of single template enclosed in a droplet. Eventually, single droplet are analyzed for being positive or negative for amplified target regions. Thus, the high precision makes ddPCR an optimal method for applications such as rare mutation detection and gene expression analysis with low starting material [126] [Figure 24].

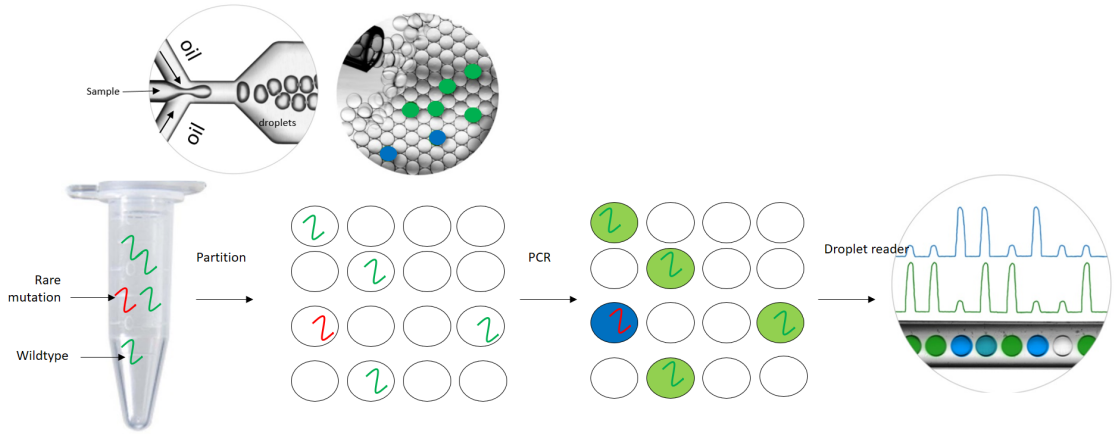

Figure 24: Schematic of the droplet digital PCR

PCR reaction mix is enveloped in oil and forms individual droplets which are amplified independently. DDPCR enables rare mutation detection and end-point analysis provides information if amplified targets were positive or negative. Partly adapted from Bio-Rad Droplet Digital™ PCR applications guide [126].

The templates in ddPCR are randomly distributed, therefore droplets can contain one or more template copies, or none at all. The partitions are amplified with PCR and the positive fractions are distinguished by the droplet reader using the Poisson distribution. Named after the French mathematician Simeon Denis Poisson, the Poisson distribution models a series of discrete probability distributions through the expression of the probability of a number of events within a fixed interval or time and space, provided that the events occur independently at a known constant rate since the last event [151].

The Poisson modeling formula is as follows [126]:

$$\text{Copies per droplet} = 1n\ (1\text{-}p)$$

Where p = fractions of positive droplets.

A thermal gradient was used for the optimization of the primer/probe annealing temperature in singleplex and duplex assays. After the ideal annealing temperature was confirmed, different probe concentrations were tested. The optimal ddPCR conditions provide the largest fluorescence amplitude difference between positive and negative droplets in the 1D amplitude plot of FAM (MUT) and HEX (WT) channels. The 2D amplitude plot should demonstrate an orthogonal separation between WT and MUT single positive, WT/MUT double positive and negative droplets [Figure 25]. The finalized annealing temperature and primer and probe concentrations are listed in Section 7.8.

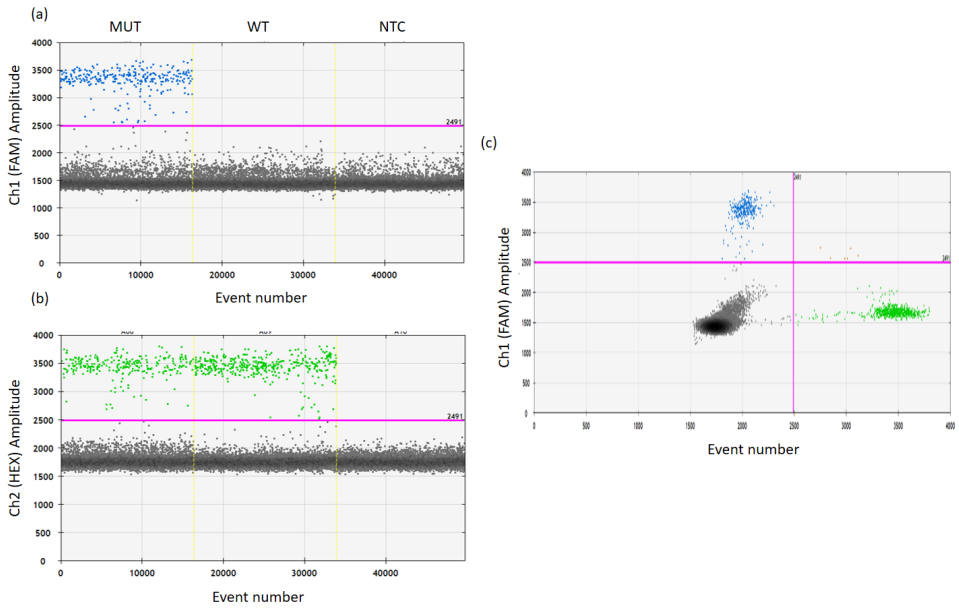

Figure 25: Optimized duplex ddPCR

ddPCR BRAF ^{V600E} assays were analyzed with Quantasoft^{TM} software and demonstrated as 1-D plots in (a) FAM channel representing mutant probes and (b) HEX channel representing wild-type probes. It is also essential to analyze assays in the (c) 2-D amplitude plot to ensure that there is a clear orthogonal separation between the different populations. Each dot on the figure represents one droplet consisting of at least one DNA target copy of either mutant (blue), wild type (green) or no DNA (black). Orange droplets contain targets of both mutant and wild type.

The false positive rate (FPR) was evaluated using the number of unspecific events in the mutation channel when analyzing non-template controls and the inclusion of high and low concentrations of wild-type cDNA (500 and 100 copies/µl, respectively). The cross-reactivity of probes was studied here, and since only non-template controls and wild-type cDNA were used, the FAM (MUT) channel should have remained eventless. The FPR for each assay ranged from zero to one event. Figure 26 describes an example of FPR ddPCR results.

As the aim was to detect rare mutations, it was critical to understand the sensitivity of the system by determining the lower limit of detection. The limit of detection (LOD) was identified with mutant cDNA diluted with a background of constant wild-type cDNA. Additionally, the performance efficiency of the primers/probes was simultaneously detected in this assay by calculating the WT/MUT ratio. In LOD and WT/MUT ratio experiments, mutant cDNA is diluted in 10-fold series from 100 to 0.01 copies/µl in a background of 100 copies/µl of wild-type cDNA. The LOD for all assays was 0.1% in a 20 µl reaction. Figure 27 describes an example of a LOD ddPCR result. The assays were also tested for specificity to ensure they were only specific for the mutation of interest. Alongside rare mutation detection assays when analyzing EV from patients' plasma, non-template control and wild-type cDNA as negative control and mutant cDNA as positive control from the cell lines were always included.

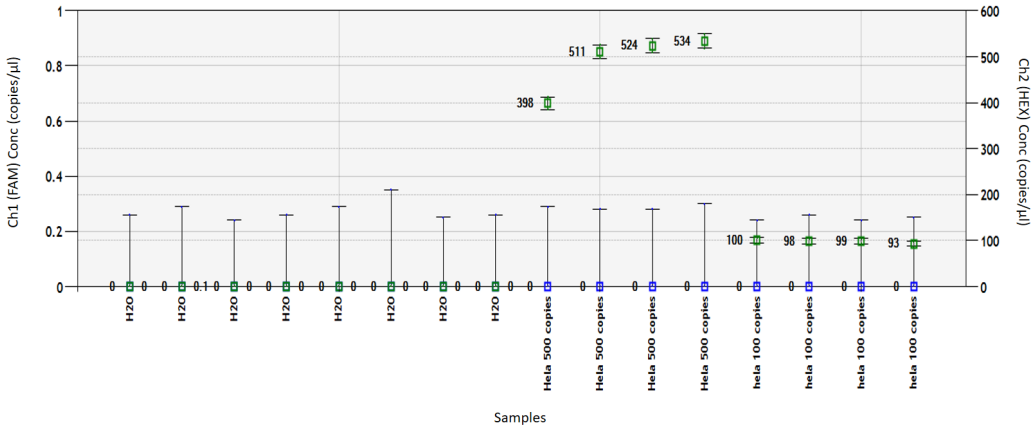

Figure 26: False positive rate for KRAS ^{G12C} assay

Concentration graph of both Channel 1 (FAM) representing MUT probes and Channel 2 (HEX) representing WT probes demonstrating concentration levels of non-template control (H2O), a high concentration of WT-cDNA (Hela 500 copies) and a low concentration of WT-cDNA (Hela 100 copies). The concentration of non-template control and Channel 1 (FAM) remained, negative demonstrating no contamination or cross-channel or cross-reactivity leakage from probes.

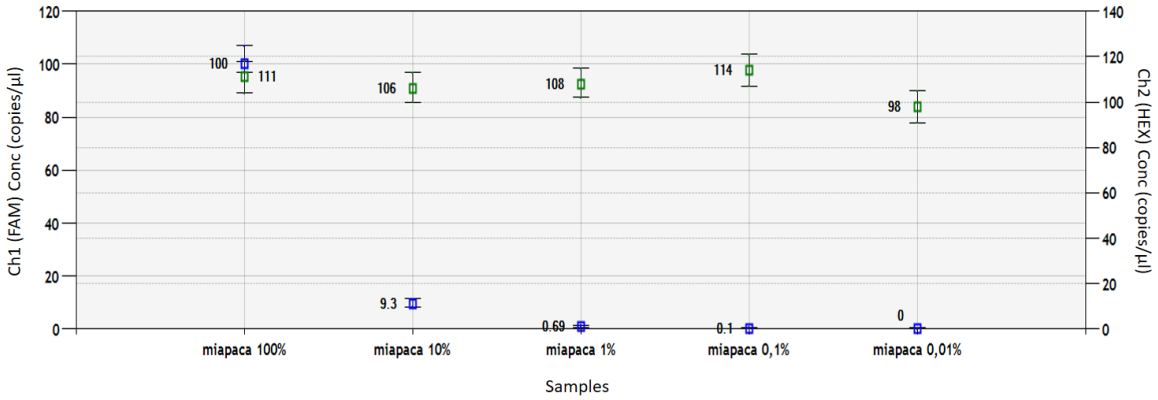

Figure 27: Limit of detection and WT/MUT ratio for KRAS ^{G12C} assay

The Concentration graph for both FAM (MUT) and HEX (WT) channels demonstrated a constant WT-cDNA concentration and serially diluted MUT-cDNA concentration. Here, it is demonstrated that the limit of detection is 0.1%. Furthermore, this graph also describes the performance efficiency of the primers and probes.

The probes for majority of the assays were labeled with the Black Hole Quencher® (BHQ1) at the 3' end of the probe (Sigma Aldrich, Missouri, USA). The positive and negative droplet populations for the *BRAF* ^{V600K} and *ALK* ^{R1275Q} assays were insufficiently separated, however, and there was also the presence of droplet rain (*droplet occurrence between positive and negative droplet clusters*), which interfered with the interpretation of positive and negative droplet populations. Therefore, for both assays the Zen™/Iowa Black™ (Z/IB) quencher was used instead. The quencher reduces signal cross-talk and generates less background [127], enabling a strong separation between both positive and negative droplets clusters. Figure 28 demonstrated a *BRAF* ^{V600K} assay with probes labeled with the BHQ1 and Z/IB quencher. The Zen™ /Iowa Black™ (Z/IB) quencher provided a better separation between the different clusters.

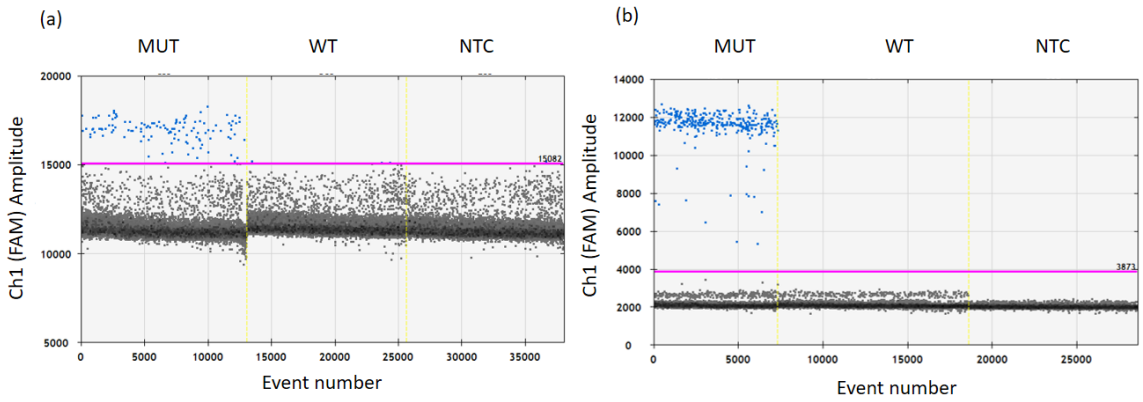

Figure 28: Comparison of different quenchers for BRAF ^{V600K} assay

ddPCR assays were compared using probes labeled with (a) Black Hole Quencher® (BHQ1) and (b) Zen™/Iowa Black™ (Z/IB). Probes with the Z/IB quencher allowed a more distinguishable separation between positive and negative population with reduced droplet rain.

Even though QuantaSoft™ Software version 1.7.4 (Bio-Rad, California, USA) automatically sets a recommended threshold upon analyzation, the thresholds were often set manually following parameters set in our group. Firstly, due to the Poisson distribution formula utilized by the software, it was important to reach 10,000 events for every well to be included in the analysis, anything lower than two events were exempted to avoid false positives. Furthermore, non-template controls should remain eventless in both FAM (MUT) and HEX (WT) channels and wild-type cDNA controls should remain eventless in the FAM (MUT) channel. The threshold for the same sample type in the same ddPCR run must lie in the same amplitude. The optimization workflow for ddPCR is described in Figure 29.

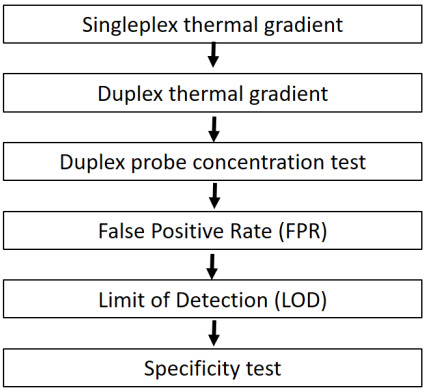

Figure 29: ddPCR optimization steps

The ddPCR was optimized first with a singleplex thermal gradient, followed by a duplex thermal gradient to identify the ideal annealing temperatures. The probe concentration was verified with a duplex PCR. This was then followed by the testing of the false positive rate, limit of detection and specificity to ensure the ddPCR assay was of quality.

9.5.3 ddPCR multiplex

Multiplex ddPCR includes more than one target sequence using either one or two pairs of primers and multiple probes targeting different targets. This technology is beneficial as a cost-efficient and quick screening tool [152]. However, ddPCR is limited to the utilization of only two reporter dyes (HEX and FAM channels), therefore multiplexing more than two targets could be challenging. In the effort of materializing this procedure, the probe concentrations and annealing temperatures were adjusted to ensure that the positive clusters representing the different targets appeared at different levels of fluorescence amplitude in the 2-D plot. Furthermore, non-specificity like cross-dimerization, competitiveness between each target and the accurate separation of fluorescent signals needs to be taken into consideration [153], and particularly in multiplex mutation assays which include targets that only differ by one nucleotide.

At the time that multiplexing with ddPCR was initiated in the group, Bio-Rad's ddPCR platform was not intended for multiplexing and therefore the software did not support this function. After ddPCR multiplexing was more popularized, QuantaSoft™ Analysis Pro Software Version 1.0 (Bio-Rad,California, USA) was released.

The multiplex assays *KRAS* $^{G12D,\ G12A,\ G12V}$, *BRAF* $^{V600E/K}$ and *ALK* $^{F1174L/R1275Q}$ were optimized. All three multiplex assays demonstrated clear orthogonal separation between the different clusters, enabling the definition of mutation of interest [Figure 30, 31, 32]. Multiplex assay conditions are listed in Section 7.8.

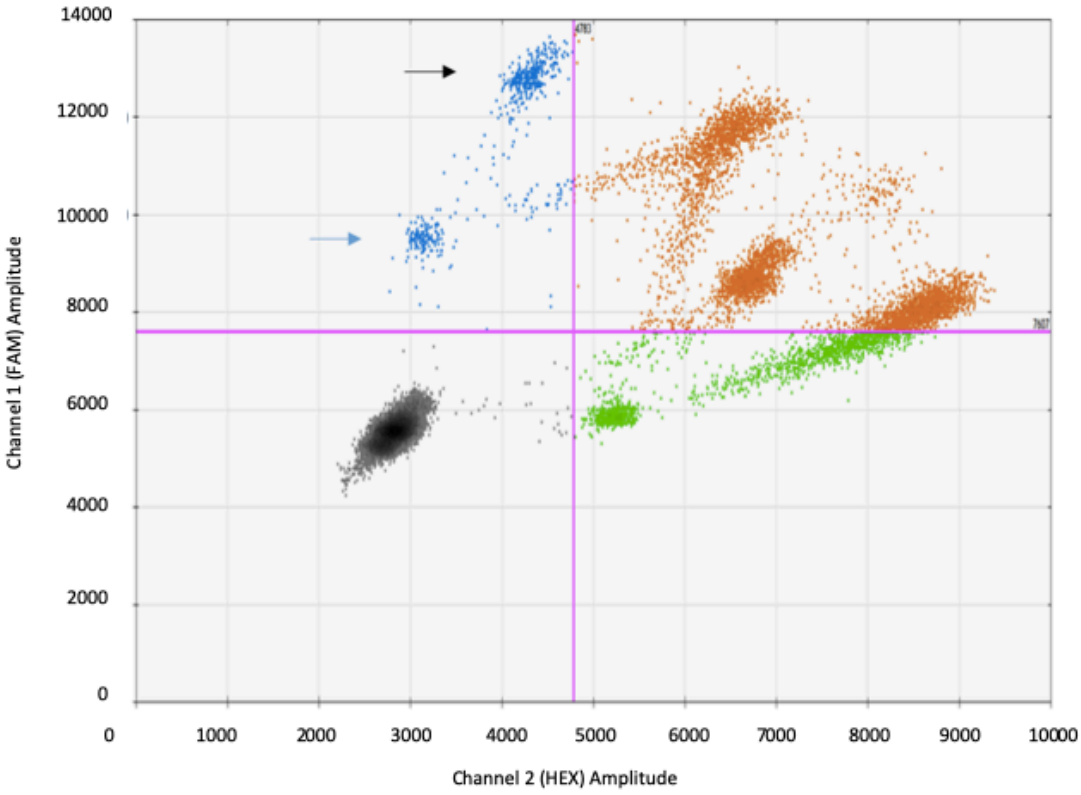

Figure 30: ALK multiplex assay

2-D amplitude plot of optimized ALK multiplex assay. The blue arrow depicts populations of ALK ^{F1174L} *and the black arrow shows populations of ALK* ^{R1275Q}*. The blue population represents mutant DNA targets, while the green population represents wild-type DNA targets. Droplets without a DNA target appear in black and double positive (containing both wild-type and mutant targets) are represented by orange dots.*

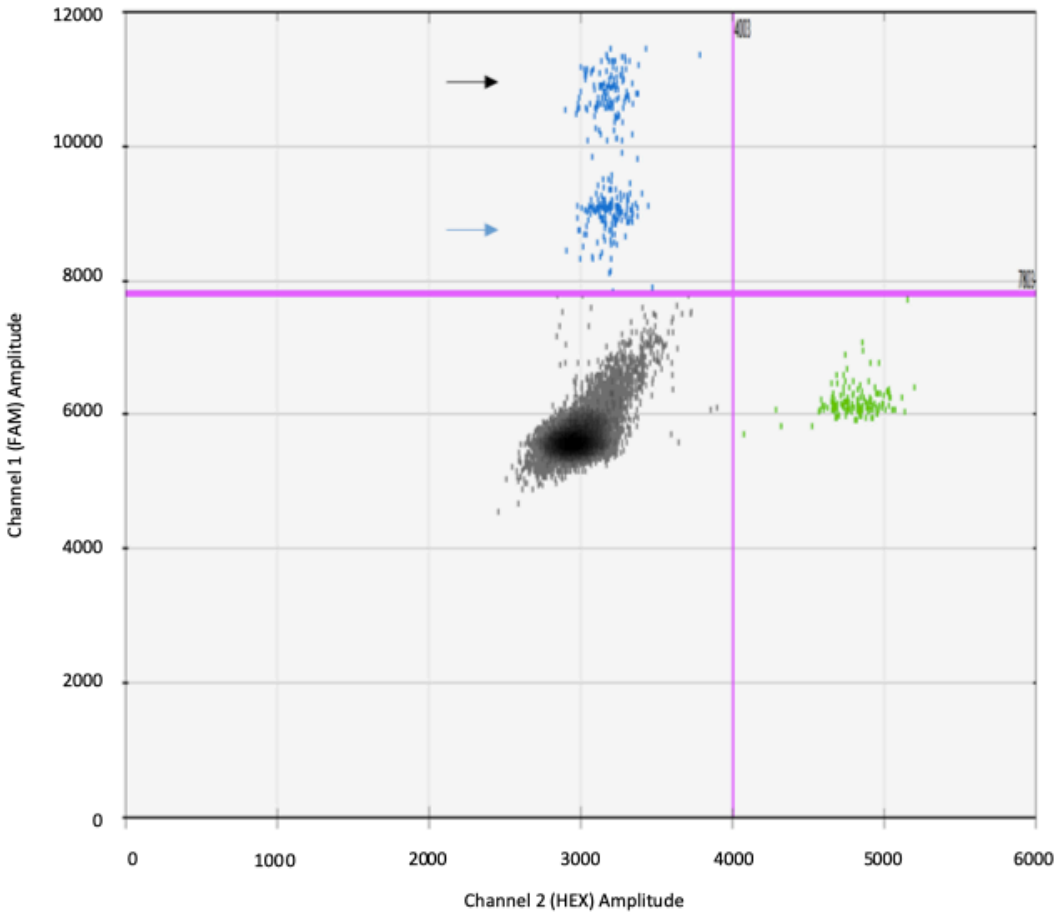

Figure 31: BRAF multiplex assay

BRAF Multiplex assay illustrated in a 2-D plot with BRAF^{V600K} (black arrow) and BRAF^{V600E} (blue arrow). The blue population represents mutant DNA targets, while the green population represents wild-type DNA targets. Droplets without DNA targets appear in black.

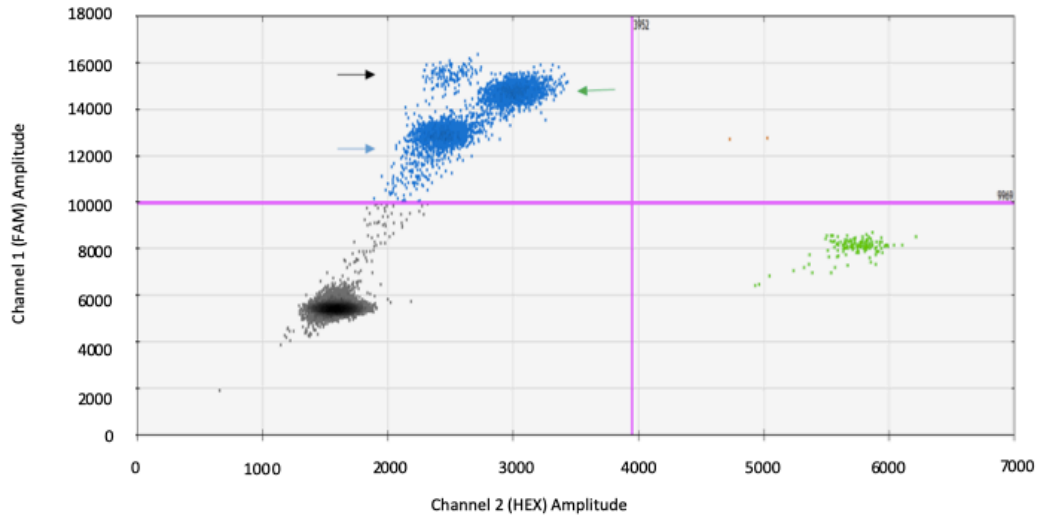

Figure 32: KRAS multiplex assay

Three KRAS *targets were included in the multiplex assay: G12D (Black arrow), G12A (blue arrow) and G12V (green arrow). The blue droplets contain mutant targets and the green droplets represent wild-type targets. The black droplets do not contain DNA targets.*

9.6 Sample collection and blood tube additives

Plasma has been described to be the physiological medium of EV [154,155]. Thus, plasma samples were preferred over serum due to the abundance of vesicles in sera. Fifty percent of EV are found in serum derived from platelets and are released after blood collection due to clot formation. According to ISEV reports, vesicles isolated from serum were used for studies regarding platelet-derived EV [156]. However, studies need to be undertaken to understand the differences in isolating the vesicles from each of these blood components.

Anticoagulant in blood tubes varies in types and purpose, which was taken into consideration when choosing the suitable medium for blood collection, as it could have influenced the function and count of the EV. As reported by Philippe *et al.,* even different produced of sodium citrate tubes could influence the quantity of the vesicles [157].

Heparin was not preferred as it is commonly linked to causing false negative PCR reads and competes with primers [158]. As our study was PCR based, this anticoagulant was avoided. Furthermore, heparin binds to EV, blocks EV uptake and reduces EV-activated platelets [159].

Sodium citrate and heparin blood increase vesicles count due to subpopulations. However, among the three most common anticoagulants (heparin, sodium citrate and EDTA), sodium citrate demonstrated lowest EV count. EDTA samples demonstrated a stable MV count derived from platelets and erythrocytes. Sodium citrate is suitable for functional analysis, whereas in clinical studies, EDTA is more appropriate [160].

When EV can be immediately analyzed after blood draw, it is ideal to utilize sodium citrate and heparin blood tubes. Logistically, immediate analysis unrealistic most of the time. Clinical routine has to be taken into consideration, including the transportation of blood sample, transport duration and in-house processing time. It has been reported that the stability of EV count could be preserved with EDTA even after 48 hours of room temperature (RT) storage [160].

For our study, we then resorted to using EDTA blood tubes for blood collection, due to their convenient accessibility in clinical settings. We wanted to remain true to the principle of introducing liquid biopsy in the clinic with the available resources. The blood samples were always centrifuged within the first hour after blood draw to separate plasma for subsequent -80^{o}C storage.

9.7 Spiking

Prior to applying the method on EV derived from patient plasma' samples, a spiking experiment was simulated for a trial run. EV were isolated via differential centrifugation from Kelly, a heterozygous neuroblastoma cell line expressing *ALK* ^{F1174L} (ref: Section 6.3.2). The isolated vesicles were then spiked into healthy blood, followed by plasma separation (ref: Section 6.3.3) and isolation of EV derived from plasma (ref: Section 6.3.3). EV-RNA was subsequently isolated from the spiked EV-plasma sample followed by whole transcriptome amplification and *ALK* ^{F1174L} mutation detection with the ddPCR. As a control, the exact workflow was repeated simultaneously, and the spiked EV plasma was visualized with the TEM. Analysis of the ddPCR demonstrated positive droplets in both FAM (MUT) and HEX (WT) channels due to the heterozygosity of the primary cell

line [Figure 33] and TEM analysis visualized CD63-positive vesicles with the typical morphology of extracellular vesicles [Figure 34].

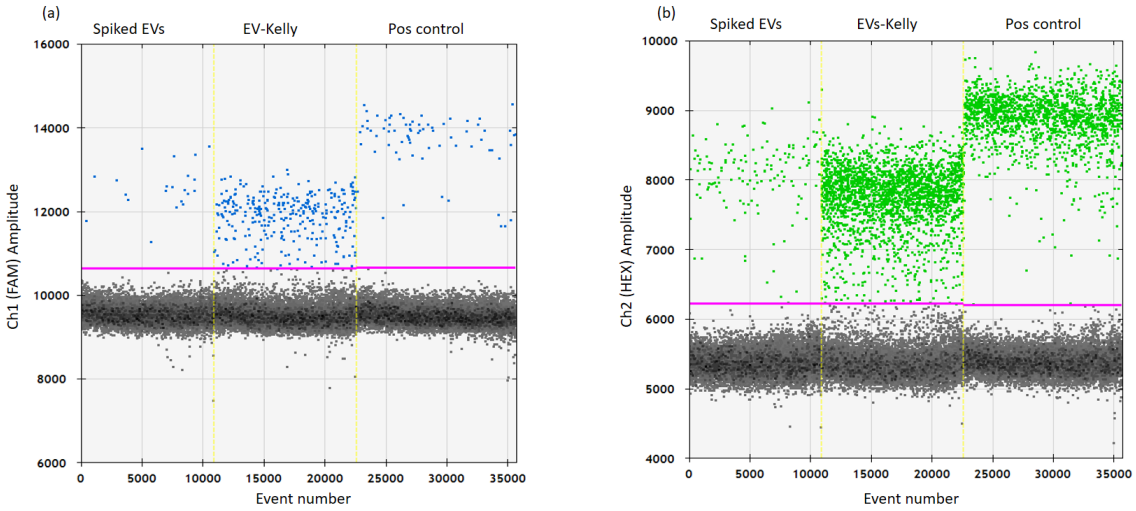

Figure 33: DDPCR analysis of spiked samples

EV-Kelly were spiked into EDTA blood (spiked EV), before EV isolation followed by analysis with the ddPCR for the mutation ALK F1174L. EV derived from Kelly (EV-Kelly) and cDNA from Kelly cell line (Pos control) were included as control. The results were depicted in 1D plot in: (a) FAM channel representing the mutation and (b) HEX channel representing WT.

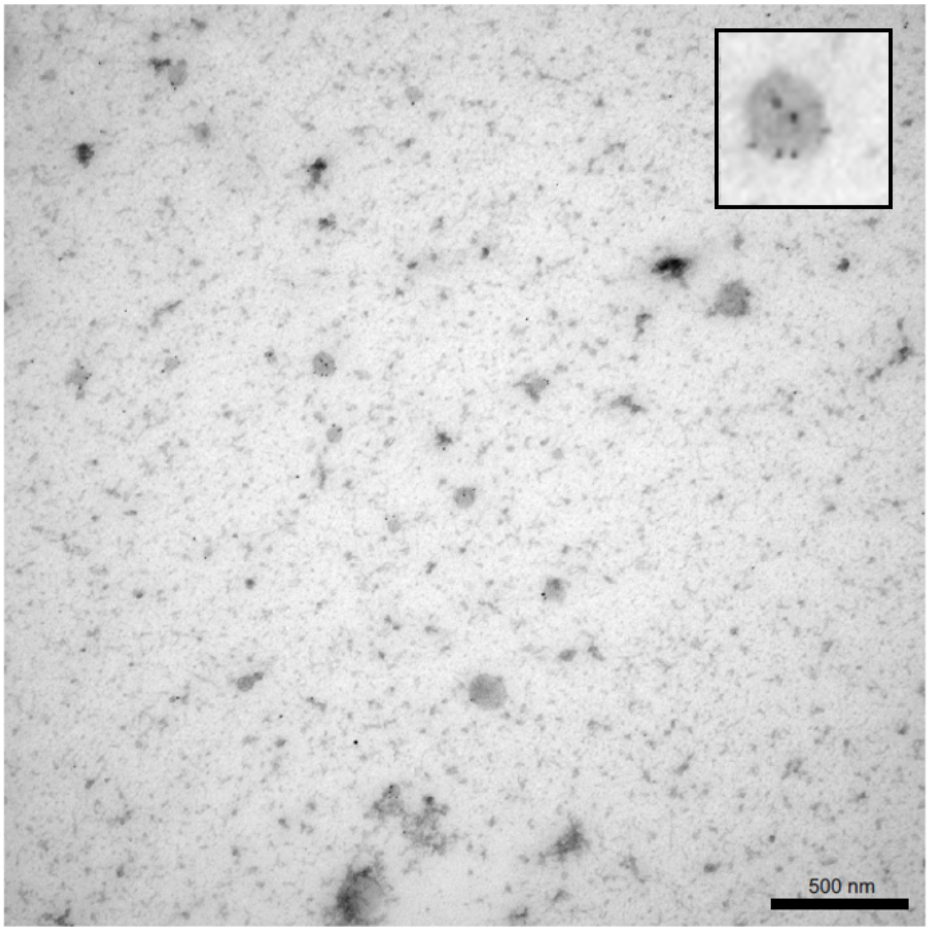

Figure 34: Whole mount immunoelectron analysis of spiked plasma sample

As an experimental control for the spiking experiment, spiked EV-Kelly in plasma samples were visualized with the transmission electron microscope.

9.8 Patients

9.8.1 Sample preparation and workflow

To optimize the maximum usage of the blood sample, efforts were applied to investigate the possibility of analyzing CTCs, cfDNA and EV from one blood tube. Therefore, plasma was separated via centrifugation and equally divided (one milliliter) for cfDNA and EV analysis, whereas the blood phase of the sample would be used for CTC analysis. After plasma separation, EV were isolated via differential centrifugation and were used either for whole-mount immune electron microscope, western blot analysis or mutational analysis with ddPCR. Figure 35 illustrates the sample processing workflow.

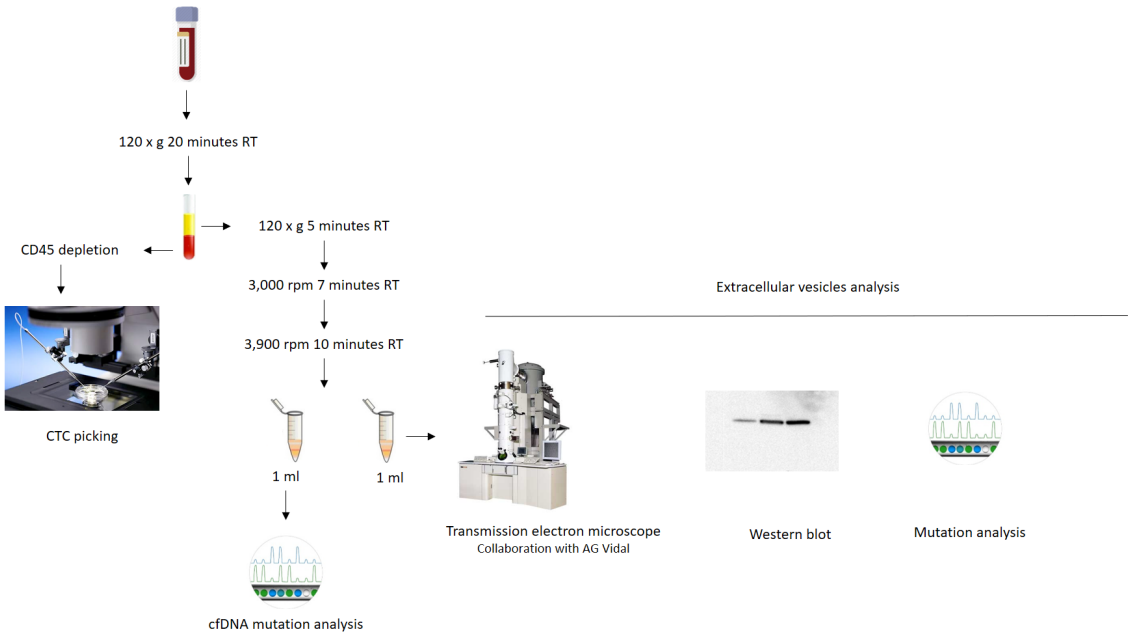

Figure 35: Liquid biopsy workflow

Whole blood was centrifuged at 120 x g for 20 minutes at room temperature. The blood phase was used for CTC picking after CD45 depletion. The plasma phase continued to be centrifuged before splitting the plasma sample equally for cfDNA and EV analysis. EV analysis was then carried out with morphological analysis via the transmission electron microscope, proteomic analysis and lastly mutational analysis.

RT: room temperature, CTC: Circulating tumor cells, cfDNA: circulating cell-free DNA

9.8.2 Analysis of extracellular vesicles derived from patients

EV from MM patients were screened with *BRAF* $^{V600E/K}$ mutation assays, whereas EV from CRC patients were screened with five *KRAS* mutations including *KRAS* $^{G12A/C/D/V}$ and *KRAS* ^{G13D}. Furthermore, EV from NB patients were screened with *ALK* $^{F1174L/R1275Q}$. In the MM cohort, *BRAF* wild type was detected in ten EV samples, mutations were present in six patients (*V600E* and *V600K* in two and four patients, respectively) and in two samples neither the wild type nor *BRAF* mutation was detected. Additionally, in the CRC cohort, *KRAS* wild type was detected in seven EV samples, mutations were present in three patients (*G12D* and *G12V* in two and one patient, respectively) and in three patients neither wild type nor *KRAS* mutation was detected. Moreover, one of the four NB patients was positive for *ALK* ^{F1174L}, and neither *ALK* mutation nor wild type was detected in the other three EV patient samples [Tables 6 and 7].

EV-based ddPCR analyses of MM and advanced CRC patients were compared with tissues profiles during routine analyses [Tables 9 and 10]. Among the 18 melanoma patients, 44% (8/18) of ddPCR results were in concordance with tissue sequencing. Wild type was detected instead of the expected mutations in 28% (5/18) of the patients and 17% (3/18) were mutation mismatched (two V600K detected instead of expected V600E and one V600E instead of WT). Additionally, 54% (7/13) of CRC patients were in concordance with tissue sequencing, with 15% (2/13) wild type detected instead of the expected mutations, and vice versa for one patient. Tissue mutation information was only available for two NB patients. One patient positive for ddPCR *ALK* ^{F1174L} assay was in concordance with the tissue sequencing results [Table 6(a)].

Table 6: Concordance between gene status of extracellular vesicles and tumor tissue for (a) melanoma and (b) colorectal cancer cohort

(a)

ddPCR results	**Number of patients (%)**
Total amount of MM patients	18
Concordance	8 (44.4 %)
BRAF WT	5 (27.7 %)
BRAF V600E	1 (5.5 %)
BRAF V600K	2 (11.2%)
Discordance	
BRAF WT instead of expected *BRAF MUT*	5 (27.7%)
BRAF V600K instead of expected *BRAF V600E*	2 (11.2%)
BRAF V600E instead of expected *BRAF WT*	1 (5.5%)
Undetectable	2 (11.2%)

(b)

ddPCR results	**Number of patients (%)**
Total amount of CRC patients	13
Concordance	7 (53.9%)
KRAS WT	5 (38.5%)
KRAS G12D	1 (7.7%)
KRAS G12V	1 (7.7%)
Discordance	
KRAS WT instead of expected *KRAS MUT*	2 (15.4%)
KRAS MUT instead of expected *KRAS WT*	1 (7.7%)
Undetectable	3 (23%)

Undetectable: no positive droplets in both WT and MUT channels.

Table 7: Cancer stages, tissue profiling and extracellular vesicles ddPCR results for (a) neuroblastoma (b) colorectal cancer and (c) melanoma cohort

(a)

Patient	Cancer stage (INSS)	Tissue sequencing	ddPCR	CPM
4	4	*ALK F1174L*	No results	No results
5	4	Unknown	No results	No results
6	4	*ALK F1174L*	*ALK F1174L*	15.7
8	4	Unknown	No results	No results

(b)

Patient	Cancer Stage (AJCC)	Tissue sequencing	ddPCR	CPM
6	4	*KRAS G12D*	*KRAS WT*	4.18
10	4	*KRAS G12D*	No results	No results
19	4	*KRAS G13D*	No results	No results
21	4	*KRAS G12D*	*KRAS WT*	33.3
22	4	*KRAS WT*	*KRAS WT*	1.87
23	4	*KRAS WT*	*KRAS WT*	3.63
25	4	*KRAS WT*	*KRAS WT*	8.58
26	4	*KRAS WT*	*KRAS WT*	39.6
27	4	*KRAS G13D*	No results	No results
30	4	*KRAS WT*	*KRAS WT*	2508
302	4	*KRAS G12D*	*KRAS G12D*	5.2
338	4	*KRAS WT*	*KRAS G12D*	13.86
356	4	*KRAS G12V*	*KRAS G12V*	3.5

(c)

Patient	Cancer Stage	Tissue sequencing	ddPCR	CPM
1	4	*BRAF WT*	*BRAF V600E*	61.6
6	3c	*BRAF WT*	*BRAF WT*	0.88
10	4	*BRAF V600E*	*BRAF WT*	3091
11	4	*BRAF V600E*	*BRAF WT*	1.6
15	4	*BRAF V600E*	*BRAF WT*	1.76
16	4	*BRAF V600K*	*BRAF V600K*	3.08
19	4	*BRAF WT*	*BRAF WT*	0.9
20	4	*BRAF V600E*	*BRAF WT*	2251
22	3a	*BRAF V600K*	*BRAF V600K*	16.5
25	4	*BRAF V600E*	*BRAF V600K*	6.26
28	4	*BRAF V600E*	No results	No results
29	3c	*BRAF V600K*	*BRAF WT*	298.1
30	4	*BRAF V600E*	*BRAF V600K*	36.6
33	1a	*BRAF V600E*	No results	No results
37	4	*BRAF V600E*	*BRAF V600E*	16.5
38	1	*BRAF WT*	*BRAF WT*	0.44
39	4	*BRAF WT*	*BRAF WT*	7.48
40	4	*BRAF WT*	*BRAF WT*	0,55

No results: No positive droplets in both WT and MUT channels.

9.8.3 Discordant cases due to treatments

Among thirty-five patients, two cases stood out with discordant mutation status. Patient 16 was diagnosed with metastatic melanoma with a brain metastasis. Sequenced archival tissue demonstrated a *BRAF* ^{V600E} mutation. Based on the positive *BRAF* ^{V600E} mutation status, the patient received dabrafenib, followed by dabrafenib and trametinib (*BRAF/MEK* inhibitor) combination therapy. The patient was recruited prior to receiving combination immunotherapy with nivolumab and ipilimumab. EV analysis revealed *BRAF* ^{V600K}. One year after recruitment, staging analysis showed a subcutaneous, cerebral, intraabdominal, intradural and vertebral metastatic progress. Furthermore, tissue sequencing was repeated due to the advanced metastatic progress, verifying the mutation switch from *BRAF* ^{V600E} to *BRAF* ^{V600K}.

Patient 338 was diagnosed with sigmoid colon cancer and synchronous hepatic metastasis. Moreover, routine pathology analysis revealed *KRAS* wild type in extracted tissue from the primary tumor. The patient received FOLFOX/cetuximab combination therapy for four months. One year after treatment, the patient presented with lung and hepatic metastasis. A blood sample was collected prior to liver metastasis resection surgery. EV-based ddPCR analysis detected resistant subclones to anti-*EGFR* therapy, harboring *KRAS* ^{G12D} mutation. With regard to both cases, a mutation switch after anti-*EGFR* or *BRAF/MEK* inhibitor therapy was detected prior to disease progression, validated via cancer staging or repeated tissue genotyping, providing a prognosis for a disease relapse.

10. DISCUSSION

This study confirmed successful mutational profiling in extracellular vesicles isolated from patient-derived plasma samples using droplet digital PCR. Thirty-four patients diagnosed with CRC, MM or NB were recruited for this study and with EV-based ddPCR analysis. DDPCR analyses were compared to tissue samples, indicating concordance rates of 54% and 44% in the CRC and MM cohort, respectively. Furthermore, EV-ddPCR analysis was detectable in only one of four NB patients, which also matched the tissue sequencing results. Two interesting cases in our patient cohort which imprinted on us that EV could demonstrate resistance as part of treatment monitoring are further discussed further in Section 9.5.

The existence of EV in biological fluids motivated the expansion of the established EV isolation protocol to also isolate EV from urine. Microscopic analysis on urinary EV hinted at the successful isolation of the vesicles. Proteomic and morphological characterization further described the ideal profile of the EV.

10.1 Isolation of extracellular vesicles

EV have been defined to have a density of 1.08-1.22 g/ml [164]. This information provided the opportunity to isolate the vesicles based on sucrose density gradient centrifugation. The samples were deposited at the top of a 2.0–0.25 M sucrose gradient, which was built into an ultracentrifuge tube. With the ultracentrifugal force, the different sample components settle to their designated isodensity zone, separating the vesicles from other components [165,166]. While satisfactory purity has been reported using this isolation method, there are other isolation techniques with shorter duration and higher end-product yield.

Another popular technique is size-based isolation via ultrafiltration, which separates particles solely depending on size or molecular weight. When isolated with this technique, larger vesicles when isolated with this technique could be sheared or deformed and therefore potentially affect analysis. Furthermore, vesicles could be trapped in the membrane filter resulting in a low yield of end product [168,169]. Size-exclusion chromatography (SEC) is another more reliable and more reproducible size-based isolation method which relies on gravity, thereby protecting the integrity of the vesicular structure [170,171]. This method produces highly purified vesicles and

can preserve the integrity, structure, and biological activity of the vesicles. Unfortunately, a dedicated instrument would need to be acquired [172].

Multiple commercially available kits are also commonly used for the isolation of extracellular vesicles, for instance Exoquick™ and Total Exosome Isolation Kit (Thermo Fischer Scientific, Massachusetts, USA), which enable quick and straight-forward isolation without the usage of specific devices. More sophisticated techniques including the ExoChip, a microfluidic device which has been utilized with different approaches for the capture of the vesicles [173]. Wang *et al.* utilized nanowires (ciliated micropillars) for vesicles segregation [174], while Davies *et al.* involved a PMMA-based (polymethyl methacrylate) membrane filter [175]. On the other hand, Chen *et al.* on the other hand approached the isolation with an immune-affinity-based capture using anti-CD63 antibody [176].

The classic approach for isolating EV is the differential centrifugation or ultracentrifugation technique. This comprises a serial centrifugation of different speeds to remove cells, cellular debris and larger vesicles [123]. This method is effective and also does not affect proteomic and nucleic acid components in the vesicles. Differential centrifugation, however, has technical drawbacks as it is labor intensive and entirely dependent on the availability of appropriate instruments in different research laboratories [177,178]. Furthermore, purification of the sample can be challenging as this method co-isolates other vesicles as well [179].

The most common isolation approach consists of classic ultracentrifugation, density gradients and filtration, or a combination of methods [6,180,181]. Although there are multiple isolation methods, and novel techniques are always being introduced, the possibilities of obtaining pure EV with less contaminant or EV restricted to population of interest are still far from being realized. Thus, more efficient isolation protocols are required.

Differential centrifugation was applied for the isolation of EV derived from cell lines and plasma samples in our study. The fundamental Théry protocol [123] was optimized, and through visualization with the transmission electron microscope, we settled with the adapted protocol which we found to have a reduction of cellular debris and heterogeneous vesicle population in the background.

10.2 Extracellular vesicles from urine

Proteomic characterization via western blot with tetraspanins CD9 and CD81 was successful for protein extracted from EV derived from cell lines and plasma samples. Furthermore, ddPCR analysis utilizing EV isolated from cell lines and plasma samples were also successful. However, both western blot and ddPCR analysis of EV urine samples were unexpectedly negative. EV were isolated from urine from neuroblastoma patients (10 milliliters per experiment), which was then analyzed with western blot, ddPCR and the whole-mount immunoelectron microscopy. EV from urine samples were microscopically visualized to be homogenously round, positively labeled with immunogold CD63 antibody, and smaller than 100 nm with a central depression. Western blot and ddPCR however was unsuccessful, with the assumption that a higher volume of urine was required for EV isolation to acquire a higher protein and nucleic acid concentration for subsequent analyzation.

Possibly, it was too ambitious to use only 10 milliliters of urine for the analysis. Multiple publications reported a higher volume of urine for EV isolation, for instance Pisitkun *et al*. pooled 400 milliliters of urine from six adult patients for proteomic analysis [182], Fernández-Llama *et al*. tested a urinary EV isolation protocol with 96 milliliters of urine [134], Zhou *et al.* reported the usage of 100 milliliters of urine for proteomic analysis [183] and lastly Cheng *et al.* successfully isolated EV from a minimum of 20 milliliters of urine [135], the lowest volume of urine in the list but still double the volume we were using. Furthermore, most groups used pooled urine samples, as the nucleic acid and proteomic content for EV urine is low and due to RNase activity in the urinary tract, a large proportion of degraded RNA was noticed in the urinary cell pellet [135].

Our target patient group for EV urine analysis was the pediatric neuroblastoma cohort, which complicated the collection of more than 10 milliliters of urine. As urine analysis to identify the markers homovanilic and vanillylmandelic acid is vital for clinical diagnostics [105,112], it was challenging to collect more than the mentioned volume or the urine collected was severely diluted due to high amount of infusion the patients received. EV urine analysis was unable to be repeated due to the end of the collaboration project.

10.3 Real-time PCR versus ddPCR

For many years, real-time PCR has assisted clinical settings with diagnostics especially in nucleic acid quantification and gene expression in the field of oncology, clinical microbiology, and gene therapy. Real-time PCR is a quantitative analysis based on the ratio of the cycle threshold (Cq values) to the enzymatic reaction curve [184]. Multiple factors like poorly optimized assays and sample quality could hinder the efficiency range of the standard curve, causing data misinterpretation and poor reproducibility [184,185].

ddPCR also uses Taq polymerase and a standard PCR reaction. The difference is that ddPCR partitions PCR reaction into 20,000 individual reactions and acquires end point data with either positive or negative calls for a single droplet [126]. ddPCR is more reliable as it is easily reproducible, precise and more sensitive even for low target concentrations and samples with possible contaminants [185].

Real-time PCR requires a housekeeping gene to normalize unknown samples, whereas for ddPCR normalization is unnecessary, as data are precise and accurate. Poor sample quality and samples with low concentration do not affect the analysis. Taylor *et al.* tested the effects of contaminants in samples and samples with low concentration on both ddPCR and qPCR. They reported that when it comes to low or no background contaminants, both systems gave a similar performance. However, ddPCR was more stable in detecting samples with low target abundance and higher levels of impurities [185].

Furthermore, ddPCR offers the opportunity to optimize multiplex assays for mutation screening. The in-house designed multiplex assays established in our group are not only cost efficient, but are also able to identify the mutation of interest based on the different clusters appearing at different amplitudes. In contrast to commercially available multiplex kits ,which are only able to provide a general screening of mutation availability and unable to identify specific mutations. Pender *et al.* investigated nine different KRAS mutations with a commercially purchased PrimePCR™ ddPCR™ Mutation Assays (Bio-Rad, California, USA) in non-small cell lung cancer patients [186]. They reported good separation in the multiplexed assays, but with the appearance of non-specific signals. Unlike the assays we designed, the commercial assays used by Pender *et al.* were not able to distinguish the different mutations based on clusters alone and only provided a yes or no answer to the availability of the different mutations in samples analyzed [186]. In-

house multiplex assays were also designed by Rowlands *et al.* using ddPCR with locked nucleic acid (LNA) base-oligos, whereas Taly *et al.* utilized non-fluorescent blockers and a different digital PCR platform, namely the RainDance Technology. Both groups reported optimal population separation on the 2D plot [187,188]. Multiplexed ddPCR assays were only used in our case as a quick screening solution prior to duplex assays. This is because when compared to duplex assays, it was noticed that using the same input volume, concentration and sample type resulted in less copies/µl in the multiplexed assays (results not shown). This could be due to the lower efficiency of the multiplex assays or competitiveness of the additional probes reducing fluorescent signals [153].

10.4 EV-based ddPCR patient analysis

The patient cohorts were comprised of 32 patients, with 2 patients in the early stages of the disease. MM and CRC patient cohorts underwent treatment during the sampling time; this was not necessary the case with the 4 NB patients recruited into the study. EV-based mutational analysis was compared to tissue samples regarding the oncogenes *BRAF, KRAS* and *ALK*. The study indicated a correlation between tumor tissues and EV of 44% and 55% for the MM and CRC cohorts, respectively. Only one of four tumor samples from the NB patients were sequenced and matched EV-based ddPCR results.

In data published previously byour group [189], CTCs were quantified and *KRAS* and *BRAF* oncogenes in cfDNA from 65 patients were analyzed and compared to tissue samples via ddPCR. Circulating cell-free DNA (cfDNA) was detectable in all patients, with 55% complementing those of the tissue samples. Concordance was mainly reported in stage IV and one patient from stage II with 2 of 10 patients with BRAF and 9 of 25 patients with *KRAS* mutation [189]. The overall concordance rates demonstrated the comparable utility of cfDNA (55%) and EV (54%) analysis for mutation detection in plasma samples from patients with CRC.

Three patients (patients 302, 338 and 356) from the study were included into the EV cohort, to directly compare both EV and cfDNA. In comparison to the cfDNA study, EV matched the gene status of the tumor more accurately, keeping in mind the humble number of patients. Patient 302 with a tissue gene status of $KRAS^{G12D}$ matched the ddPCR results of both cfDNA and EV. Nevertheless, patient 356 with a tissue gene status of $KRAS^{G12V}$ matched the EV ddPCR results,

whereas when analyzing cfDNA with ddPCR, only wild type was detected. Disease progression in patient 338 correlated with EV results, demonstrating a mutation switch, whereas only wild type was detected in cfDNA.

This correlates with the comparison of exoDNA (exosomes-derived DNA) and cfDNA with tissue profiling in pancreatic ductal adenocarcinoma patients,where it was reported that exoDNA exceeded cfDNA in *KRAS* detection of metastatic pancreatic cancer patients with 85% for exoDNA and 57.9% for cfDNA [10]. Möhrmann *et al.* compared cfDNA from advanced cancer patients via ddPCR and BEAMing digital PCR analysis and EV via next generation sequencing, targeting the oncogenes *BRAF* ^{V600} and *KRAS* $^{G12/G13}$. In this study, the concordance rate for EV and cfDNA were comparable. When compared to sequenced FFPE archival tissues, 95% of exosomes samples were in correlation with tissue samples. The concordance rate for cfDNA was 90% for ddPCR and 92% for BEAMing digital PCR [11].

10.5 Discordant results

Discordance can be explained by several limitations and a lack of uniformity while conducting the study. The study group was not only smaller than many other studies [10,11,190], but also consisted of various tumor entities with a variety of treatment options. Furthermore, the heterogeneous landscape of the tumor or the different time point of plasma sample and tissue collection could influence the inconsistent results. Blood samples were collected after patients received the allocated therapy with a median time of 6 months between pre-treatment tissue sampling and post-treatment blood collection. Thus, it was explored whether extracellular vesicles could provide information on how the treatment affects the disease. Discrepancies when analyzing gene status in exo-nucleic acid and archival tissue samples due to different time points of plasma samples and tissue collection were reported by Möhrman *et al.* [11]. A discordance rate of 5% between exo-nucleic acid and archival tissues was reported, and in comparison to our study the duration between blood and sample collection was much longer (median time difference: 20 months) [11], whereas we have reported a median time difference of six months.

Intratumor heterogeneity has been reported in all three tumor entities (CRC, MM and NB). The information transmitted is dependent on the cell of origin in which vesicles were released from, either from synchronous primary tumors within the same patient or between primary tumor and

metastasis [191,192]. Furthermore, the operative extraction of tumor tissues stems from only a single geographic location and does not represent the possible mutation variability actually expressed by the disease [193]. On the other hand, EV appear to capture events not represented in tumor tissue, suggesting the ability to capture heterogeneous events not profiled in a single tissue biopsy [78]. Intratumor heterogeneity is no longer an exception, but a characteristic feature in high grade tumor. Therefore, it is now of importance for it to be evaluated for biomarker or drug studies.

10.6 Limitations in the pediatric neuroblastoma cohort

Neuroblastoma (NB) is the hallmark for high cellular heterogeneity and entails a wide range of low-frequency mutations [194]. NB heterogeneous attributes which influence the broad clinical presentation 'mark' this disease as an interesting study subject. However, due to the low-frequency mutations it was challenging to detect mutations of interest in the small cohort recruited (only four patients were successfully recruited). Therefore, of the four patients, only one patient was positive for the *ALK* ^{F1174L} mutation, complementing the corresponding tissue analysis.

In comparison to adult cancer diseases, NB proved to be challenging in terms of sample collection, being a pediatric illness. Ten milliliters of blood was collected from patients of both CRC and MM cohorts, while only three to five milliliters of blood was collected from pediatric NB patients. Furthermore, the blood volume was not solely employed for the EV studies but shared for the diagnostics of CTCs. The low blood volume complicated the analyzation by the significant reduction of proteomic and nucleic acid concentration. Urine samples collected from NB patients were limited to ten milliliters, a much lower volume in comparison to volumes used by other EV research groups [134,135,182,183]. The initial low sample volume contributed to the non-detectability of some samples during analysis of EV.

10.7 Clonal evolution

Targeted therapy interrupts the signaling pathway or receptors, weakening cancer progression, seeking a balance between killing cancer cells and sparing off-target side effects [195]. The initial promise of improved patient survival and tumor regression was subsequently met with secondary resistance. Due to genetic variations, cancer cells can evolve and adapt to the treatment, thereby dysregulating the immune system or developing a different mechanism to evade immune recognition, thus inevitably causing disease relapse and ineffectiveness of the targeted therapy[65].

Clinical trials demonstrated improved progression-free survival and overall survival in melanoma patients who received selective *BRAF* (dabrafenib, vemurafenib) and *MEK* (trametinib) inhibitors in comparison to systemic therapy, for instance dacarbazine, interferon or interleukin-2 [196]. The COMBI-AD study demonstrated an improved recurrence-free survival rate of 58% versus 39% at 3 years and an improved overall survival of 86% versus 77% when comparing dabrafenib/trametinib combination therapy versus two placebos in fully resected high-risk stage 3 melanoma [104]. Unavoidably, subclonal activation occurred at a median rate of 4 to 7 months post treatment [197]. This then caused a mutation shift, proliferation of the subclones and eventually their detection by mutational testing. Van Allen *et al.* sequenced tissue samples originating from *BRAF* ^{V600} mutant advanced melanoma patients and reported genetic alterations in the *MAPK(ERK)* signal transduction pathway in 51% of the patient cohort [98,198]. This was noticed in Case 16, who demonstrated significant progress ten months after treatment pause and the presence of a mutation switch *(BRAF* ^{V600E} to *BRAF* ^{V600K}). Contrarily to the sequenced pre-*BRAF/MEK* inhibitor-treatment tissue, EV-based analysis demonstrated *BRAF* ^{V600K} mutation. Interestingly, the EV-ddPCR results were reconfirmed with the sequencing results of newly biopsied submammary metastatic skin tissue.

Anti-epidermal growth factor receptor (anti-*EGFR*) inhibitor cetuximab was approved as a first line therapy to be used as a single agent or in combination with standard chemotherapy for metastatic CRC patients who are intolerant to chemotherapy, *EGFR* expressing or *RAS* wild type [199]. Clinical trials demonstrated that cetuximab in combination with FOLFOX versus FOLFOX alone improved patient's overall survival (23.5 versus 20 months) and improved progression-free survival (9.9 versus 8.4 months) [200]. However, patients appeared to acquire secondary resistance

upon cetuximab withdrawal. Molecular alterations occurred in colorectal cancer that are *RAS* wild type at baseline, eventually shifting to a mutated status resulting in a secondary resistance to anti-*EGFR* therapy [201]. The acquired resistance was noticed in our study in Case 338 when we made comparison via EV-ddPCR analysis one year after cetuximab treatment and with primary tumor tissue biopsied prior to the administration of anti-*EGFR* monoclonal antibody. This disease progression was interestingly not detectable in our cfDNA study [189]. In both cases from MM and CRC patient cohort, EV-ddPCR indicated the mutation switch before known disease progression, detected either by disease staging or routine tissue sequencing analysis.

10.8 Challenges in extracellular vesicle research

Research on extracellular vesicles has grown rapidly in the past decade; substantial research and progress has been made despite frustrations occurring. There is a lack of uniformity when it comes to EV research. The appearance of different isolation methods and biofluid collection could result in different results and efficiency regarding the sample analysis. This induces interlaboratory variability, regarding the accuracy and sensitivity of the EV diagnostics [202]. Furthermore, the protocol for EV isolation is time consuming and may not be convenient when it comes to clinical settings. Recently, EV have been targeted to be studied as a drug delivery system. However, trials will need to be conducted thorougly to validate the purity before implementation.

A major problem in EV research is the low yield of nucleic acid and protein extracted from the vesicles. Concentrations of EV, whether nucleic acid or protein, are expected to be in a certain range, although this is not a standard.Typically, one µg of protein could be extracted from one milliliter of culture medium, and even less when it comes to patients' biofluid [203,204].

Furthermore, detected EV are heterogeneous, and to date it is not possible to track the parent cell which EV are released from [205]. Studies have reported different subpopulations and vesicular content could vary based on different anticoagulants in blood tubes [160] and different isolation methods [167,206].

Our study depicts the value of extracellular vesicles as a notable liquid biopsy component and this was highlighted with the discordant cases. The mutation switch after anti-*EGFR* or *BRAF/MEK* inhibitor therapy mirrored in the extracellular vesicles isolated from patients' plasma has important implications for the ability of EV to provide information on the heterogenous landscape of the disease, therefore providing necessary information for disease prognosis and therapy planning.

11. FUTURE PERSPECTIVES

Extracellular vesicles, when compared to the intricate isolation and rarity of CTCs in the bloodstream and the high wild-type DNA background when analyzing cfDNA, are an efficient partner for liquid biopsy diagnostics [66]. EV have the potential to be used alongside or independent from other liquid biopsy markers as a quick cancer screening or real-time disease and treatment monitoring tool. Tissue biopsy will most probably remain as a gold standard for disease monitoring in the years to come. However, the inclusion of liquid biopsy markers could provide more thorough information on the heterogeneous characteristics of the disease missed by tissue genotyping. Furthermore, due to the minimal invasiveness with only a simple blood draw, it would be less of a hassle to have repetitive tests in comparison to operative retrieval of the tumor tissue. Despite only being isolated from blood like CTCs and their abundance in other biofluids, EV allow for a wider range of diagnostic sources [24]. While CTCs and cfDNA diagnostics acquired U.S.A Food and Drug Administration (FDA) approval for certain tumor entities [207,208], EV being proven competent is still at its infancy in the field of liquid biopsy. Larger clinical trials are required to validate the different components of liquid biopsy for it to reach its full potential and assist disease management in clinical settings.

The multiple functions featured in EV have allowed for the venture of appointing EV as a therapeutic platform. EV biogenesis pathways garnered interest and pathways were explored to reduce production, release and EV uptakes. For further elaboration, ceramide is vital in the ESCRT pathway and therefore plays an important role in EV biogenesis [209]. The synthesis of ceramide can be inhibited by the introduction of neutral sphingomyelinase 2 (nSMase2), which successfully decreases miR-10b transfer via EV in breast cancer and diminishes miR-10b cell proliferation in recipient cells [210].

EV are most praised for their role in intercellular communication, and have therefore has been studied regarding loading drugs into the nanostructures and transporting the drugs to their designated location. Kim *et al*. demonstrated the encapsulation of paclitaxel in macrophage-derived exosomes (exoPTX) via sonification. The exoPTX gathered in cancer cells and reduced metastasis when compared to counterparts like liposomes and polymer-based carriers [211]. Doxorubicin was successfully encapsulated into EV with electroporation and tested on breast cancer cell lines, leading to reduced toxicity, immunogenicity and tumor growth [212].

The current EV purification technologies are limited, restricting the implementation of using EV as a possible oncology treatment. A reliable, reproducible, fast and cost-effective EV manufacturing platform needs to be set up for this hypothetical therapeutic option to be realized.

12. CONCLUSION

Liquid biopsy provides a comprehensive profiling of the oncogenic genes, and the mechanism of metastasis and therapy resistance [3,5,6]. It could further complement tissue biopsy, which only provides information from areas where tissue was extracted [3]. EV serve as an important liquid biopsy component due to their role as an intracellular information shuttle and stable carriers of cellular information in the circulation. These vesicles have been reported to play a role in therapy resistance and potentially provide organ-specific metastatic information depending on the cell of origin which the EV were released from [2,7].

Extracellular vesicles were initially isolated from cell line supernatant via differential centrifugation, then eventually ventured to biofluids (plasma and urine). EV were studied as a feasible liquid biopsy component and the mutational status of EV in plasma was compared to tissue samples. Proteomic characterization demonstrated the enrichment of tetraspanins CD9 and CD81 in EV samples isolated from cell lines and plasma samples. Morphological characterization assisted with immunogold CD63 labeling described the vesicles of interest as CD63 positive, 10-100 nm, and ranging from spherical to round in shape.

Urine-based EV were successfully isolated and visible with the whole mount immunoelectron microscope. Application of urinary EV was unsuccessful in protein and PCR-based analysis due to the inadequately low volume of samples collected. This was unable to be tested again due to the end of the collaboration project.

Multiplexing with ddPCR was introduced to maximize sample usage and to be used as a potential screening platform for patient samples. The multiplex assays were superior to commercial assays because the exact mutation could be defined. However, in comparison to duplex ddPCR assays, copy numbers fluctuate for identical sample. This could be due to the fluorescence competition of the different probes.

EV were analyzed for their mutational load in plasma samples isolated from patients of the CRC, MM and NB cohorts. Here, the novel method of Droplet Digital^{TM} PCR was utilized, demonstrating a concordance of 44% and 55% with MM and CRC patient cohorts, respectively. Furthermore, one out of four NB patients was positive for *ALK* ^{F1174L} via ddPCR-EV analysis, which also matched the sequenced tumor tissue.

The discordance reported could be influenced by several factors, for example the limited number of patients recruited, the variety of tumor entities included in the study and the different treatment received by patients. The intertumoral heterogeneity detected in blood-based biomarkers could have differed from the mutations found in biopsied tissues. Furthermore, the medical backgrounds of patients 16 and 338 were highlighted to demonstrate that EV were able recognize clonal evolution in terms of mutational switch prior to clinical evidence after prescription of *BRAF/MEK* inhibitor and anti-*EGFR* therapy.

Instead of looking at patients as a single entity, medicine has evolved to introduce personalized medicine based on different genetic subsets. Liquid biopsy, being a part of personalized medicine, could collaborate with standard clinical diagnostics for real-time monitoring of the disease and treatment monitoring. Extracellular vesicles, initially only a rubbish truck removing cellular waste out of the way, are now a vital member of the liquid biopsy team, and not only confined for disease surveillance but also as a nano-drug delivery system.

13. REFERENCES

1. Pantel K and Alix-Panabieres C. Liquid biopsy and minimal residual disease - latest advances and implications for cure. *Nat. Rev. Clin. Oncol.*, vol. 16, no. 7, pp. 409–4242019.
2. Lo Cicero A, Stahl PD, Raposo G. Extracellular vesicles shuffling intercellular messages: for good or for bad. *Current opinion in cell biology,* 35: 69-77, 2015.
3. Babayan A, Pantel K. Advances in liquid biopsy approaches for early detection and monitoring of cancer. *Genome Med.,* 10(1):21, 2018.
4. Heijnen HF, Schiel AE, Fijnheer R, Geuze HJ, Sixma JJ. Activated platelets release two types of membrane vesicles: microvesicles by surface shedding and exosomes derived from exocytosis of multivesicular bodies and alpha-granules. *Blood,* 94(11):3791–9, 1999.
5. Xu X, Lai Y, Hua ZC. Apoptosis and apoptotic body: disease message and therapeutic target potentials. *Biosci. Rep.*, 39 (1): BSR20180992, 2019.
6. Pan BT, Johnstone RM. Fate of the transferrin receptor during maturation of sheep reticulocytes in vitro: selective externalization of the receptor. *Cell,* 33(3):967–78, 1983.
7. Harding C, Heuser J, Stahl P. Receptor-mediated endocytosis of transferrin and recycling of the transferrin receptor in rat reticulocytes. *J. Cell Biol*.,97(2):329–39,1983.
8. Demory Beckler M, Higginbotham JN, Franklin JL, Ham AJ, Halvey PJ, Imasuen IE, Whitwell C, Li M, Liebler DC, Coffey RJ .Proteomic analysis of exosomes from mutant KRAS colon cancer cells identifies intercellular transfer of mutant KRAS. *Mol. Cell Proteomics,* 12(2):343–55, 2013.
9. Kowal J, Tkach M, Théry C. Biogenesis and secretion of exosomes. *Current Opinion in Cell Biology, Elsevier*, 2014, 29, pp.116-125,10.1016/j.ceb.2014.05.004, 2014.
10. Barile L, Moccetti T, Marbán E, Vassalli G. Roles of exosomes in cardioprotection. *Eur. Heart J.,* 38(18):1372–9, 2017.
11. Mizutani K, Kawakami K, Horie K, Fujita Y, Kameyama K, Kato T, Nakane K, Tsuchiya T, Yasuda M, Masunaga K, Kasuya Y. Urinary exosome as a potential biomarker for urinary tract infection. *Cellular Microbiology,* 21:e13020, 2019.
12. Castaño C, Novials A, Párrizas M. Exosomes and diabetes. *Diabetes Metab. Res. Rev.,*35(3):e3107, 2019.
13. Allenson K, Castillo J, San Lucas FA, Scelo G, Kim DU, Bernard V, Davis G, Kumar T, Katz M, Overman MJ, Foretova L. High prevalence of mutant KRAS in circulating exosome-derived DNA from early-stage pancreatic cancer patients. *Ann. Oncol.,*28(4):741–7,2017.
14. Möhrmann L, Huang HJ, Hong DS, Tsimberidou AM, Fu S, Piha-Paul SA, Subbiah V, Karp DD, Naing A, Krug A, Enderle D. Liquid biopsies using plasma exosomal nucleic acids and plasma cell-free DNA compared with clinical outcomes of patients with advanced cancers. *Clin. Cancer Res.*,24(1):181–8,2018.
15. Gould SJ, Raposo G. As we wait: coping with an imperfect nomenclature for extracellular vesicles. *J. Extracell. Vesicles,* 2:10.3402/jev.v2i0.20389,2013.
16. Morwood J. The pocket Oxford Classical Greek Dictionary. Cambridge, UK: Oxford University Press; 449 p.,2002.
17. Chen T, Wang C, Yu H, Ding M, Zhang C, Lu X, Zhang CY, Zhang C. Increased urinary exosomal microRNAs in children with idiopathic nephrotic syndrome. *EBioMedicine*, 39:552–61,2019.
18. Zhang X, Yuan X, Shi H, Wu L, Qian H, Xu W. Exosomes in cancer: small particle, big player. *J Hematol. Oncol.,*8:83,2015.
19. Théry C, Witwer KW, Aikawa E, Alcaraz MJ, Anderson JD, Andriantsitohaina R, Antoniou A, Arab T, Archer F, Atkin-Smith GK, Ayre DC. Minimal information for studies of extracellular vesicles 2018 (MISEV2018): a position statement of the International Society for Extracellular Vesicles and update of the MISEV2014 guidelines. *J. Extracell. Vesicles*, 7(1):1535750, 2018.
20. Sahu R, Kaushik S, Clement CC, Cannizzo ES, Scharf B, Follenzi A, Potolicchio I, Nieves E, Cuervo AM, Santambrogio L. Microautophagy of cytosolic proteins by late endosomes. *Dev. Cell,* 20(1):131–9,2011.
21. Théry C, Zitvogel L, Amigorena S. Exosomes: composition, biogenesis and function. *Nat. Rev. Immunol.,* **2,** 569–579,2002.
22. Hurley JH, Hanson PI. Membrane budding and scission by the ESCRT machinery: it's all in the neck. *Nat. Rev. Mol. Cell Biol.*, 11(8):556-566, 2010.
23. Trajkovic K, Hsu C, Chiantia S, Rajendran L, Wenzel D, Wieland F, Schwille P, Brügger B, Simons M. Ceramide triggers budding of exosome vesicles into multivesicular endosomes. *Science*, 319.5867:1244–7, 2008.
24. de Gassart A, Géminard C, Février B, Raposo G, Vidal M. Lipid raft-associated protein sorting in exosomes. *Blood,* 102.13,4336-4344, 2003.

25. Van Niel G, Charrin S, Simoes S, Romao M, Rochin L, Saftig P, Marks MS, Rubinstein E, Raposo G. The tetraspanin CD63 regulates ESCRT-independent and -dependent endosomal sorting during melanogenesis. *Dev. Cell*, 21(4):708–21,2011.
26. Andreu Z, Yáñez-Mó M. Tetraspanins in extracellular vesicle formation and function. *Front. Immunol.*,5, 442,2014.
27. Bebelman MP, Smit MJ, Pegtel DM, Baglio SR. Biogenesis and function of extracellular vesicles in cancer. *Pharmacol. Ther.,*188:1–11,2018.
28. McKelvey KJ, Powell KL, Ashton AW, Morris JM, McCracken SA. Exosomes: mechanisms of uptake. *Journal of circulating biomarkers*, *4*, 7, 2015.
29. Bobrie A, Colombo M, Raposo G, Théry C. Exosome Secretion: Molecular Mechanisms and Roles in Immune Responses. Vol. 12, *Traffic*, *12* (12), pp.1659-1668, 2011.
30. Ostrowski M, Carmo NB, Krumeich S, Fanget I, Raposo G, Savina A, Moita CF, Schauer K, Hume AN, Freitas RP, Goud B. Rab27a and Rab27b control different steps of the exosome secretion pathway. *Nat. Cell Biol., 12*(1), pp.19-30, 2010.
31. Hsu C, Morohashi Y, Yoshimura SI, Manrique-Hoyos N, Jung S, Lauterbach MA, Bakhti M, Grønborg M, Möbius W, Rhee J, Barr FA. Regulation of exosome secretion by Rab35 and its GTPase-activating proteins TBC1D10A-C. *J. Cell Biol.,*189(2):223–32,2010.
32. Wu Y, Wu W, Wong WM, Ward E, Thrasher AJ, Goldblatt D, Osman M, Digard P, Canaday DH, Gustafsson K. Human gamma delta T cells: a lymphoid lineage cell capable of professional phagocytosis. *J. Immunol.,*183(9):5622–9, 2009.
33. Tian T, Zhu YL, Zhou YY, Liang GF, Wang YY, Hu FH, Xiao ZD. Exosome uptake through clathrin-mediated endocytosis and macropinocytosis and mediating miR-21 delivery. *J. Biol. Chem.,*289(32):22258–67,2014.
34. Wajant H, Moosmayer D, Wüest T, Bartke T, Gerlach E, Schönherr U, Peters N, Scheurich P, Pfizenmaier K. Differential activation of TRAIL-R1 and -2 by soluble and membrane TRAIL allows selective surface antigen-directed activation of TRAIL-R2 by a soluble TRAIL derivative. *Oncogene,* 20(30):4101–6, 2001.
35. Taylor DD, Gerçel-Taylor C, Lyons KS, Stanson J, Whiteside TL. T- Cell apoptosis and suppression of T-cell receptor/CD3-zeta by Fas ligand-containing membrane vesicles shed from ovarian tumors. *Clin. Cancer Res.,*9(14):5113–9, 2003.
36. Campos A, Salomon C, Bustos R, Díaz J, Martínez S, Silva V, Reyes C, Díaz-Valdivia N, Varas-Godoy M, Lobos-González L, Quest AF. Caveolin-1-containing extracellular vesicles transport adhesion proteins and promote malignancy in breast cancer cell lines. *Nanomedicine*,13(20), 2018.
37. Chen M, Xu R, Rai A, Suwakulsiri W, Izumikawa K, Ishikawa H, Greening DW, Takahashi N, Simpson RJ. Distinct shed microvesicle and exosome microRNA signatures reveal diagnostic markers for colorectal cancer. *PLoS One,* 14(1):e0210003,2019.
38. Rabinowits G, Gercel-Taylor C, Day JM, Taylor DD, Kloecker GH. Exosomal microRNA: a diagnostic marker for lung cancer. *Clin. Lung Cancer,*2009;10(1):42–6,2019.
39. Matsuno Y, Kanke T, Maruyama N, Fujii W, Naito K, Sugiura K. Characterization of mRNA profiles of the exosome-like vesicles in porcine follicular fluid. *PLoS One*, 14(6):e0217760,2019.
40. Thakur BK, Zhang H, Becker A, Matei I, Huang Y, Costa-Silva B, Zheng Y, Hoshino A, Brazier H, Xiang J, Williams C. Double-stranded DNA in exosomes: a novel biomarker in cancer detection. *Cell Res.,*24(6):766–9, 2014.
41. Sun Y, Huo C, Qiao Z, Shang Z, Uzzaman A, Liu S, Jiang X, Fan LY, Ji L, Guan X, Cao CX. Comparative Proteomic Analysis of Exosomes and Microvesicles in Human Saliva for Lung Cancer. *J. Proteome Res.,*17(3):1101–7, 2018.
42. Palazzolo G, Albanese NN, Di Cara G, Gygax D, Vittorelli ML, Pucci-Minafra I. Proteomic analysis of exosome-like vesicles derived from breast cancer cells. *Anticancer Res.*,32(3):847–60,2012.
43. Cheruiyot C, Pataki Z, Ramratnam B, Li M. Proteomic Analysis of Exosomes and Its Application in HIV-1 Infection. Vol. 12, *Proteomics - Clinical Applications. 12*(5), p.1700142, 2018.
44. Keerthikumar S, Chisanga D, Ariyaratne D, Al Saffar H, Anand S, Zhao K, Samuel M, Pathan M, Jois M, Chilamkurti N, Gangoda L. ExoCarta: A Web-Based Compendium of Exosomal Cargo. *J. Mol. Biol.,*428(4):688–92,2016.
45. Helwa I, Cai J, Drewry MD, Zimmerman A, Dinkins MB, Khaled ML, Seremwe M, Dismuke WM, Bieberich E, Stamer WD, Hamrick MW. A Comparative Study of Serum Exosome Isolation Using Differential Ultracentrifugation and Three Commercial Reagents. *PLoS One*, 12(1):e0170628–e0170628,2017.
46. Lim JH, Lee CH, Kim KY, Jung HY, Choi JY, Cho JH, Park SH, Kim YL, Baek MC, Park JB, Kim YH. Novel urinary exosomal biomarkers of acute T cell-mediated rejection in kidney transplant recipients: A cross-sectional study. *PLoS One*, 13(9):e0204204,2018.
47. Welton JL, Loveless S, Stone T, von Ruhland C, Robertson NP, Clayton A. Cerebrospinal fluid extracellular vesicle enrichment for protein biomarker discovery in neurological disease; multiple sclerosis. *J. Extracell. vesicles,* 6(1):1369805,2017.
48. Huang, X., Hu, X., Zhao, M. and Zhang, Q. Analysis of salivary exosomal proteins in young adults with severe periodontitis. *Oral*

Diseases, *26*(1), pp.173-181, 2020.

49. Ståhl AL, Arvidsson I, Johansson KE, Chromek M, Rebetz J, Loos S, Kristoffersson AC, Békássy ZD, Mörgelin M, Karpman D. A novel mechanism of bacterial toxin transfer within host blood cell-derived microvesicles. *PLoS Pathog*., 11(2):e1004619, 2015.
50. Bhatnagar S, Shinagawa K, Castellino FJ, Schorey JS. Exosomes released from macrophages infected with intracellular pathogens stimulate a proinflammatory response in vitro and in vivo. *Blood*, 110(9):3234–44,2007.
51. Heijnen HFG, Schiel AE, Fijnheer R, Geuze HJ, Sixma JJ. Activated platelets release two types of membrane vesicles: Microvesicles by surface shedding and exosomes derived from exocytosis of multivesicular bodies and a-granules. *Blood*, 94(11):3791–9, 1999.
52. Spronk HMH, Ten Cate H, Van Der Meijden PEJ. Differential roles of Tissue Factor and Phosphatidylserine in activation of coagulation. *Thromb. Res.,* 133, pp.S54-S56,2014.
53. Zarà M, Guidetti GF, Camera M, Canobbio I, Amadio P, Torti M, Tremoli E, Barbieri SS. Biology and Role of Extracellular Vesicles (EV) in the Pathogenesis of Thrombosis. *Int. J. Mol. Sci.,*20(11):2840, 2019.
54. Boilard E. Extracellular vesicles and their content in bioactive lipid mediators: more than a sack of microRNA. J. *Lipid Res*., 59(11):2037–46,2018.
55. Abd Elmageed ZY, Yang Y, Thomas R, Ranjan M, Mondal D, Moroz K, Fang Z, Rezk BM, Moparty K, Sikka SC, Sartor O. Neoplastic reprogramming of patient-derived adipose stem cells by prostate cancer cell-associated exosomes. *Stem Cells,* 32(4):983–97, 2014.
56. Melo SA, Sugimoto H, O'Connell JT, Kato N, Villanueva A, Vidal A, Qiu L, Vitkin E, Perelman LT, Melo CA and Lucci A. Cancer exosomes perform cell-independent microRNA biogenesis and promote tumorigenesis. *Cancer cell, 26*(5), pp.707-721, 2014.
57. Roccaro AM, Sacco A, Maiso P, Azab AK, Tai YT, Reagan M, Azab F, Flores LM, Campigotto F, Weller E, Anderson KC. BM mesenchymal stromal cell-derived exosomes facilitate multiple myeloma progression. *J. Clin. Invest.,*123(4):1542–55, 2013.
58. Soldevilla B, Rodríguez M, San Millán C, García V, Fernández-Periañez R, Gil-Calderón B, Martín P, García-Grande A, Silva J, Bonilla F, Domínguez G. Tumor-derived exosomes are enriched in ΔNp73, which promotes oncogenic potential in acceptor cells and correlates with patient survival. *Hum. Mol. Genet*., 23(2):467–78,2014.
59. Umezu T, Ohyashiki K, Kuroda M, Ohyashiki JH. Leukemia cell to endothelial cell communication via exosomal miRNAs. *Oncogene,* 32(22):2747–55, 2013.
60. Tadokoro H, Umezu T, Ohyashiki K, Hirano T, Ohyashiki JH. Exosomes derived from hypoxic leukemia cells enhance tube formation in endothelial cells. *J. Biol. Chem.,*288(48):34343–51, 2013.
61. Umezu T, Tadokoro H, Azuma K, Yoshizawa S, Ohyashiki K, Ohyashiki JH. Exosomal miR-135b shed from hypoxic multiple myeloma cells enhances angiogenesis by targeting factor-inhibiting HIF-1. *Blood,* 124(25):3748–57, 2014.
62. Hoshino A, Costa-Silva B, Shen TL, Rodrigues G, Hashimoto A, Mark MT, Molina H, Kohsaka S, Di Giannatale A, Ceder S, Singh S. Tumour exosome integrins determine organotropic metastasis. *Nature*, 527(7578):329–35, 2015.
63. Chen G, Huang AC, Zhang W, Zhang G, Wu M, Xu W, Yu Z, Yang J, Wang B, Sun H, Xia H. Exosomal PD-L1 contributes to immunosuppression and is associated with anti-PD-1 response. *Nature*, *560*(7718), pp.382-386, 2018.
64. Wang J, Hendrix A, Hernot S, Lemaire M, De Bruyne E, Van Valckenborgh E, Lahoutte T, De Wever O, Vanderkerken K, Menu E. Bone marrow stromal cell-derived exosomes as communicators in drug resistance in multiple myeloma cells. *Blood,* 124(4):555–66, 2014.
65. Battke C, Ruiss R, Welsch U, Wimberger P, Lang S, Jochum S, Zeidler R. Tumour exosomes inhibit binding of tumour-reactive antibodies to tumour cells and reduce ADCC. *Cancer Immunol. Immunother*.,60(5):639–48, 2011.
66. König IR, Fuchs O, Hansen G, von Mutius E, Kopp M V. What is precision medicine? *Eur. Respir. J.,* 50(4), 2017.
67. Greaves M, Maley CC. Clonal evolution in cancer. Vol. 481, *Nature*. 2012. p. 306–13.
68. Spranger S, Gajewski TF. Tumor-intrinsic oncogene pathways mediating immune avoidance. *Oncoimmunology*, 5(3):e1086862, 2016.
69. Brock G, Castellanos-Rizaldos E, Hu L, Coticchia C, Skog J. Liquid biopsy for cancer screening, patient stratification and monitoring. *Transl. Cancer Res.*,4(3):280–90, 2015.
70. Zhang Y, Liu Y, Liu H, Tang WH. Exosomes: Biogenesis, biologic function and clinical potential.*Cell & bioscience*, *9*(1), p.19, 2019.
71. Neumann MHD, Bender S, Krahn T, Schlange T. ctDNA and CTCs in Liquid Biopsy – Current Status and Where We Need to Progress. *Computational and structural biotechnology journal*, *16*, pp.190-195, 2018.
72. Miller MC, Doyle G V, Terstappen LWMM. Significance of Circulating Tumor Cells Detected by the CellSearch System in Patients with Metastatic Breast Colorectal and Prostate Cancer. *J. Oncol.,*617421, 2010.
73. Douma S, Van Laar T, Zevenhoven J, Meuwissen R, Van Garderen E, Peeper DS. Suppression of anoikis and induction of metastasis by the neurotrophic receptor TrkB. *Nature*, 430(7003):1034–9, 2004.

74. Mitchell MJ, King MR. Computational and experimental models of cancer cell response to fluid shear stress. *Front. Oncol.,* 3:44, 2013.
75. Jie XX, Zhang XY, Xu CJ. Epithelial-to-mesenchymal transition, circulating tumor cells and cancer metastasis: Mechanisms and clinical applications. *Oncotarget*, *8*(46), p.81558, 2017.
76. Lu D, Graf RP, Harvey M, Madan RA, Heery C, Marte J, Beasley S, Tsang KY, Krupa R, Louw J, Wahl J. Detection and Characterization of Circulating Tumour Cells from Frozen Peripheral Blood Mononuclear Cells. *Journal of circulating biomarkers*, *4*, p.4, 2015.
77. Kustanovich A, Schwartz R, Peretz T, Grinshpun A. Life and death of circulating cell-free DNA. Vol. 20, *Cancer biology & therapy*, *20*(8), pp.1057-1067, 2019.
78. Cohen JD, Li L, Wang Y, Thoburn C, Afsari B, Danilova L, Douville C, Javed AA, Wong F, Mattox A, Hruban RH.Detection and localization of surgically resectable cancers with a multi-analyte blood test.*Science*, 359(6378):926-930, 2018.
79. Samanta S, Rajasingh S, Drosos N, Zhou Z, Dawn B, Rajasingh J. Exosomes: New molecular targets of diseases. *Acta Pharmacologica Sinica* 39.4: 501-513, 2018.
80. Onódi Z, Pelyhe C, Terézia Nagy C, Brenner GB, Almási L, Kittel Á, Manček-Keber M, Ferdinandy P, Buzás EI, Giricz Z. Isolation of High-Purity Extracellular Vesicles by the Combination of Iodixanol Density Gradient Ultracentrifugation and Bind-Elute Chromatography From Blood Plasma. *Front. Physiol.,* 9:1479, 2018.
81. Dan L. Longo MD. Harrisons Hämatologie und Onkologie. second. Berlin, Deutschland: ABW Wissenschaftsverlagsgesellschaft mbH (Verlag); 946 p., 2016.
82. Robert Koch-Institution. Colorectal cancer ICD-10 C18-21,Zentrum für Krebsregisterdaten. 2016.
83. Iacopetta B. Are there two sides to colorectal cancer*? Int. J. cancer*, 101(5):403–8, 2002.
84. Benedix F, Kube R, Meyer F, Schmidt U, Gastinger I, Lippert H. Comparison of 17,641 patients with right- and left-sided colon cancer: Differences in epidemiology, perioperative course, histology, and survival. *Dis Colon Rectum*, 53(1):57–64, 2010.
85. Hutchins G, Southward K, Handley K, Magill L, Beaumont C, Richman S, Seymour MT, Kerr DJ, Gray RG, Quirke P, QUASAR Collaborative Group. Value of mismatch repair, KRAS, and BRAF mutations in predicting recurrence and benefits from chemotherapy in colorectal cancer. *J. Clin. Oncol.,* 29(10):1261–70, 2011.
86. Lan YT, Jen-Kou L, Lin CH, Yang SH, Lin CC, Wang HS, Chen WS, Lin TC, Jiang JK, Chang SC. Mutations in the RAS and PI3K pathways are associated with metastatic location in colorectal cancers. *J. Surg. Oncol.,* 111(7):905–10, 2015.
87. Ghidini M, Petrelli F, Tomasello G. Right Versus Left Colon Cancer: Resectable and Metastatic Disease. *Curr. Treat Options Oncol.,* 19(6):31, 2018.
88. American Joint Committee on cancer. AJCC Cancer Staging Manual. seventh. Edge Stephen B., Byrd David R., Compton Carolyn C., Fritz April G., Greene Frederick L. TA, editor. Chicago, IL, USA: Springer New York Dordrecht Heidelberg London, 672 p.,2015.
89. Akkoca AN, Yanık S, Özdemir ZT, Cihan FG, Sayar S, Cincin TG, Çam A, Özer C. TNM and Modified Dukes staging along with the demographic characteristics of patients with colorectal carcinoma. *Int. J. Clin. Exp. Med.,* 7(9):2828–35, 2014.
90. DiPiro JT, Talbert RL, Yee GC, Matzke GR, Weils BG PL. Pharmacotherapy: A Pathophysiologic Approach. tenth. Weitz Michael K, Brian, editors. United States of America: McGraw-Hill Education; 2017.
91. Lynch HT, Snyder CL, Shaw TG, Heinen CD, Hitchins MP. Milestones of Lynch syndrome: 1895-2015. *Nat. Rev. Cancer*,15(3):181–94, 2015.
92. Jafar nouri nojadeh, shahin behrouz sharif ebrahim sakhinia. Microsatellite instability in colorectal cancer. *EXCLI journal*, 17,159, 2018.
93. Tate JG, Bamford S, Jubb HC, Sondka Z, Beare DM, Bindal N, Boutselakis H, Cole CG, Creatore C, Dawson E, Fish P. COSMIC: The Catalogue Of Somatic Mutations In Cancer. *Nucleic Acids Res.,* 47(D1):D941–7, 2019.
94. AWMF. Leitlinienprogramm Onkologie (Deutsche Krebsgesellschaft, Deutsche Krebshilfe, AWMF): S3-Leitlinie Kolorektales Karzinom, Langversion 2.1. Berlin, p. 328, 2019.
95. Park T, Choi C ju, Choi Y, Suh DC. Cost-effectiveness of cetuximab for colorectal cancer. *Expert Rev Pharmacoeconomics Outcomes Res.,*16(6):667–77, 2016.
96. Bevacizumab (Antineoplastic). LiverTox: Clinical and Research Information on Drug-Induced Liver Injury.Bethesda (MD): National Institute of Diabetes and Digestive and Kidney Diseases, 2012.
97. Inos E, Swetter SM, Cockburn MG, Colditz GA, Clarke CA. Increasing burden of melanoma in the United States. *J. Invest. Dermatol.,* 129(7):1666–74, 2009.
98. Matthews NH, Li WQ, Qureshi AA, Weinstock MA, Cho E. "Epidemiology of melanoma." *Cutaneous melanoma: aetiology and therapy* Codon Publications, 2017.
99. Brenner M, Hearing VJ. The protective role of melanin against UV damage in human skin *Photochemistry and photobiology,* 84.3: 539-549,

2008.

100. McCain J. The MAPK (ERK) pathway: Investigational combinations for the treatment of BRAF- mutated metastatic melanoma *Pharmacy and Therapeutics*, 38.2: 96, 2013.
101. Forbes SA, Beare D, Gunasekaran P, Leung K, Bindal N, Boutselakis H, Ding M, Bamford S, Cole C, Ward S, Kok CY. COSMIC: exploring the world's knowledge of somatic mutations in human cancer. *Nucleic Acids Res*.,43(D1):D805–11, 2015.
102. Michielin O, van Akkooi A, Ascierto P, Dummer R, Keilholz U, Committee EG. Cutaneous melanoma: ESMO Clinical Practice Guidelines for diagnosis, treatment and follow-up. *Annals of Oncology,* 30.12: 1884-1901, 2019.
103. Ives NJ, Suciu S, Eggermont AM, Kirkwood J, Lorigan P, Markovic SN, Garbe C, Wheatley K, Bufalino R, Cameron D, Cascinelli N. Adjuvant interferon-alpha for the treatment of high-risk melanoma: An individual patient data meta-analysis. *Eur. J. Cancer*,82:171–83, 2017.
104. Eggermont AM, Chiarion-Sileni V, Grob JJ, Dummer R, Wolchok JD, Schmidt H, Hamid O, Robert C, Ascierto PA, Richards JM, Lebbé C. Prolonged Survival in Stage III Melanoma with Ipilimumab Adjuvant Therapy. *N. Engl. J. Med.,* 375(19):1845–55, 2016.
105. Weber JS, Mandalà M, Del Vecchio M, Gogas H, Arance AM, Cowey CL, Dalle S, Schenker M, Chiarion-Sileni V, Marquez Rodas I, Grob JJ. Adjuvant therapy with nivolumab (NIVO) versus ipilimumab (IPI) after complete resection of stage III/IV melanoma: Updated results from a phase III trial (CheckMate 238). 9502-950, 2018.
106. Long GV, Hauschild A, Santinami M, Atkinson V, Mandalà M, Chiarion-Sileni V, Larkin J, Nyakas M, Dutriaux C, Haydon A, Robert C. Adjuvant Dabrafenib plus Trametinib in Stage III BRAF-Mutated Melanoma. *N. Engl. J. Med.,* 377(19):1813–23, 2017.
107. Brodeur GM. Neuroblastoma: biological insights into a clinical enigma. *Nat. Rev. Cancer*, 3(3):203–16, 2003.
108. Amiel J, Laudier B, Attie-Bitach T, Trang H, de Pontual L, Gener B, Trochet D, Etchevers H, Ray P, Simonneau M, Vekemans M, Munnich A, Gaultier C, Lyonnet S. Polyalanine expansion and frameshift mutations of the paired-like homeobox gene PHOX2B in congenital central hypoventilation syndrome. *Nat. Genet.,* 33(4):459–61, 2003.
109. Takahashi M. The GDNF/RET signaling pathway and human diseases. *Cytokine Growth Factor Rev*., 12(4):361–73, 2001.
110. Maris JM, Weiss MJ, Mosse Y, Hii G, Guo C, White PS, Hogarty MD, Mirensky T, Brodeur GM, Rebbeck TR, Urbanek M. Evidence for a hereditary neuroblastoma predisposition locus at chromosome 16p12-13. *Cancer Res.,* 62(22):6651–8, 2002.
111. cancer.sanger.ac.uk.v.2016 p. COSMIC: Catalogue of somatic mutations in cancer, 2016.
112. Peifer M, Hertwig F, Roels F, Dreidax D, Gartlgruber M, Menon R, Krämer A, Roncaioli JL, Sand F, Heuckmann JM, Ikram F. Telomerase activation by genomic rearrangements in high-risk neuroblastoma. *Nature*, 526(7575):700–4, 2015.
113. Hertwig F, Peifer M, Fischer M. Telomere maintenance is pivotal for high-risk neuroblastoma. *Cell Cycle,* 15.3: 311, 2016.
114. Cheung Nai-Kong V. CSL. Neuroblastoma. New York, USA: Springer, Berlin, Heidelberg; 2005. 303 p.
115. Greengard EG. Molecularly Targeted Therapy for Neuroblastoma. *Child*, 5(10):142, 2018.
116. Monclair T, Brodeur GM, Ambros PF, Brisse HJ, Cecchetto G, Holmes K, Kaneko M, London WB, Matthay KK, Nuchtern JG, von Schweinitz D. The International Neuroblastoma Risk Group (INRG) staging system: an INRG Task Force report. *J. Clin. Oncol*., 27(2):298–303, 2009.
117. Rawnaq T, Quaas A, Zander H, Gros SJ, Reichelt U, Blessmann M, Wilzcak W, Schachner M, Sauter G, Izbicki JR, Kaifi JT. L1 is highly expressed in tumors of the nervous system: a study of over 8000 human tissues. *J. Surg. Res*.,173(2):314–9, 2012.
118. Sokol E, Desai A V. The Evolution of Risk Classification for Neuroblastoma. *Child,* 6(2):27, 2019.
119. Strother DR, London WB, Schmidt ML, Brodeur GM, Shimada H, Thorner P, Collins MH, Tagge E, Adkins S, Reynolds CP, Murray K. Outcome after surgery alone or with restricted use of chemotherapy for patients with low-risk neuroblastoma: results of Children's Oncology Group study P9641. *J. Clin. Oncol.,* 30(15):1842–8, 2012.
120. Pinto NR, Applebaum MA, Volchenboum SL, Matthay KK, London WB, Ambros PF, Nakagawara A, Berthold F, Schleiermacher G, Park JR, Valteau-Couanet D.Advances in Risk Classification and Treatment Strategies for Neuroblastoma. *J. Clin. Oncol*., 33(27):3008–17, 2015.
121. Kushner BH, LaQuaglia MP, Bonilla MA, Lindsley K, Rosenfield N, Yeh S, Eddy J, Gerald WL, Heller G, Cheung NK. Highly effective induction therapy for stage 4 neuroblastoma in children over 1 year of age. *J. Clin. Oncol.,* 12(12):2607–13, 1994.
122. Berthold F, Boos J, Burdach S, Erttmann R, Henze G, Hermann J, Klingebiel T, Kremens B, Schilling FH, Schrappe M, Simon T. Myeloablative megatherapy with autologous stem-cell rescue versus oral maintenance chemotherapy as consolidation treatment in patients with high-risk neuroblastoma: a randomised controlled trial. *Lancet Oncol.,* 6(9):649–58, 2005.
123. Yu AL, Gilman AL, Ozkaynak MF, London WB, Kreissman SG, Chen HX, Smith M, Anderson B, Villablanca JG, Matthay KK, Shimada H. Anti-GD2 antibody with GM-CSF, interleukin-2, and isotretinoin for neuroblastoma. *N. Engl. J. Med.,* 363(14):1324–34, 2010.
124. Krytska K, Ryles HT, Sano R, Raman P, Infarinato NR, Hansel TD, Makena MR, Song MM, Reynolds CP, Mossé YP. Crizotinib Synergizes with Chemotherapy in Preclinical Models of Neuroblastoma. *Clin. Cancer Res.,* 22(4):948–60, 2016.

125. Thery C, Amigorena S, Raposo G, Clayton A. Isolation and characterization of exosomes from cell culture supernatants and biological fluids. *Curr Protoc Cell Biol*., 30.1: 3-22, 2016.
126. Schütte M, Risch T, Abdavi-Azar N, Boehnke K, Schumacher D, Keil M, Yildiriman R, Jandrasits C, Borodina T, Amstislavskiy V, Worth CL. Molecular dissection of colorectal cancer in pre-clinical models identifies biomarkers predicting sensitivity to EGFR inhibitors. *Nat. Commun.,* 8(1):14262, 2017.
127. Ye J, Coulouris G, Zaretskaya I, Cutcutache I, Rozen S MT. Primer-BLAST: A tool to design target-specific primers for polymerase chain reaction. *BMC Bioinformatics,* 13:134, 2012.
128. Biorad. Droplet digital application guide. http://www.bio-rad.com/webroot/web/pdf/lsr/literature/Bulletin_6407.pdf
129. Prediger E. qPCR Probes—selecting the best reporter dye and quencher.*Integrated DNA Technologies*. 2015. https://eu.idtdna.com/pages/education/decoded/article/qpcr-probes-selecting-the-best-reporter-dye-and-quencher
130. Van der Valk J, Bieback K, Buta C, Cochrane B, Dirks WG, Fu J, Hickman JJ, Hohensee C, Kolar R, Liebsch M, Pistollato F. Fetal Bovine Serum (FBS): Past - Present - Future. *ALTEX,* 35(1):99–118, 2018.
131. Shelke G V, Lässer C, Gho YS, Lötvall J. Importance of exosome depletion protocols to eliminate functional and RNA-containing extracellular vesicles from fetal bovine serum. *Journal of extracellular vesicles,* 3.1:24783, 2014.
132. Price P, Stiles B, Staines D, Evege E, Fatunmbi F, Wagner K. Cultures in Advanced MEM and Advanced D-MEM demonstrated comparable or better growth to those grown in its classical counterparts. *Focus (Madison),* 25:3–6, 2003.
133. Lobb RJ, Becker M, Wen Wen S, Wong CS, Wiegmans AP, Leimgruber A, Möller A. Optimized exosome isolation protocol for cell culture supernatant and human plasma. *Journal of extracellular vesicles,* 4.1: 27031, 2015.
134. Lee DH, Yoon H, Park S, Kim JS, Ahn YH, Kwon K, Lee D, Kim KH. Urinary Exosomal and cell-free DNA Detects Somatic Mutation and Copy Number Alteration in Urothelial Carcinoma of Bladder. *Sci. Rep.,* 8(1):14707, 2018.
135. Nilsson J, Skog J, Nordstrand A, Baranov V, Mincheva-Nilsson L, Breakefield XO, Widmark A. Prostate cancer-derived urine exosomes: a novel approach to biomarkers for prostate cancer. *Br. J. Cancer,* 100(10):1603–7, 2009.
136. Fernández-Llama P, Khositseth S, Gonzales PA, Star RA, Pisitkun T, Knepper MA. Tamm-Horsfall protein and urinary exosome isolation. *Kidney Int*., 77(8):736–42, 2010.
137. Cheng L, Sun X, Scicluna BJ, Coleman BM, Hill AF. Characterization and deep sequencing analysis of exosomal and non-exosomal miRNA in human urine. *Kidney Int.,* 86(2):433–44, 2014.
138. Peak TC, Praharaj PP, Panigrahi GK, Doyle M, Su Y, Schlaepfer IR, Singh R, Vander Griend DJ, Alickson J, Hemal A, Atala A. Exosomes secreted by placental stem cells selectively inhibit growth of aggressive prostate cancer cells. *Biochem. Biophys. Res. Commun.,* 499(4):1004–10, 2018.
139. Pospichalova V, Svoboda J, Dave Z, Kotrbova A, Kaiser K, Klemova D, Ilkovics L, Hampl A, Crha I, Jandakova E, Minar L. Simplified protocol for flow cytometry analysis of fluorescently labeled exosomes and microvesicles using dedicated flow cytometer. *J. Extracell. vesicles*, 4:25530, 2015.
140. Rikkert LG, Nieuwland R, Terstappen LWMM, Coumans FAW. Quality of extracellular vesicle images by transmission electron microscopy is operator and protocol dependent. *J. Extracell. vesicles,* 8(1):1555419, 2019.
141. Chuo ST-Y, Chien JC-Y, Lai CP-K. Imaging extracellular vesicles: current and emerging methods. *J. Biomed. Sci.,*25(1):91, 2018.
142. Williams David, B., and C. Barry Carter. Transmission Electron Microscopy. *Transmission Electron Microscopy,* 3-22,1996
143. György B, Szabó TG, Pásztói M, Pál Z, Misják P, Aradi B, László V, Pállinger E, Pap E, Kittel A, Nagy G. Membrane vesicles, current state-of-the-art: emerging role of extracellular vesicles. *Cell Mol. Life Sci.,* 68(16):2667–88, 2011.
144. Théry C, Ostrowski M, Segura E. Membrane vesicles as conveyors of immune responses. *Nat .Rev. Immunol.,* 9(8):581–93, 2009.
145. Zhang L, Song J, Newhouse Y, Zhang S, Weisgraber KH, Ren G. An optimized negative-staining protocol of electron microscopy for apoE4•POPC lipoprotein. *J. Lipid Res*.,51(5):1228–36, 2010.
146. Raposo G, Stoorvogel W. Extracellular vesicles: Exosomes, microvesicles, and friends. *J. Cell Biol.,* 200(4):373 LP – 383, 2013.
147. Brum JR, Steward GF. Morphological characterization of viruses in the stratified water column of alkaline, hypersaline Mono Lake. *Microb. Ecol.,* 60(3):636–43, 2010.
148. Kondratov KA, Petrova TA, Mikhailovskii VY, Ivanova AN, Kostareva AA, Fedorov A V. A study of extracellular vesicles isolated from blood plasma conducted by low-voltage scanning electron microscopy. *Cell tissue biol.,*11(3):181–90, 2017.
149. Nguyen DB, Ly TB, Wesseling MC, Hittinger M, Torge A, Devitt A, Perrie Y, Bernhardt I. Characterization of Microvesicles Released from Human Red Blood Cells. *Cell Physiol. Biochem.,*38(3):1085–99, 2016.

150. Shao H, Chung J, Balaj L, Charest A, Bigner DD, Carter BS, Hochberg FH, Breakefield XO, Weissleder R, Lee H. Protein typing of circulating microvesicles allows real-time monitoring of glioblastoma therapy. *Nat. Med.,*18(12):1835–40, 2012.
151. Lasken RS. Single-cell genomic sequencing using Multiple Displacement Amplification*. Current opinion in microbiology* 10.5: 510-516, 2007.
152. Spits C, Le Caignec C, De Rycke M, Van Haute L, Van Steirteghem A, Liebaers I, Sermon K. Whole-genome multiple displacement amplification from single cells. *Nat. Protoc.,*1(4):1965–70, 2006.
153. Haight FA. Handbook of the Poisson Distribution. New York, USA; 18.4: 478-479, 1967.
154. Elnifro EM, Ashshi AM, Cooper RJ, Klapper PE. Multiplex PCR: optimization and application in diagnostic virology. *Clin. Microbiol. Rev.,* 13(4):559–70, 2000.
155. Sint D, Raso L, Traugott M. Advances in multiplex PDCR: balancing primer efficiencies and improving detection success. *Methods Ecol. Evol.,* 3(5):898–905, 2012.
156. George JN, Thoi LL, McManus LM, Reimann TA. Isolation of human platelet membrane microparticles from plasma and serum. *Blood,* 60(4):834–40, 1982.
157. Gemmell CH, Sefton M V, Yeo EL. Platelet-derived microparticle formation involves glycoprotein IIb-IIIa. Inhibition by RGDS and a Glanzmann's thrombasthenia defect*. J. Bio.l Chem.,* 268(20):14586–9, 1993.
158. Witwer KW, Buzás EI, Bemis LT, Bora A, Lässer C, Lötvall J, Nolte-'t Hoen EN, Piper MG, Sivaraman S, Skog J, Théry. Standardization of sample collection, isolation and analysis methods in extracellular vesicle research. *Journal of extracellular vesicles,* 2.1: 20360, 2013.
159. Philippe J, De Logi E, Baele G. Comparison of five different citrated tubes and their in vitro effects on platelet activation. *Clin. Chem.,* 50(3):656–8, 2004.
160. Yokota M, Tatsumi N, Nathalang O, Yamada T, Tsuda I. Effects of heparin on polymerase chain reaction for blood white cells. *Journal of clinical laboratory analysis,* 13.3: 133-140, 1999.
161. Maguire CA, Balaj L, Sivaraman S, Crommentuijn MH, Ericsson M, Mincheva-Nilsson L, Baranov V, Gianni D, Tannous BA, Sena-Esteves M, Breakefield XO.Microvesicle-associated AAV vector as a novel gene delivery system. *Mol. Ther.,* 20(5):960–71, 2012.
162. Wisgrill L, Lamm C, Hartmann J, Preißing F, Dragosits K, Bee A, Hell L, Thaler J, Ay C, Pabinger I, Berger A. Peripheral blood microvesicles secretion is influenced by storage time, temperature, and anticoagulants. *Cytometry A*., 89(7):663–72, 2016.
163. Mader S, Pantel K. Liquid biopsy: Current status and future perspectives. *Oncology research and treatment* 40.7-8: 404-408, 2017.
164. Alix-Panabières C, Pantel K. Circulating Tumor Cells: Liquid Biopsy of Cancer. *Clin. Chem*.,59(1):110–8, 2013.
165. Iliev D, Strandskog G, Nepal A, Aspar A, Olsen R, Jørgensen J, Wolfson D, Ahluwalia BS, Handzhiyski J, Mironova R.Stimulation of exosome release by extracellular DNA is conserved across multiple cell types. *FEBS J*., 285(16):3114–33, 2018.
166. Whiteside TL. The potential of tumor-derived exosomes for noninvasive cancer monitoring. *Expert Rev. Mol. Diagn*., 15(10):1293–310, 2015.
167. Kamerkar S, LeBleu VS, Sugimoto H, Yang S, Ruivo CF, Melo SA, Lee JJ, Kalluri R. Exosomes facilitate therapeutic targeting of oncogenic KRAS in pancreatic cancer. *Nature*, 546(7659):498–503, 2017.
168. Van Deun J, Mestdagh P, Sormunen R, Cocquyt V, Vermaelen K, Vandesompele J, Bracke M, De Wever O, Hendrix A. The impact of disparate isolation methods for extracellular vesicles on downstream RNA profiling. *Journal of extracellular vesicles,* 3.1: 24858, 2014.
169. Liga A, Vliegenthart ADB, Oosthuyzen W, Dear JW, Kersaudy-Kerhoas M. Exosome isolation: a microfluidic road-map. *Lab Chip*, 15(11):2388–94, 2015.
170. Xin H, Li Y, Buller B, Katakowski M, Zhang Y, Wang X, Shang X, Zhang ZG, Chopp M. Exosome-mediated transfer of miR-133b from multipotent mesenchymal stromal cells to neural cells contributes to neurite outgrowth. *Stem Cells,* 30(7):1556–64, 2012.
171. Navajas R, Corrales FJ, Paradela A. Serum Exosome Isolation by Size-Exclusion Chromatography for the Discovery and Validation of Preeclampsia-Associated Biomarkers. *Methods Mol. Biol.,* 1959:39–50, 2019.
172. Guerreiro EM, Vestad B, Steffensen LA, Aass HC, Saeed M, Øvstebø R, Costea DE, Galtung HK, Søland TM. Efficient extracellular vesicle isolation by combining cell media modifications, ultrafiltration, and size-exclusion chromatography. *PLoS One,* 13(9):e0204276, 2018.
173. Yu LL, Zhu J, Liu JX, Jiang F, Ni WK, Qu LS, Ni RZ, Lu CH, Xiao MB. A Comparison of Traditional and Novel Methods for the Separation of Exosomes from Human Samples. *BioMed. research international*, 2018.
174. Kanwar SS, Dunlay CJ, Simeone DM, Nagrath S. Microfluidic device (ExoChip) for on-chip isolation, quantification and characterization of circulating exosomes. *Lab Chip*, 14(11):1891–900, 2014.

175. Wang Z, Wu HJ, Fine D, Schmulen J, Hu Y, Godin B, Zhang JX, Liu X. Ciliated micropillars for the microfluidic-based isolation of nanoscale lipid vesicles. *Lab Chip*, 13(15):2879–82, 2013.
176. Davies RT, Kim J, Jang SC, Choi E-J, Gho YS, Park J. Microfluidic filtration system to isolate extracellular vesicles from blood. *Lab Chip,* 12(24):5202–10, 2012.
177. Chen C, Skog J, Hsu CH, Lessard RT, Balaj L, Wurdinger T, Carter BS, Breakefield XO, Toner M, Irimia D. Microfluidic isolation and transcriptome analysis of serum microvesicles. *Lab Chip*,10(4):505–11, 2010.
178. Liang LG, Kong MQ, Zhou S, Sheng YF, Wang P, Yu T, Inci F, Kuo WP, Li LJ, Demirci U, Wang S. An integrated double-filtration microfluidic device for isolation, enrichment and quantification of urinary extracellular vesicles for detection of bladder cancer. *Sci. Rep*., 7(1):46224.
179. Merchant ML, Rood IM, Deegens JKJ, Klein JB. Isolation and characterization of urinary extracellular vesicles: implications for biomarker discovery. *Nat. Rev. Nephrol.,* 13(12):731–49, 2017.
180. Ludwig N, Whiteside TL, Reichert TE. Challenges in Exosome Isolation and Analysis in Health and Disease. *International journal of molecular sciences,* 20.19: 4684, 2019.
181. Mol EA, Goumans M-J, Doevendans PA, Sluijter JPG, Vader P. Higher functionality of extracellular vesicles isolated using size-exclusion chromatography compared to ultracentrifugation. *Nanomedicine*.13(6):2061–5, 2017.
182. Welton JL, Webber JP, Botos L-A, Jones M, Clayton A. Ready-made chromatography columns for extracellular vesicle isolation from plasma. *Journal of extracellular vesicles,* 4.1: 27269, 2015.
183. Pisitkun T, Shen R-F, Knepper MA. Identification and proteomic profiling of exosomes in human urine. Proc. Natl. Acad. Sci., 101.36: 13368-13373, 2004.
184. Zhou H, Yuen PS, Pisitkun T, Gonzales PA, Yasuda H, Dear JW, Gross P, Knepper MA, Star RA. Collection, storage, preservation, and normalization of human urinary exosomes for biomarker discovery. *Kidney Int.,* 69(8):1471–6, 2006.
185. Hayden RT, Gu Z, Ingersoll J, Abdul-Ali D, Shi L, Pounds S, Caliendo AM. Comparison of droplet digital PCR to real-time PCR for quantitative detection of cytomegalovirus. J. Clin. Microbiol. 51.2: 540-546, 2013.
186. Taylor SC, Laperriere G, Germain H. Droplet Digital PCR versus qPCR for gene expression analysis with low abundant targets: from variable nonsense to publication quality data. *Sci. Rep*.,7(1):2409, 2017.
187. Pender A, Garcia-Murillas I, Rana S, Cutts RJ, Kelly G, Fenwick K, Kozarewa I, de Castro DG, Bhosle J, O'Brien M, Turner NC. Efficient Genotyping of KRAS Mutant Non-Small Cell Lung Cancer Using a Multiplexed Droplet Digital PCR Approach. *PLoS One*, 10(9):e0139074, 2015.
188. Rowlands V, Rutkowski AJ, Meuser E, Carr TH, Harrington EA, Barrett JC. Optimisation of robust singleplex and multiplex droplet digital PCR assays for high confidence mutation detection in circulating tumour DNA. *Sci. Rep.,* (1):12620, 2019.
189. Taly V, Pekin D, Benhaim L, Kotsopoulos SK, Le Corre D, Li X, Atochin I, Link DR, Griffiths AD, Pallier K, Blons H. Multiplex Picodroplet Digital PCR to Detect Mutations in Circulating DNA from the Plasma of Colorectal Cancer Patients. *Clin. Chem.,* 59(12):1722 LP – 1731, 2013.
190. Liebs S, Keilholz U, Kehler I, Schweiger C, Hayback J, Nonnenmacher A. Detection of mutations in circulating cell-free DNA in relation to disease stage in colorectal cancer. *Cancer Med.,* 8(8):3761–9, 2019.
191. Kim Y, Shin S, Kim B, Lee K-A. Selecting short length nucleic acids localized in exosomes improves plasma EGFR mutation detection in NSCLC patients. *Cancer Cell Int.,* 19:251, 2019.
192. Blank A, Roberts 2nd DE, Dawson H, Zlobec I, Lugli A. Tumor Heterogeneity in Primary Colorectal Cancer and Corresponding Metastases. Does the Apple Fall Far From the Tree? *Front. Med.,* 5:234, 2018.
193. Grzywa TM, Paskal W, Włodarski PK. Intratumor and Intertumor Heterogeneity in Melanoma. *Transl. Oncol.,* 10(6):956–75, 2017.
194. Alizadeh AA, Aranda V, Bardelli A, Blanpain C, Bock C, Borowski C, Caldas C, Califano A, Doherty M, Elsner M, Esteller M, Fitzgerald R, Korbel JO, Lichter P, Mason CE, Navin N, Pe'er D, Polyak K, Roberts CW, Siu L, Snyder A, Stower H, Swanton C, Verhaak RG, Zenklusen JC, Zuber J, Zucman-Rossi J. Toward understanding and exploiting tumor heterogeneity. *Nat. Med.,* 21(8):846–53, 2015.
195. Ngan ES-W. Heterogeneity of neuroblastoma. *Oncoscience*, 2(10):837–8, 2015.
196. Comoli P, Chabannon C, Koehl U, Lanza F, Urbano-Ispizua A, Hudecek M, Ruggeri A, Secondino S, Bonini C, Pedrazzoli P. Development of adaptive immune effector therapies in solid tumors. *Annals of Oncology* 30.11: 1740-1750, 2019.
197. Menzies AM, Long G V., Murali R. Dabrafenib and its potential for the treatment of metastatic melanoma. *Drug design, development and therapy* 6: 391, 2012.
198. Johnson DB, Flaherty KT, Weber JS, Infante JR, Kim KB, Kefford RF, Hamid O, Schuchter L, Cebon J, Sharfman WH, McWilliams RR, Sznol M, Lawrence DP, Gibney GT, Burris HA 3rd, Falchook GS, Algazi A, Lewis K, Long GV, Patel K, Ibrahim N, Sun P, Little S, Cunningham E, Sosman

JA, Daud A, Gonzalez R. Combined BRAF (Dabrafenib) and MEK inhibition (Trametinib) in patients with BRAFV600-mutant melanoma experiencing progression with single-agent BRAF inhibitor. *J. Clin. Oncol.,* 32(33):3697–704, 2014.

199. Van Allen EM, Wagle N, Sucker A, Treacy DJ, Johannessen CM, Goetz EM, Place CS, Taylor-Weiner A, Whittaker S, Kryukov GV, Hodis E. The Genetic Landscape of Clinical Resistance to RAF Inhibition in Metastatic Melanoma. *Cancer Discov*., 4(1):94 LP – 109, 2014.
200. Van Cutsem E, Kohne CH, Láng I, Folprecht G, Nowacki MP, Cascinu S, Shchepotin I, Maurel J, Cunningham D, Tejpar S, Schlichting M. Cetuximab plus irinotecan, fluorouracil, and leucovorin as first-line treatment for metastatic colorectal cancer: Updated analysis of overall survival according to tumor KRAS and BRAF mutation status. *J. Clin. Oncol.,* 29(15):2011–9, 2011.
201. Maughan TS, Adams RA, Smith CG, Meade AM, Seymour MT, Wilson RH, Idziaszczyk S, Harris R, Fisher D, Kenny SL, Kay E. Addition of cetuximab to oxaliplatin-based first-line combination chemotherapy for treatment of advanced colorectal cancer: results of the randomised phase 3 MRC COIN trial. *The Lancet,* 377.9783: 2103-2114, 2011.
202. Parseghian CM, Loree JM, Morris VK, Liu X, Clifton KK, Napolitano S, Henry JT, Pereira AA, Vilar E, Johnson B, Kee B. Anti-EGFR-resistant clones decay exponentially after progression: implications for anti-EGFR re-challenge. *Ann. Oncol.,* 30(2):243–9, 2019.
203. Li X, Corbett AL, Taatizadeh E, Tasnim N, Little JP, Garnis C, Daugaard M, Guns E, Hoorfar M, Li IT. Challenges and opportunities in exosome research-Perspectives from biology, engineering, and cancer therapy. *APL Bioeng*, 3(1):11503, 2019.
204. Charoenviriyakul C, Takahashi Y, Morishita M, Matsumoto A, Nishikawa M, Takakura Y. Cell type-specific and common characteristics of exosomes derived from mouse cell lines: Yield, physicochemical properties, and pharmacokinetics. *Eur. J. Pharm. Sci.,* 96:316–22, 2017.
205. Yamashita T, Takahashi Y, Nishikawa M, Takakura Y. Effect of exosome isolation methods on physicochemical properties of exosomes and clearance of exosomes from the blood circulation. *Eur. J. Pharm. Biopharm.,* 98:1–8, 2016.
206. Li X, Corbett AL, Taatizadeh E, Tasnim N, Little JP, Garnis C, Daugaard M, Guns E, Hoorfar M, Li IT. Challenges and opportunities in exosome research—Perspectives from biology, engineering, and cancer therapy. *APL Bioeng.,* 3(1):011503, 2019.
207. Tauro BJ, Greening DW, Mathias RA, Ji H, Mathivanan S, Scott AM, Simpson RJ. Comparison of ultracentrifugation, density gradient separation, and immunoaffinity capture methods for isolating human colon cancer cell line LIM1863-derived exosomes. *Methods,* 56(2):293–304, 2012.
208. Millner LM, Linder MW, Valdes Jr R. Circulating tumor cells: a review of present methods and the need to identify heterogeneous phenotypes. *Ann. Clin. Lab. Sci.,* 43(3):295–304, 2013.
209. Morgan TM. Liquid biopsy: Where did it come from, what is it, and where is it going? *Investig. Clin. Urol.,* 60(3):139–41, 2019.
210. Colombo M, Raposo G, Thery C. Biogenesis, secretion, and intercellular interactions of exosomes and other extracellular vesicles. *Annu. Rev. Cell Dev. Biol*.,30:255–89, 2014.
211. Singh R, Pochampally R, Watabe K, Lu Z, Mo Y-Y. Exosome-mediated transfer of miR-10b promotes cell invasion in breast cancer. *Mol. Cancer.*256, 2014.
212. Kim MS, Haney MJ, Zhao Y, Mahajan V, Deygen I, Klyachko NL, Inskoe E, Piroyan A, Sokolsky M, Okolie O, Hingtgen SD. Development of exosome-encapsulated paclitaxel to overcome MDR in cancer cells. *Nanomedicine*.12(3):655–64, 2016.
213. Tian Y, Li S, Song J, Ji T, Zhu M, Anderson GJ, Wei J, Nie G. A doxorubicin delivery platform using engineered natural membrane vesicle exosomes for targeted tumor therapy. *Biomaterials.*35(7):2383–90, 2014.

14. STATUTORY DECLARATION

"I, Soo Ann Yap, by personally signing this document in lieu of an oath, hereby affirm that I prepared the submitted dissertation on the topic „ **Extracellular vesicles as cancer liquid biopsy biomarker / Extrazelluläre Vesikel als prädiktive Liquid Biopsy Biomarker in der Onkologie"** independently and without the support of third parties, and that I used no other sources and aids than those stated.

All parts which are based on the publications or presentations of other authors, either in letter or in spirit, are specified as such in accordance with the citing guidelines. The sections on methodology (in particular regarding practical work, laboratory regulations, statistical processing) and results (in particular regarding figures, charts and tables) are exclusively my responsibility.

Furthermore, I declare that I have correctly marked all of the data, the analyses, and the conclusions generated from data obtained in collaboration with other persons, and that I have correctly marked my own contribution and the contributions of other persons (cf. declaration of contribution). I have correctly marked all texts or parts of texts that were generated in collaboration with other persons.

My contributions to any publications to this dissertation correspond to those stated in the below joint declaration made together with the supervisor. All publications created within the scope of the dissertation comply with the guidelines of the ICMJE (International Committee of Medical Journal Editors; www.icmje.org) on authorship. In addition, I declare that I shall comply with the regulations of Charité – Universitätsmedizin Berlin on ensuring good scientific practice.

I declare that I have not yet submitted this dissertation in identical or similar form to another Faculty.

The significance of this statutory declaration and the consequences of a false statutory declaration under criminal law (Sections 156, 161 of the German Criminal Code) are known to me."

Date Signature

15. DECLARATION OF OWN CONTRIBUTION TO ANY PUBLICATIONS

Soo Ann Yap has included into this thesis some data and results, which has already been published:

Publication 1:

Analysis of cancer related mutations in extracellular vesicles RNA by Droplet Digital PCR.

Yap S.A, Münster-Wandowski A., Nonnenmacher A., Keilholz U., Liebs S.

BioTechniques Journal, 25 June 2020.

Contributions:

Yap S.A. contributed to the conception of the work, established all protocols and performed all experiments, except for protocols and experiments related to whole mount immunoelectron microscopy. Results of whole mount electron microscopy was discussed with Münster-Wandowski A. (Figure 12, 14, 16, 17, 18, 19 and 34). Manuscript for the above mentioned publication was drafted by Yap S.A..
Münster-Wandowski A. performed and analyzed transmission electron microscopic analysis. Results from Figure 12, 14, 16, 17, 18, 19 and 34 were kindly provided by Münster-Wandowski A.
Keilholz U. and Liebs S. contributed to the conception of the work and supervised the project.
Nonnenmacher A. assisted in results interpretation, primarily in ddPCR multiplex assays (Figure 31 and 32).
All authors discussed the results, contributed to and approved the final manuscript of the above mentioned publication

_____

Signature, date and stamp of first supervising university professor / lecturer

_____

Signature of doctoral candidate

16. CURRICULLUM VITAE

My curriculum vitae does not appear in the electronic version of my paper for reasons of data protection.

17. ACKNOWLEDGEMENTS

I am grateful for the chance provided by Prof. Dr. Ulrich Keilholz for opening the doors of science to me by giving me the opportunity to be part of an amazing team. Thank you to my lab colleagues from AG Keilholz. Special thanks to Stefano Meucci for installing the courage in me to embark on the exosome journey, Christoph Hapke for my first pipetting lesson, Sandra Liebs for showing me the dedication to science, Anika Nonnenmacher for being the pleasant person you are and Gabriela Pachnikova for our fun coffee outings and all the assistance. Anna Kotarac and Henriette Thau, I really appreciate the positive vibes in the office. Thank you to Dr. Agnieszka Münster-Wandowski for such a lovely and productive collaboration. Thank you to the Berliner Krebsgesellschaft e.V for the Ernst-von-Leyden Stipendium for financing me for two years.

My amazing long-distanced support system Dr. Andreas Schönfeld and Leticia Figueiredo , thank you for the advices and patience over the years. Jenny Graterol who stood by me during my whole Berlin experience.

My family scattered all over the world; my forever supportive parents and my dearest sisters, my Canadian family .I am almost never by your side but I always felt your love and support. I would have never been able to come this far without you. The many people I met along the different time point in my life. I am grateful for all the opportunities, experiences and moments we shared.

To the late Miss Heike Lange, I have always told you how grateful I am to every kind word you said and always loved baking for you. I am forever grateful for your kindness, encouragements, for always telling me I am doing well and that everything is going to be just fine.

The oncology research field came a long way from the introduction of chemotherapy, which was then thought of as the ultimate cure for this deadly disease to the sophisticated advancements made today. The battle is weary and will continue on for years to come. It might not be a possible to save every patient, but every single life save is worthwhile. Thank you to the doctors and nurses standing in the front line battling this disease and researchers working behind the scenes.

Yours sincerely,

18. PUBLICATION LIST

1. Analysis of cancer related mutations in extracellular vesicles RNA by Droplet Digital PCR.
   Yap S.A., Münster-Wandowski A., Nonnenmacher A., Keilholz U., Liebs S.
   BioTechniques Journal, 25 June 2020